DESIGN SCALING OF AEROBALLISTIC RANGE MODELS

A THESIS SUBMITTED TO
THE GRADUATE SCHOOL OF NATURAL AND APPLIED SCIENCES
OF
MIDDLE EAST TECHNICAL UNIVERSITY

BY

ÜMİT KUTLUAY

IN PARTIAL FULFILLMENT OF THE REQUIREMENTS
FOR
THE DEGREE OF MASTER OF SCIENCE
IN
DEPARTMENT OF MECHANICAL ENGINEERING

DECEMBER 2004

Approval of the Graduate School of Natural and Applied Sciences

_____

Prof. Dr. Canan ÖZGEN

Director

I certify that this thesis satisfies all the requirements as a thesis for the degree of Master of Science.

_____

Prof. Dr. S. Kemal İDER

Head of Department

This is to certify that we have read this thesis and that in our opinion it is fully adequate, in scope and quality, as a thesis for the degree of Master of Science.

_____	_____
Dr. Gökmen MAHMUTYAZICIOĞLU	Prof. Dr. Tuna BALKAN
Co - Supervisor	Supervisor

Examining Committee Members

Prof. Dr. Kemal ÖZGÖREN	(METU, ME)	_____
Prof. Dr. Tuna BALKAN	(METU, ME)	_____
Dr. Gökmen MAHMUTYAZICIOĞLU	(TÜBİTAK-SAGE)	_____
Prof. Dr. Metin AKKÖK	(METU, ME)	_____
Dr. Mutlu Devrim CÖMERT	(TÜBİTAK-SAGE)	_____

I hereby declare that all information in this document has been obtained and presented in accordance with academic rules and ethical conduct. I also declare that, as required by these rules and conduct, I have fully cited and referenced all material and results that are not original to this work.

Name, Last name: Ümit KUTLUAY

Signature :

ABSTRACT

DESIGN SCALING OF AEROBALLISTIC RANGE MODELS

Kutluay, Ümit
M.Sc., Department of Mechanical Engineering
Supervisor: Prof. Dr. Tuna Balkan
Co-supervisor: Dr. Gökmen Mahmutyazıcıoğlu

December 2004, 144 pages

The aim of this thesis is to develop a methodology for obtaining an optimum configuration for the aeroballistic range models. In the design of aeroballistic range models, there are mainly three similarity requirements to be matched between the model and the actual munition: external geometry, location of the centre of gravity and the ratio of axial mass moment of inertia to the transverse mass moment of inertia. Furthermore, it is required to have a model with least possible weight, so that the required test velocities can be obtained with minimum chamber pressure and by use of minimum propellant while withstanding the enormous launch accelerations. This defines an optimization problem: to find the optimum model internal configuration and select materials to be used in the model such that the centre of gravity location and the inertia ratio are matched as closely as possible while the model withstands the launch forces and has minimum mass. To solve this problem a design methodology is devised and an optimization code is developed based on this methodology. Length, radius and end location of an optimum cylinder which has to be drilled out from the model are selected as the design variables for the optimization problem. Built–in functions from the *Optimization Toolbox* of Matlab® are used in the optimization routine, and also a graphical user interface is

designed for easy access to the design variables. The developed code is a very useful tool for the designer, although the results are not meant to be directly applied to the final product, they form the starting points for the detailed design.

Keywords: Aeroballistics, Aeroballistic Range, Aeroballistic Range Testing, Aeroballistic Range Models, constrained optimization

ÖZ

ÖLÇEKLENDİRİLMİŞ AEROBALİSTİK DENEME MODELLERİNİN TASARIMI

Kutluay, Ümit
Yüksek Lisans, Makina Mühendisliği Bölümü
Tez Yöneticisi: Prof. Dr. Tuna Balkan
Ortak Tez Yöneticisi: Dr. Gökmen Mahmutyazıcıoğlu

Aralık 2004, 144 sayfa

Bu çalışmanın amacı, aerobalistik deneme modellerinin en iyi konfigürasyonlarının belirlenmesinde kullanılacak bir yöntem geliştirilmesidir. Aerobalistik Model tasarımında, model ile gerçek mühimmat arasında sağlanması gereken başlıca üç benzerlik gereksinimi vardır: dış geometri, ağırlık merkezinin konumu, eksenel eylemsizlik değerinin yanal eylemsizlik değerine oranı. Bunlara ek olarak, istenen test hızına en düşük miktarda barut kullanarak, en düşük yanma odası basınçları altında ulaşılabilmesi için modelin mümkün olduğunca hafif olması da gerekmektedir. Bu gereksinimler, ağırlık merkezi konumunu ve eylemsizliklerin oranını mümkün olduğunca yakın bir şekilde tuttururken, en düşük kütleye sahip olan ve fırlatma yüklerine dayanan en iyi model iç konfigürasyonunun bulunması ve modelde kullanılan malzemelerin seçilmesi şeklinde bir eniyileme problemi tanımlamaktadır. Bu problemin çözümü için bir tasarım yöntemi geliştirilmiş ve bu yöntem kullanılarak bir kod yazılmıştır. En iyilime probleminin tasarım değişkenleri olarak, modelin içerisinden çıkartılması gereken bir silindirin uzunluğu, yarıçapı ve bittiği nokta seçilmiştir. Eniyileme alt programı olarak,

Matlab® yazılımının *Optimization Toolbox* fonksiyonları kullanılmış ve tasarım parametrelerinin kullanıcı tarafından kolaylıkla değiştirilebilmesi için bir de grafik arayüz tasarlanmıştır. Bu çalışma sonunda geliştirilen kod, tasarımcı için çok faydalı bir araç olsa da çıktıları son ürün üzerinde kullanılmak için değil, detaylı tasarıma girdi oluşturmak içindir.

Anahtar kelimeler: Aerobalistik, Aerobalistik Test Altyapısı, Aerobalistik Test, Aerobalistik Test Modeli, kısıtılı eniyileme

ACKNOWLEDGEMENT

I would like to express my special thanks to my supervisor Prof. Dr. Tuna BALKAN for his guidance, tolerance and understanding. I would like to state my deepest gratitude to my co-supervisor Dr. Gökmen MAHMUTYAZICIOĞLU for his guidance, patience and motivation.

I would like to thank TÜBİTAK-SAGE for all their support throughout this study. I would like state my gratitude to my colleagues Sevsay AYTAR ORTAÇ for her support, guidance and discussions on the subject, İ. Murat KARBANCIOĞLU for his ideas and invaluable help as a "debugger", Şamil KORKMAZ, Çağlar SULAR, Umut DURAK and Mümtaz A. ESİ for their discussions on the subject. I would like to extend my gratitude to Vedat EKÜTEKİN and Koray DAYANÇ for their motivation, support and advices.

I would like to thank my family who supported me throughout my life for their trust, understanding and patience.

TABLE OF CONTENTS

APPENDICES

LIST OF TABLES

LIST OF FIGURES

LIST OF SYMBOLS

A	Cross sectional area
a	Acceleration
b	Span
br	Body section radius
$\widetilde{C},\widetilde{c}$	Constraints matrix
c	Chord length
d	Differentiation, search direction
H	Hessian
I	Moment of inertia
m	Mass
nl	Nose section length
nr	Nose section end radius
R	Rotation matrix, radius
tr	Tail section radius
V	Velocity
w	Weighting factor
x	Design variables
α	Fin angle
λ	Lagrangian multipliers, scale factor
ρ	Density
σ	Stress
∇	Gradient

Superscripts

0	Initial condition
T	Transpose

Acronyms

CFD	Computational Fluid Dynamics
CM, *cg*	Centre of Gravity
FML	Flight Mechanics Laboratory
FOM	Figure of Merit
GP	General Purpose
GUI	Graphical User Interface
LD	Low Drag

CHAPTER 1

INTRODUCTION

Aeroballistics is the science of motion of projectiles[1] in flight. The motion of a projectile in flight is characterized by the aerodynamic parameters such as drag and lift coefficients and also by stability derivatives. To obtain these parameters, the first method that comes to mind is full scale flight testing. However, full scale flight testing is usually not feasible because of high costs and difficulties of controlling the test conditions. Furthermore, it is often not possible to flight test the projectile in the early stages of the design work.

These difficulties related to aerodynamic parameter estimation from the results of full scale flight testing are overcome by the use of alternative methods where the required parameters are obtained at relatively low costs and under controlled conditions. These methods can be classified as [1]:

- Computational Aerodynamics
- Theoretical and Empirical Aerodynamics
- Experimental Aerodynamics (Wind Tunnel Testing)
- Experimental Flight Dynamics (Aeroballistic Range Testing)

The importance of computational methods in engineering can not be neglected. However, Computational Aerodynamics, often referred as CFD – Computational Fluid Dynamics, is far from being the best tool for the prediction for the

[1] Projectile is the common name given to the flying objects that follow a ballistic flight path. The word “ballistic” is derived from the Roman weapon “ballista”.

aerodynamic parameters for the projectiles, mostly because of the computational speed limitations. The results of CFD analysis are of little importance unless they are validated using experimental data [1], [2].

The most fundamental aerodynamic parameters for simple projectile geometries can be obtained by the use of the results of theoretical and empirical aerodynamics with relatively high computational speed and acceptable accuracy. However, when new and complex geometries are considered, the empirical aerodynamics fails to give satisfactory results. Furthermore, like CFD, the results of the empirical aerodynamics are not reliable unless there exists experimental data for justification.

There are basically two types of aerodynamic facilities used for the derivation of aerodynamic parameters experimentally: wind tunnels and aeroballistic ranges. The major difference between a wind tunnel and aeroballistic range is the way the flight conditions are simulated.

In wind tunnels the medium, which is usually air, is accelerated mostly by the help of propeller(s). The body, for which the aerodynamic parameters are sought is mostly constrained and balanced so that the desired flight conditions such as the angle of attack or pitch angle are simulated. Although wind tunnel testing has an important place in research on projectile aerodynamics, different wind tunnels are needed for the wide Mach number range a projectile flies through, which can increase the test costs drastically. The most important drawback of wind tunnel testing for predicting the aerodynamic parameters of projectiles is the way models are mounted in the test section. The pressure distribution on the base of the projectile is very important from ballistic point of view. However, this pressure distribution is distorted due to the base sting, which holds the model, which in turn, affects the accuracy of the test results [1].

In contrast to wind tunnel testing, the model itself is accelerated to the required test velocities using some kind of gun in aeroballistic range testing (i.e. the model is “launched” from the gun). The motion of the dynamically scaled model is tracked

by data acquisition systems downrange and the aerodynamic parameters are predicted from the flight data acquired.

Although the purpose of the aeroballistic range tests was the optimization of the spin stabilized shells for munitions until 1940's [3], aeroballistic range facilities are widely used in the development of transonic, supersonic and hypersonic missiles and airplanes as well as investigation of atmospheric re-entry of long range missiles and re-entry vehicles. Flight dynamics characteristics, aerophysics of wake phenomena, aerodynamic heating and aerodynamic parameters for the flight vehicles can be determined from aeroballistic range tests [4]. These ranges are also used for research on material behavior under very high loads, high speed impact and investigation of the effects of space debris on satellites and other orbital vehicles. After the tragic events of September 11th 2001 and the loss of the Space Shuttle Columbia during re-entry in February 1st 2003, most of the research in aeroballistic ranges world-wide is concentrated on the hyper velocity impact and new material development for shock absorbing.

There are basically three types of guns that are used in aeroballistic ranges: powder gas guns, compressed air guns and light gas guns. Powder gas guns are traditional guns that are operated by the ignition of the gunpowder and are very useful tools for low to intermediate (up to Mach 5.0) velocities. When higher velocities are needed, compressed air guns and light gas guns are feasible solutions. Compressed air guns, as the name suggests, works on the principle of accelerating the models by the sudden expansion of compressed air. They reach higher speeds when compared to powder gas guns. Light gas guns use highly compressed hydrogen or helium and by sudden expansion of the gasses models are accelerated to very high speeds (up to 13 km/s – nearly Mach 40). The other types of guns that are used in aeroballistic ranges are railguns, coilguns and ram accelerators [5]. The first two are electromagnetic guns, where the last one is derived from the ramjet concept.

The flight history of the model is recorded by the help of either photographic or yaw-card stations and sometimes both methods are applied together. In

photographic stations, a photograph of the model or its shadow is captured along with the time information from a time/velocity measurement system. These images are later processed to obtain the attitude of the model and subsequently, the required aerodynamic parameters are estimated. In yaw-card stations, the model punches the cards as it travels downrange the facility and time information of the punching instant is kept. The cards are post processed to find the model's attitude at the time of the punching and the model's attitude throughout the range, i.e. flight history, is obtained.

With the advances in the technology, very high speed motion cameras are also used to visualize some special events like the muzzle exit or sabot separation. There are cameras capable of recording images up to 120,000 frames per second. In open-air facilities, it is also possible to track the flight of the model for very long distances using special mirrors and motion systems especially designed for ballistic testing.

Figure 1.1 Powder gas gun used at FML

TÜBİTAK-SAGE, a member of Aeroballistic Range Association (ARA) since 1996, owns the only aeroballistic range facility in Turkey: the Flight Mechanics

Laboratory (FML). FML was constructed as an open air aeroballistic range facility in 1997, [6] and the test section was later covered in 1999, [7], [8]. The length of the test section was originally 100 m, although it has been increased to 200 m in 2002, making it one of the longest in the world. A view of the test section is shown in Figure 1.2. The models are accelerated to velocities in excess of M 5.0 by the powder gas gun of diameter 100 mm and barrel length of 5.5 m. The operating chamber pressure of the gun is 2000 bars (Figure 1.1).

The facility currently has 30 yawcard stations and 8 photographic stations to gather the flight data of the projectiles. Examples of images taken from both type of stations are given in Figure 1.3 and Figure 1.4. The time of the flight is measured by sensors at every station and also by the velocity measurement system.

Figure 1.2 Test section of the Flight Mechanics Laboratory (TÜBİTAK-SAGE)

Figure 1.3 Image from a yaw card after the test

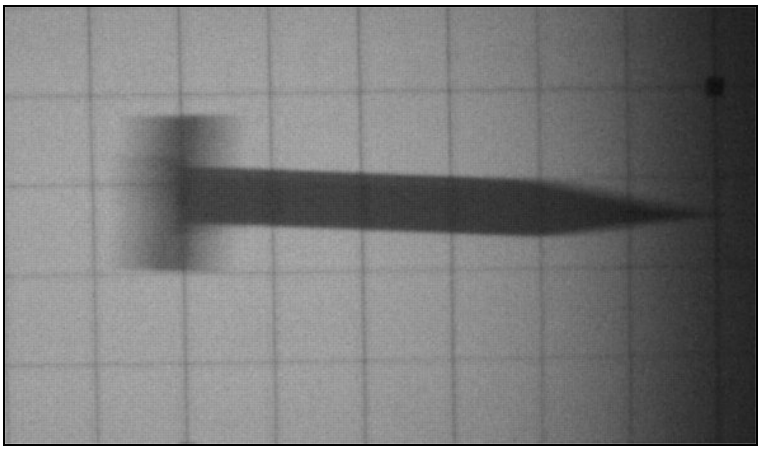

Figure 1.4 Image from a photographic station after the test

For aerodynamic testing where the similarity of the flow patterns are important, the Reynolds number, which is the ratio of inertia forces to viscous forces is kept constant, [9]. Mach number, which is defined as the ratio of the flow velocity to the

ratio of the speed of sound, is equally important to the experimental aerodynamics as the Reynolds number, [9], [10].

Aeroballistic range tests are performed at full-scale Mach numbers. Although there are a small number of aeroballistic ranges where the medium can be changed so that the test Reynolds number is matched to that of the full-scale Reynolds number, FML does not have such a capability. However, as the Mach number increases, the scaling effects of the unmatched Reynolds numbers become less and less important. So for the Mach number range where the FML used, the scale effects due the Reynolds number is neglected.

Another issue in free-flight model testing is the effect of gravity. Since the gravity can not be scaled, an error is introduced to the results of the tests. However, contribution of this error is small, since the duration of an aeroballistic range test is very short [9].

The projectile itself is the very heart of successful aeroballistic range testing. The models that are to be tested should be dynamically scaled. That is, the dimensions, and the centre of gravity location of the actual munition should be scaled down while the ratio of the axial inertia to the transverse inertia of the model should be matched to the actual munition value. Once these scaling requirements are satisfied, the flow pattern as well as the model's translational and rotational motion will be similar to the actual munition's motion. However, in scale model testing, all of the scaling requirements are not fulfilled at the same time, but tests are designed for certain similitude requirements that are important to the goals of the specific test under consideration [11]. Most of the time, it is not possible to scale down every geometrical detail of the original body due to the manufacturing and material constraints. Also it is not possible to match the centre of gravity location and the inertia ratio at the exact scaled down value but they are matched within some tolerance. So the models used in aeroballistic ranges are never true scaled models but often adequate models, which will give satisfactory results with negligible effects of scaling.

In this study, the model design is the main concern.

1.1 AIM OF THE STUDY

The projectile used in aeroballistic range testing usually consists of two parts, the model and the sabot[2] [3].

The model is the scaled replica of the actual body, for which the aerodynamic parameters are required. The sabot's duty is to protect and support the model within the barrel of the gun and accelerate it to the desired test velocity. There are basically two types of sabot in use for aeroballistic range testing: pusher type sabots and puller type sabots. For pusher type sabots, the model is accelerated by "pushing" it from the base while supporting it from the sides. The base part of the pusher type sabot is often named as pusher (Figure 1.5) [8]. Puller type sabots are used when the base area of the model does not provide a sufficient surface for pusher contact (Figure 1.6) [12], [13], [14].

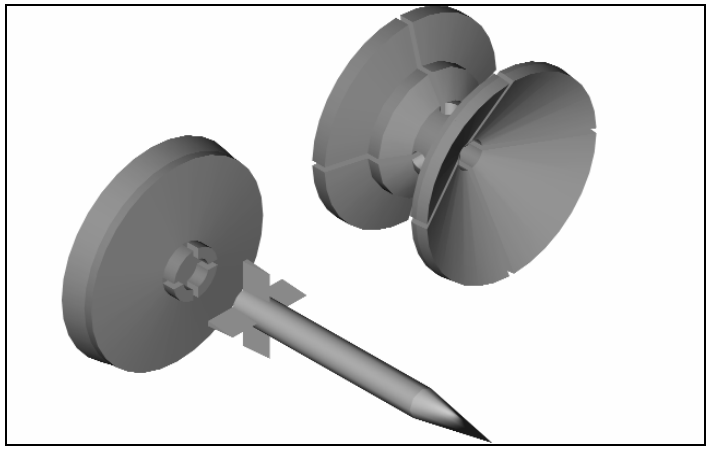

Figure 1.5 Model, sabot and pusher

[2] "Sabot" is a French word meaning wooden shoe. When used in aeroballistics, it refers to the support which is used to launch aeroballistic range models and sub-caliber projectiles.

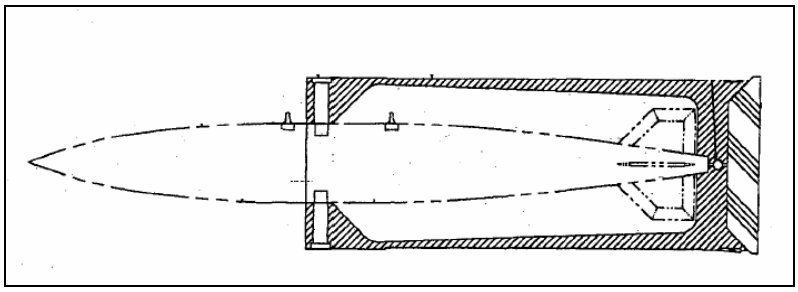

Figure 1.6 Model and puller type sabot

The design process of an aeroballistic range model is not a straightforward work. There are many strict requirements imposed on the designer some of which can be summarized as follows [2], [3], [7], [15]:

- The projectile should be scaled such that it fits into the gun.
- The original exterior geometry should be matched.
- The location of the center of gravity should be scaled and matched.
- The ratio of the axial inertia to the transverse inertia of the model should be matched to that of the actual munition.
- The model should withstand the launch accelerations, since the launch loads are far more greater than the inflight loads.
- The surface quality of the original body should be scaled.
- The weight of the model should be as small as possible to keep the required chamber pressure minimum.

In general, it is not possible to scale every geometrical detail of the actual munition. This is mostly due to the difficulties in production and costs.

The approach to aeroballistic range model design is given in [2] as a flow chart and it is obvious that this process is an iterative work (Figure 1.7). In fact, the

aeroballistic range model design process includes the mechanical design of sabot as well. However, sabot design is a very broad and complex subject and is not included in this study. Most of the time, it is not possible to obtain the optimum model configuration by calculations alone but a corrective redesign is necessary after proof firing tests that are performed to see if the model fulfills the above mentioned requirements. This design work takes a great deal of time and effort of the engineer, thus a need for a computer aided design methodology arose at TÜBİTAK-SAGE.

This thesis study is done in order to develop a methodology which will be the basis for a computer code that will be used to obtain the optimum aeroballistic model configuration which will match the center of gravity and ratios of inertia criteria with minimum possible error while minimizing the weight. The aim of this study is neither to decide on the best optimization method in designing aeroballistic range models, nor to design the optimum aeroballistic range model of a low-drag general purpose aircraft bomb or an unguided artillery rocket. The code will be used as a first order computer aided design tool in the design and scaling of the aeroballistic range models. Once the outputs of the code are obtained, they are used as inputs for detailed mechanical design before the manufacturing.

The goals of the study can be summarized as follows:

- The methodology should be generic, i.e. it should cover all type of models.
- The code should run on Windows operating systems.
- The code should have a graphical user interface (GUI) for ease of usage.
- The results of the code should be saved to files for later reference.
- The code should be capable of modeling the most common geometries used in aeroballistic range testing.
- The code should perform a preliminary stress analysis of the model.

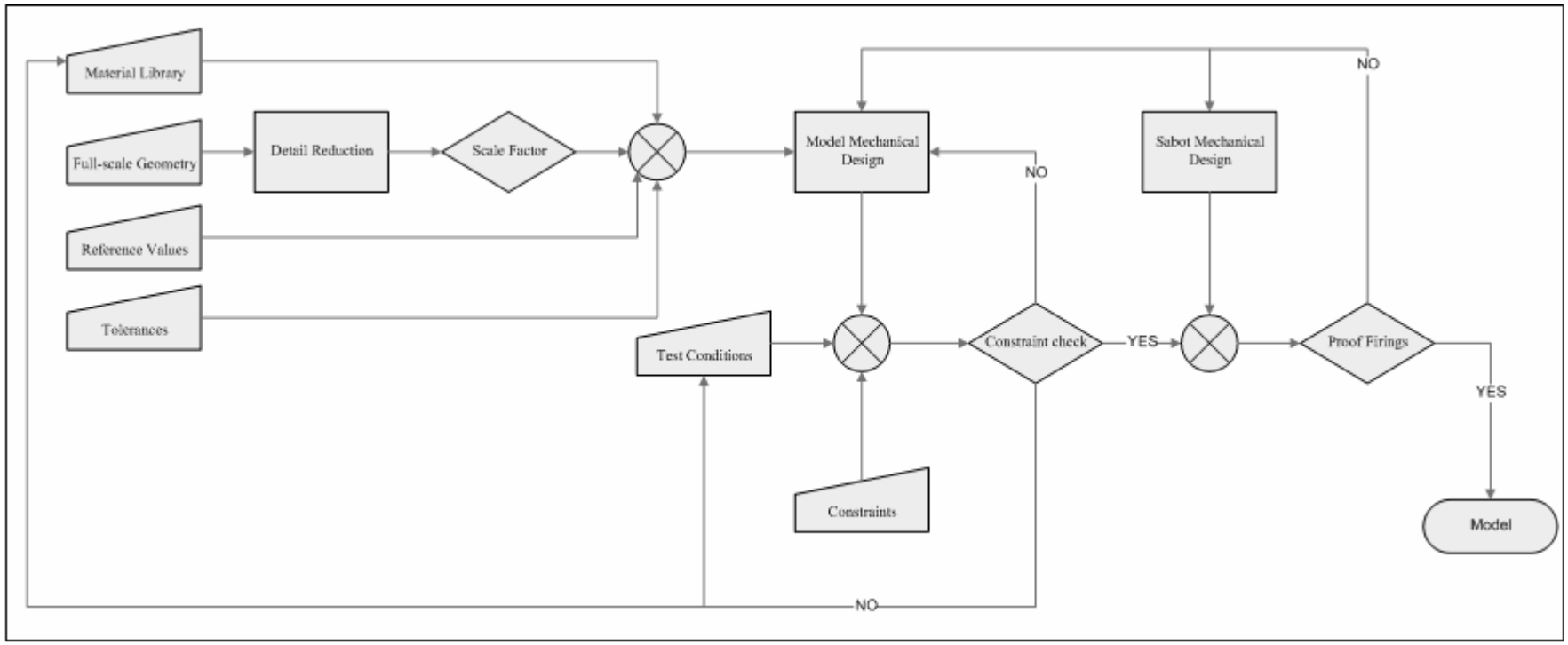

Figure 1.7 Flowchart for aeroballistic range model design

MathWorks Inc.'s Matlab® 6.5.1 is selected as the development platform for the code. There are basically two reasons behind this selection: first the advantages of Matlab® as a programming language when compared to the traditional languages like C and FORTRAN, and second the Optimization Toolbox, which is a collection of functions that are specifically developed for optimization problems. This approach eliminated the need to create the optimization functions from scratch but to use the existing and proven functions and embed them into the aeroballistic range models' optimization code.

1.2 SCOPE OF THE STUDY

The foundations of the work are primarily based on calculus and strength of materials. In Chapter 2, the detailed mathematical formulations for the geometrical calculations and the solid modeling methods are presented. Also a simple method for estimating the dynamic stress on the model during launch is formulated in detail. The derivation of the objective function for the general optimization problem of the design scaling of aeroballistic range models is also done in this chapter together with the constraints function.

In Chapter 3, a brief overview of the optimization techniques that are used commonly in the literature are presented. The methods are not investigated in detail, since the main concern of the study is to develop a design methodology to be used in actual design work and not to discuss the optimization methods.

The flowchart of the code is given and design methodology is explained in detail in Chapter 4. This chapter also includes the test cases selected to test, debug and verify the code. The first test case is a medium range unguided artillery rocket. The second test case is a Low Drag General Purpose (LDGP) Aircraft Bomb.

In Chapter 5, the evaluation of the study is done, concluding remarks are made and recommendations on the future work are presented.

CHAPTER 2

FORMULATION

2.1 AEROBALLISTIC RANGE MODEL DESIGN

The challenge in the design of an aeroballistic range model is to find the optimum model configuration which matches the location of the centre of gravity and the ratio of the axial inertia to the transverse inertia of the model. It is also important to minimize the model weight so that the required test velocities can be reached with smaller chamber pressures. This is important in material selection, since the smaller the pressure is the easier and cheaper to find a material that holds the launching stresses.

Obviously, above mentioned requirements define an optimization problem. There are three objectives in this optimization:

1. Match the centre of gravity location
2. Match the inertia ratio
3. Minimize the weight.

The first objective can be formulated as follows:

$$f_1 = \left[\frac{Cg_{model}}{Cg_{goal}} - 1 \right]^2 \tag{2.1}$$

where Cg_{model} denotes the location of the centre of gravity of the model. Cg_{goal} is the scaled location of the actual centre of gravity location and obtained by

multiplying the actual location of centre of gravity from the nose with scale factor (λ) as shown in Equation (2.2).

$$Cg_{goal} = Cg_{actual} \cdot \lambda \tag{2.2}$$

The second objective can be formulated as:

$$f_2 = \left[\frac{\left(I_x / I_y \right)_{model}}{\left(I_x / I_y \right)_{goal}} - 1 \right]^2 \tag{2.3}$$

where I_x is the axial inertia and I_y is the transverse inertia.

There are two coordinate frames used in the calculations. One of them is located at the centre of gravity of the munition and x axis is along the symmetry axis of the body and the other is located at the nose tip and the x axis is coincident with the first frame (Figure 2.1). The centre of gravity location is calculated with respect to frame 2 and moments of inertia are calculated with respect to frame 1.

The third objective can be formulated as:

$$f_3 = \frac{m_{model}}{1000} \tag{2.4}$$

where m_{model} denotes the weight of the model and it is normalized with a reference weight of 1000 grams (most aeroballistic range models tested at FML weights about 1kg) in order to have a dimensionless objective function

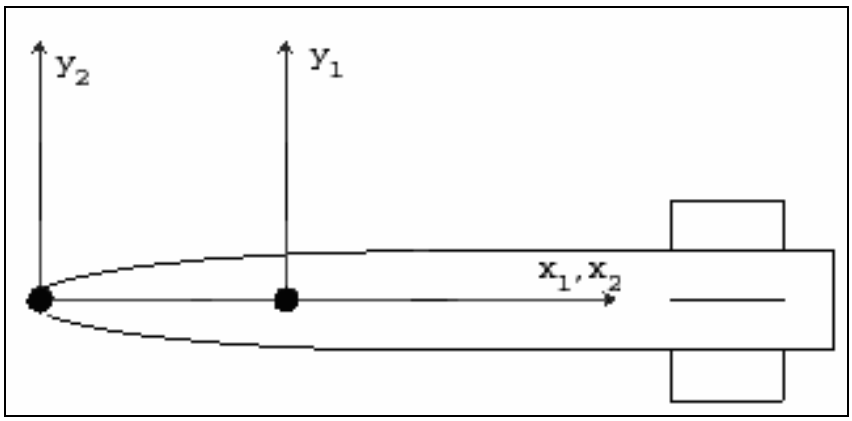

Figure 2.1 Coordinate frames used in calculations

Obviously, this multi-objective optimization problem can be redefined as a single objective optimization problem by the use of appropriate weights. Then the objective function becomes [2]:

$$f = \left[\frac{Cg_{model}}{Cg_{goal}} - 1\right]^2 \times w_1 + \left[\frac{\left(I_x / I_y\right)_{model}}{\left(I_x / I_y\right)_{goal}} - 1\right]^2 \times w_2 + \frac{m_{model}}{1000} \times w_3 \qquad (2.5)$$

In the flow of the design work (Figure 1.7) the problem is to minimize the differences in the cg location and the ratio of the inertias of the model with a fixed external geometry and the goal values while minimizing the weight. This is done in an iterative manner starting with an initial guess of the model configuration (i.e. initial material selection for the parts of the model as well as initial internal configuration) and trying to find an optimum value by changing the design parameters.

Most aeroballistic range models are manufactured with cylindrical holes drilled inside. This is due to the ease of manufacturability, since it is really easy to drill out a cylinder from the model to match the required parameters. Then, this

manufacturing approach can be applied directly to the optimization problem in hand:

"Find the optimum cylinder that has to be drilled out from the model"

First step is to define the cylinder: any cylinder can be defined with a length, radius and start/end point with respect to some axis. Then, the "optimum cylinder" can be defined with the following states (Figure 2.2):

- x_1: the length of the cylinder
- x_2: the radius of the cylinder
- x_3: the end point of the cylinder on x axis

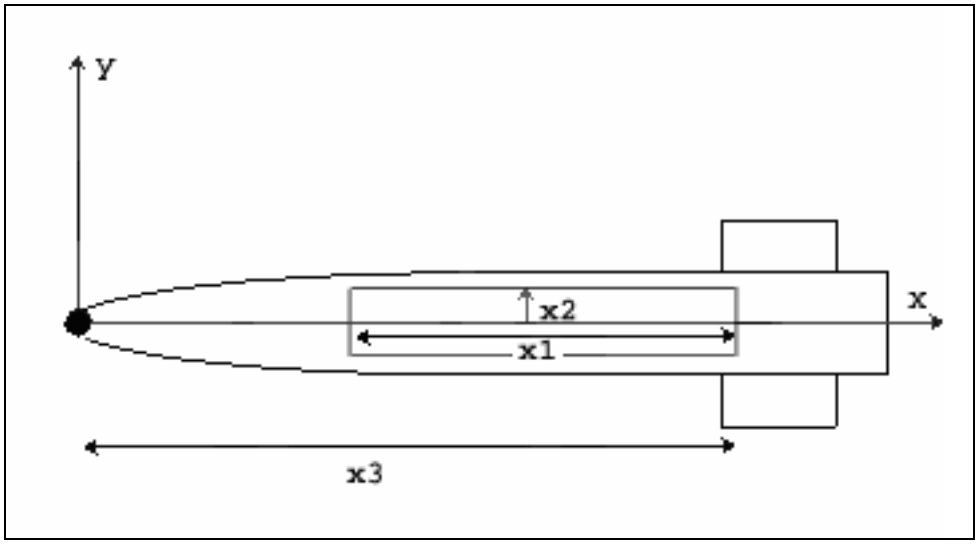

Figure 2.2 The definition of the optimum cylinder

So the objective function given in Equation (2.5) is in fact a function of x_1, x_2 and x_3 since all the mass properties of the model is now dependent on the parameters of the cylinder that is drilled out as well as the materials used in the model and the

external dimensions of the model (scale). Then, the difference between the centre of gravity location and inertia ratio of the model and the goal values is simply the mass properties of the cylinder provided that the external dimensions and materials selected are fixed.

Having defined the objective function, the next step in the optimization is to define the constraints. First of all there are lower and upper bounds for the states. These are simple geometrical facts and can be summarized as follows:

$$x_1 < x_3 \tag{2.6}$$

$$x_3 < x_f \tag{2.7}$$

$$x_2 < \min_{x1,x3}(O(x)) \tag{2.8}$$

$$0 < x_1 \tag{2.9}$$

$$0 < x_2 \tag{2.10}$$

$$0 < x_3 \tag{2.11}$$

where x_f is the length of the model and O(x) denotes the offset curve of the model external geometry, which is generated due to manufacturability considerations (i.e. the model should have a finite wall thickness).

Another constraint is related to the strength of the model. Since the model will be under axial compressive loads during launch [16], the value of the axial compressive stress at any cross-section of the model should not exceed the yield strength of the material at that section Equation (2.12).

$$\sigma_{compression} < \sigma_{yield} \tag{2.12}$$

Then the constraints can be shown in matrix notation as

$$\tilde{c} = \begin{bmatrix} x_1 - x_3 \\ x_3 - x_f \\ x_2 - \min_{x1,x3}(R(x)) \\ -x_1 \\ -x_2 \\ -x_3 \\ \sigma_{compression} - \sigma_{yield} \end{bmatrix} \tag{2.13}$$

$$\tilde{c} < 0 \tag{2.14}$$

2.2 AEROBALLISTIC RANGE MODEL GEOMETRIES

The geometries of the projectiles are usually axisymmetric or mirror symmetric, regardless of their type (i.e. air to ground/ground to ground, guided/unguided, etc.), but in this study only axisymmetric projectiles are considered. The typical projectile geometry has an aerodynamically shaped nose (cone or blunt), a cylindrical body and an afterbody (cylindrical, flare, boat tail). All of these geometries can be approximated by use of simple mathematical functions.

2.2.1 Nose Profile

The typical geometry of the nose section of a projectile has a special name: ogive[3]. There are mainly four types of ogives used in aeroballistics [17]:

- Tangent Ogive
- Von Karman Ogive
- ½ Power Parabolic Ogive

[3] "Ogive" is a French word meaning the arch or rib which crosses a Gothic vault diagonally. When used in ballistics, it refers to the front consisting of the conical head of a missile or rocket that protects the payload from heat during its passage through the atmosphere.

- Conical Ogive

However, simplest and mostly used one of the four is the tangent ogive. Tangent ogive is basically an arc, fit to the nose of the projectile with the following boundary conditions (Figure 2.3):

1. The arc passes through the nose start location (0, 0).
2. The arc passes through the nose end location (*nl*, *nr*)
3. Derivative of the arc equation with respect to x is zero at the nose end location.

General equation of a circle with centre at (*a*, *b*) and radius R is given in Equation (2.15).

$$(x-a)^2+(y-b)^2=R^2 \tag{2.15}$$

Above mentioned boundary conditions are applied and equations (2.16), (2.17) and (2.20) are obtained where *nl* denotes the nose length and nr denotes the nose radius at the nose end.

$$y=b+\sqrt{R^2-(x-a)^2} \tag{2.16}$$

$$a^2+b^2=R^2 \tag{2.17}$$

$$(nl-a)^2+(nr-b)^2=R^2 \tag{2.18}$$

$$\left.\frac{dy}{dx}\right|_{x=nl}=\frac{a-nl}{\sqrt{R^2-(nl-a)^2}} \tag{2.19}$$

Equation (2.19) implies that:

$$a = nl \tag{2.20}$$

That is, the x coordinate of the centre of the circle is nose length distance away from the origin of the Coordinate Frame 2 (Figure 2.1). Substituting Equation (2.20) into Equation (2.17) and Equation (2.18) y coordinate of the center of the arc is obtained as Equation (2.21). Then it can be easily shown that the radius of the arc is given by Equation (2.22). Furthermore the equation of the tangent ogive is given in Equation (2.23).

$$b = \frac{nr^2 - nl^2}{2 \cdot nr} \tag{2.21}$$

$$R = \left| \sqrt{nl^2 + \left(\frac{nr^2 - nl^2}{2 \cdot nr} \right)^2} \right| \tag{2.22}$$

$$y = \frac{nr^2 - nl^2}{2 \cdot nr} + \sqrt{nl^2 + \left(\frac{nr^2 - nl^2}{2 \cdot nr} \right)^2 - (x - nl)^2} \tag{2.23}$$

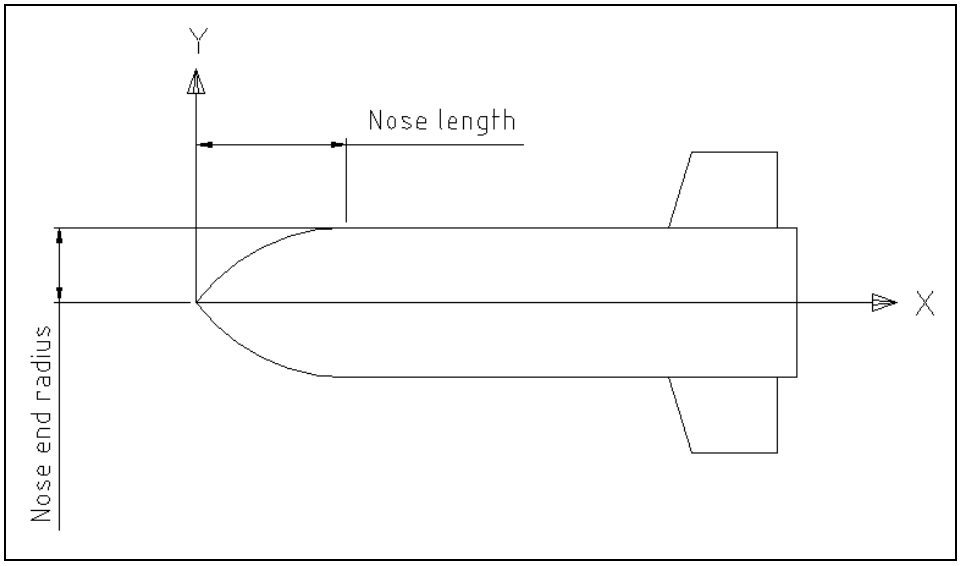

Figure 2.3 Tangent Ogive

2.2.2 Body Profile

The body of the projectile is usually a cylinder. However, there are some projectiles with expanding/contracting bodies (truncated cone). So it is best to model the body with a generic line equation as Equation (2.24) where b_{start} denotes the body start location, b_{end} denotes the body end location, br_{start} denotes the body radius at the start and br_{end} denotes the body radius at the end.

$$y = \left(\frac{br_{end} - br_{start}}{b_{end} - b_{start}} \right) \cdot x + \frac{br_{end} \cdot (b_{end} - b_{start}) + b_{end} \cdot (br_{end} - br_{start})}{b_{end} - b_{start}} \tag{2.24}$$

2.2.3 Tail Profile

The tail section of a projectile is usually a boat tail or a flare. The geometry equation for the tail section can be obtained in a similar manner to Equation (2.24), as,

$$y = \left(\frac{tr_{end} - tr_{start}}{t_{end} - t_{start}} \right) \cdot x + \frac{tr_{end} * (t_{end} - t_{start}) + t_{end} * (tr_{end} - tr_{start})}{t_{end} - t_{start}} \tag{2.25}$$

2.2.4 Fin Planform

The most general fin planform is formed by four simpler geometric parts (Figure 2.4). Then 6 parameters are needed to define this figure:

- Root chord (c)
- Maximum span (b)
- Leading edge sweep angle 1 ($\alpha 1$)
- Leading edge sweep angle 2 ($\alpha 2$)
- Trailing edge sweep angle ($\alpha 3$)

- Fin start location (fin_{start})

Using these 6 parameters, the formula of the fin can be derived as follows:

$$y = x \cdot \tan(\alpha 1) \tag{2.26}$$

$$z = \frac{b}{\tan(\alpha 3)} \tag{2.27}$$

$$\tan(\alpha 2) = \frac{b - y}{c - (x + z)} \tag{2.28}$$

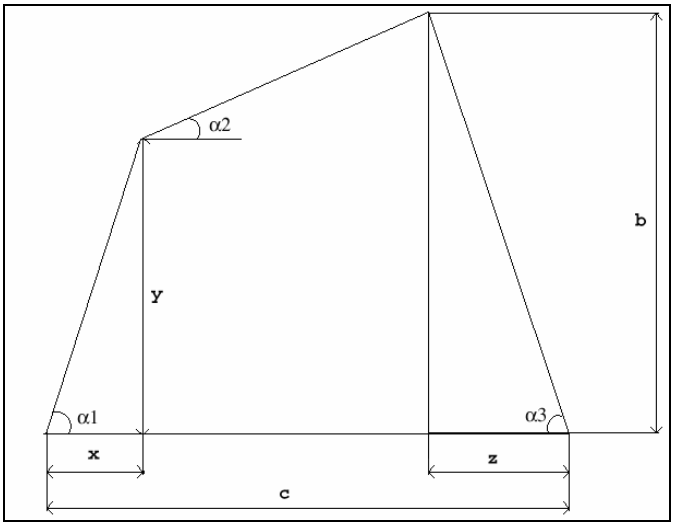

Figure 2.4 General fin planform

Substituting Equation (2.26) and Equation (2.27) into Equation (2.28) x is obtained in terms of known values as.

$$x = \frac{c \cdot \tan(\alpha 2) \cdot \tan(\alpha 3) - b \cdot [\tan(\alpha 3) + \tan(\alpha 2)]}{\tan(\alpha 2) \cdot \tan(\alpha 3) - \tan(\alpha 1) \cdot \tan(\alpha 3)} \tag{2.29}$$

Since all of the vertices are known, then the equations for the fin can be easily obtained in terms of body radius at the fin start ($fin_{startradius}$) and the above defined parameters as line equations.

2.3 ESTIMATING THE LAUNCH LOADS

One of the greatest challenges in aeroballistic range model design is the prediction of the models' strength under launch loads. The projectile (i.e. model and the sabot) is subjected to extreme accelerations during launch (in the order of 1000g's). Although there are a number of analytical and experimental methods derived to estimate whether the model will hold these stresses or fail, the design of model and sabot packages is largely a trial and error procedure based on experience, [18], [19].

The experimental approach is to statically test the sabot/model packages in a compression test machine and predict the failing load, [19],[20]. This approach gives acceptable predictions for most of the time, although there are cases in which the dynamic behavior of the sabot/model is different from the static behavior.

The analytical approach tries to estimate the launch loads and employs stress analysis under static loading making use of the elementary principles of strength of materials neglecting the dynamic effects [3],[18],[19]. Although this approach may seem as oversimplified, it has not been necessary to make it more complex, since a successful model/sabot design is usually obtained with a small number of proof firings and great deal of experience [3].

In this approach, first step is to calculate the acceleration during the model travel in the barrel of the gun, which would give the desired test velocity. Thus, once the length of the barrel (l_{barrel}) and the test velocity (V_{muzzle}) is known, the constant acceleration (a) is obtained from the basic acceleration formula as:

$$a = \frac{1}{2} \cdot \frac{V_{muzzle}^{\ 2}}{l_{barrel}} \tag{2.30}$$

A correction factor is multiplied to the constant acceleration of Equation (2.30) in order to get a better prediction of dynamic loads, since the peak acceleration will be higher than this constant value. The proper way to estimate the peak acceleration factor is based on the previous acceleration measurements in the gun with similar projectiles at similar muzzle velocities. It is stated in [3] that this value lies within the range 3-5.

This is also verified with the results presented in [21]. Figure 2.5 shows the acceleration versus time plot for the FML model of Reference [21], obtained as a by-product of a dynamic finite element analysis (FEA), which was carried out in order to predict whether the designed model could withstand the expected chamber and barrel pressures. FEA was carried out using MARC Mentat 2003 software. The velocity versus time plot for the same model is shown in Figure 2.6. It is seen that for a muzzle velocity of 504 m/s, maximum acceleration experienced by the model is 51200 m/s^2. For a barrel length of 5.5 meters, the constant acceleration value obtained by using Equation (2.30) is 23092 m/s^2. According to the range given in [3] the peak acceleration is between 69276 m/s^2 and 115460 m/s^2. So, the limits given in [3] are in fact conservative values and can be used in aeroballistic range model design if no other data are available.

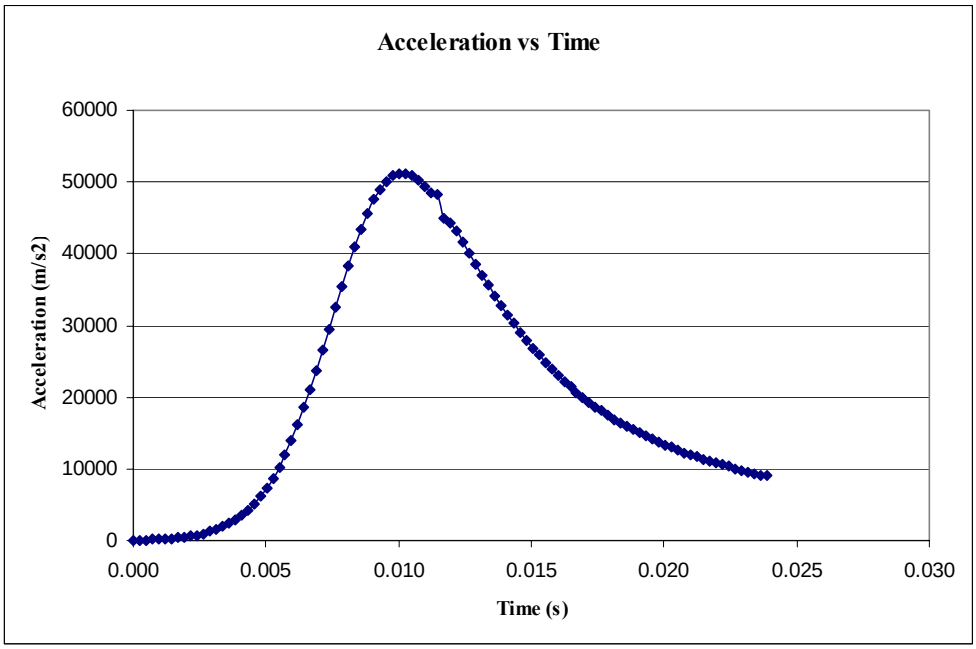

Figure 2.5 Acceleration versus time for a FML model (FEA Result)

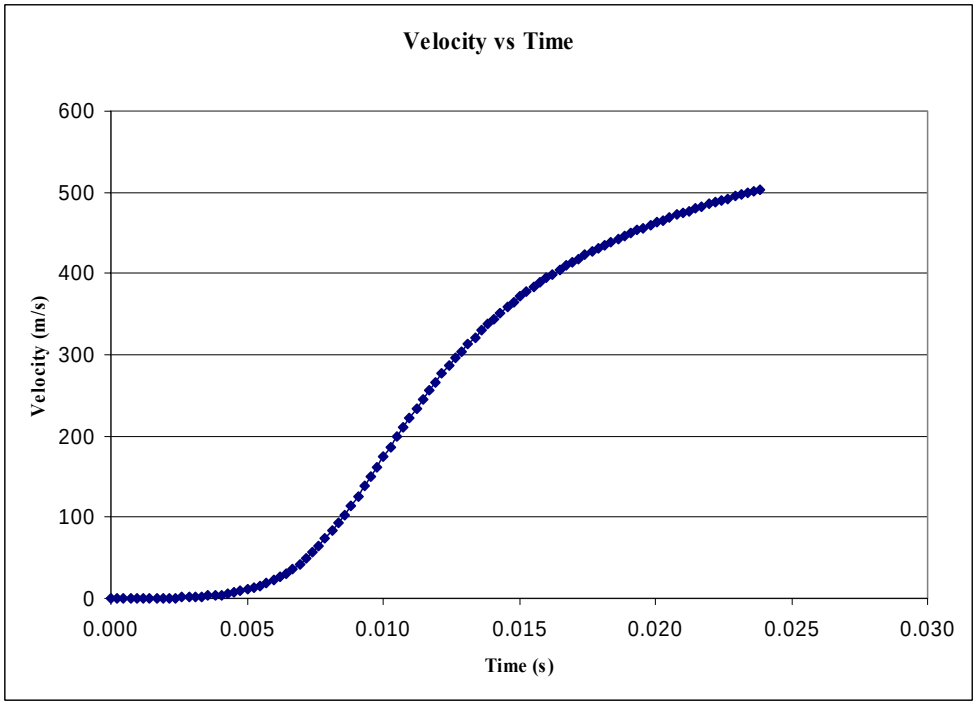

Figure 2.6 Velocity versus time for a FML model (FEA Result)

Then the maximum force acting on the base of the model during the launch is a axial compressive force caused by the acceleration of the mass ahead of it [19]. Thus, for any cross-section of the model, the axial compressive stress is defined as, [3], [16]:

$$\sigma_c = \frac{a_{peak} \cdot m'}{A_i} \tag{2.31}$$

where a_{peak} is the peak acceleration, m` is the total mass of all sections ahead of the particular section for which the axial compressive stress is calculated and A_i is the cross-sectional area. The model is assumed to withstand the launch loads unless the value of the axial compressive stress at any transverse section is greater that the yield strength of the material at that particular cross section.

Although the analytical approach gives acceptable approximations, it is better to carry out a finite element analysis of the projectile before the proof tests using commercial FEA tools, in order to validate the results foreseen by the static stress analysis approach [21].

CHAPTER 3

OPTIMIZATION TECHNIQUES

3.1 OPTIMIZATION THEORY

A system is defined as optimal, if it satisfies the performance criteria better than any other possible system while not violating the defined constraints [22].

The general optimization problem is defined as:

$$\begin{aligned} &\textit{Minimize} \quad f(\vec{x}) \\ &\textit{Subject to} \quad g_i(\vec{x}) \le 0 \quad \textit{for} \quad i = 1,...,m \\ &\qquad\qquad\quad g_i(\vec{x}) = 0 \quad \textit{for} \quad i = m+1,...,l \\ &\qquad\qquad\quad \vec{X}_{low} \le \vec{x} \le \vec{X}_{up} \end{aligned} \tag{3.1}$$

where x is a vector of length n design parameters, $f, g_1,...,g_2, h_1,...,h_l$ are design functions where the function *f* is called the *objective function,* the constraint $g_i(\vec{x}) \le 0 \quad for \quad i = 1,...,m$ is called an *inequality constraint,* and the constraint $g_i(\vec{x}) = 0 \quad for \quad i = m+1,...,l$ is called an *equality constraint*. The design parameter x is limited by upper and lower limits, which are often named as side constraints [23], [24], [25].

The problem given in Equation (3.1) can be stated as follows [24]:

"*Minimize the objective function f, subject to l equality constraints and m inequality constraints, with n design variables lying between the prescribed lower and upper limits*"

A vector x satisfying all the inequality and equality constraints is called a *feasible solution* to the problem. The collection of all these type of solutions forms the *feasible region.*

3.2 MULTI OBJECTIVE OPTIMIZATION

Most of the time, the real engineering problems are highly non-linear with more than one objective to minimize. So, the objective function is usually a vector of objectives, which must be traded off in some way to reach an optimal. This leads to the concept of noninferiority [25]:

"*A noninferior solution is the one in which an improvement in one of the objective requires a degradation of another*".

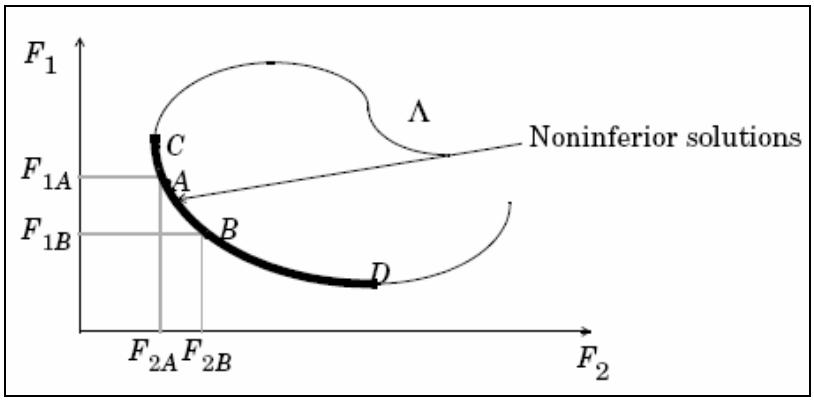

Figure 3.1 Set of non-inferior solutions

Consider the feasible region of Λ in Figure 3.1. The points denoted by A and B represent two specific non-inferior solution points, since an improvement in one objective F_1, requires a degradation in the other objective F_2, i.e.:

$$F_{1B} < F_{1A}, F_{2B} > F_{2A} \tag{3.2}$$

It is clear that, for any point defined in Λ, if an improvement can be obtained in the objectives then that point is not a noninferior point, thus is of no use to the solution of the optimization problem.

Multi objective optimization concerns the generation and selection of noninferior points. Although there are a number of methods for multi objective optimization, the one used in this study is the weighted sum strategy.

The weighted sum strategy converts the multi objective optimization problem to a single objective scalar problem by constructing a weighted sum of all of the objectives (3.3) [25].

$$\min_{x \in \Lambda} f(x) = \sum_{i=1}^{m} w_i \cdot F_i(x)^2 \tag{3.3}$$

The weighting coefficients do not necessarily indicate the relative importance of the objectives or allow trade offs between the objectives to be expressed.

3.3 UNCONSTRAINED OPTIMIZATION

There are many methods used for unconstrained optimization, which are classified according to the derivative information that they are (not) using. Some methods only use function evaluations, while others employ the gradient information to reach the optimal solution.

Gradient methods are more efficient when the function to be minimized is continuous in its first derivative, where higher order methods like Newton's method are only feasible when the second order information is readily known or easily calculated. The methods that only use function evaluations, such as pattern search method, are most suitable for problems that are very nonlinear or have a number of discontinuities.

Proceeding two sections give brief information about the most common method that is used for unconstrained minimization, Quasi-Newton Method and line search algorithm. Detailed information and the implementation steps are available in references [24], [25].

3.3.1 Quasi-Newton Methods

The most popular methods that use the gradient information are Quasi–Newton methods. These methods calculate curvature information at each iteration step and formulate a quadratic problem of the form:

$$\min_x \frac{1}{2} x^T H x + c^T x + b \tag{3.4}$$

where H is a positive definite symmetric matrix (the Hessian matrix), c is a constant vector and b is a constant. The optimal solution is obtained when:

$$\nabla f(x^*) = Hx^* + c = 0 \tag{3.5}$$

where the optimal solution point x* is:

$$x^* = -H^{-1}c \tag{3.6}$$

The mostly used method to calculate and update the Hessian matrix at each iteration step is the Broyden – Fletcher – Goldfarb – Shanno (BFGS) method.

BFGS has an advantage of quadratic convergence and also robustness by carrying forward information from previous iterations [24]. The BFGS method is formulated as:

$$H_{k+1} = H_k + \frac{q_k q_k^T}{q_k^T s_k} - \frac{H_k^T s_k^T s_k H_k}{s_k^T H_k s_k} \tag{3.7}$$

where

$$s_k = x_{k+1} - x_k \tag{3.8}$$

$$q_k = \nabla f(x_{k+1}) - \nabla f(x_k) \tag{3.9}$$

The gradient information can be obtained analytically or numerically by using finite differences. Thus, at each iteration step, the design variables are perturbed in order to calculate the rate of change of the objective function.

At each major iteration step (k), a line search is performed in the direction of:

$$d_k = -H_k^{-1} \nabla f(x_k) \tag{3.10}$$

3.3.2 Line Search

Line search is a search method that is used as part of a larger optimization algorithm. At each iteration step of the main algorithm, the line-search method searches along the line containing the current point, x_k, parallel to the search direction as given in Equation (3.10). Then the next iterate is of the form:

$$x_{k+1} = x_k + \alpha^* \cdot d_k \tag{3.11}$$

where x_k denotes the current iterate, d_k is the search direction, and α^* is a scalar step size.

The line search method attempts to decrease the objective function along the line by minimizing polynomial interpolation models of the objective function. The line search procedure has two main steps [25]:

- Bracketing the points to be searched on the line. This step is used to decide on the step length, α.
- Sectioning the bracket to subintervals, where the minimum of the objective function is approximated by using polynomial interpolation (cubic or quadratic).

The resulting step length α satisfies the Wolfe conditions [25]:

$$f(x_k + \alpha \cdot d_k) \leq f(x_k) + c_1 \cdot \alpha \cdot \nabla f(x_k)^T \cdot d_k \tag{3.12}$$

$$\nabla f(x_k + \alpha \cdot d_k)^T d_k \geq c_2 \cdot \alpha \cdot \nabla f(x_k)^T \cdot d_k \tag{3.13}$$

where c_1 and c_2 are constants with $0 < c_1 < c_2 < 1$.

The first condition Equation (3.12) requires that α sufficiently decreases the objective function. The second condition Equation (3.13) ensures that the step length is not too small.

3.4 CONSTRAINED OPTIMIZATION

The common approach to constrained optimization problems is to transform the problem into a simpler subproblem, which can be solved iteratively. Although early optimization methods employed a translation of the constrained minimization problem to an unconstrained minimization problem through application of a

penalty function, modern methods are focused on the solution of Kuhn-Tucker (KT) equations.

The KT equations are necessary conditions for optimality for a constrained optimization problem. If the problem is a convex problem, that is, *f(x)* and $g_i(\vec{x}),\ \ i = 1,...,m$, are convex functions, then the KT equations are both necessary and sufficient for a global solution point.

In addition to the constraints of Equation (3.1), the Kuhn-Tucker equations can be stated as:

$$\begin{aligned} \nabla f(x^*) + \sum_{i=1}^{m} \lambda_i^* \cdot \nabla g_i(x^*) = 0 \\ \lambda_i^* \cdot g_i(x^*) = 0 \qquad i = 1,....,m \\ \lambda_i^* \geq 0 \qquad i = m+1,....,l \end{aligned} \tag{3.14}$$

The first equation describes a canceling of the gradients between the objective function and the active constraints at the solution point. For the gradients to be canceled, Lagrange multipliers ($\lambda i, i=1,...,m$) are necessary to balance the deviations in magnitude of the objective function and constraint gradients. Because only active constraints are included in this canceling operation, Lagrange multipliers of the non-active constraints are set to zero. This is stated implicitly in the last two equations of Equation set (3.14).

The solution of the KT equations forms the basis to many nonlinear programming algorithms such as constrained quasi-Newton methods. These methods are commonly referred to as Sequential Quadratic Programming (SQP) methods, since a Quadratic Programming (QP) subproblem is solved at each major iteration step (also known as Iterative Quadratic Programming, Recursive Quadratic Programming, and Constrained Variable Metric methods).

Next two sections give brief information about the SQP. Detailed information about this method and the implementation steps are available in references [24], [25].

3.4.1 Sequential Quadratic Programming (SQP)

SQP allows the use of Newton's method for constrained optimization as done for unconstrained optimization.

At each major iteration step, the Hessian matrix is approximated using the Lagrange multiplier through an application of quasi-Newton method. This is then used to generate a QP subproblem, whose solution is used to form a search direction for line searching procedure.

3.4.2 Quadratic Programming (QP) Subproblem

The bounds of the design variables of Equation (3.1) are expressed as inequality constraints and a quadratic approximation for the Lagrangian function is obtained as:

$$L(x,\lambda) = f(x) + \sum_{i=1}^{m} \lambda_i \cdot g_i(x) \tag{3.15}$$

Then the QP subproblem is defined as [25]:

$$\begin{aligned} &\min_{d \in R^n} \frac{1}{2} d^T H_k d + \nabla f(x_k)^T d \\ &\nabla g_i(x_k)^T d + g_i(x_k) = 0 \qquad i = 1,...,m \\ &\nabla g_i(x_k)^T d + g_i(x_k) \le 0 \qquad i = m+1,...,l \end{aligned} \tag{3.16}$$

The solution of this subproblem is used to form a new iterate

$$x_{k+1} = x_k + \alpha_k \cdot d_k \tag{3.17}$$

where the step size α_k is determined by line search procedure. The H_k matrix is the positive definite approximation of the Hessian matrix of the Lagrangian function Equation (3.15). The most common method used to update the H_k is BFGS method.

3.5 GLOBAL OPTIMIZATION

The optimization methods described in the previous section are called "classical" methods and they have a common drawback: global optimization is not guaranteed. Thus, depending on the initial guess, the algorithm may or may not converge to a solution, and even if it converges to a solution this solution point may only be a local extremum of the objective function.

To deal with this problem, non-classical methods have been derived such as simulated annealing and genetic algorithms. The names are not coincidental since the basic ideas behind these algorithms are derived from processes of nature.

Simulated annealing is analogous to a metallurgical process in which metals are cooled to obtain different crystalline structures based on minimum potential energy. Genetic algorithm is based on the natural selection phenomena seen in nature, leading to better and stronger generations.

The classical methods tend to move towards the local extremum closest to the starting point and they can not identify if this point is a local or global extremum. However, global optimization techniques are primarily searching algorithms, which sweep the entire solution domain to find the best possible solution, i.e. the global optimum solution. In simulated annealing a search direction is generated randomly and the minimum of the objective function is sought. Sometimes, an increase in the function value is permitted in the search direction to escape from a potential sticking to a local minimum. In genetic algorithms, a population of solutions is generated and is evolved towards a global optimum solution.

The main disadvantage of the global optimization techniques is that, they require huge amount of iterations and take very long to find the solution. Detailed information about the global optimization techniques can be found in references [22] and [24].

3.6 OPTIMIZATION USING MATLAB®

The world wide known and respected commercial engineering package Matlab® has a collection of special functions that are used for optimization of a wide range of real world problems. This collection of functions is named as the Optimization Toolbox. The types of problems that can be solved using the toolbox are given in Optimization Toolbox User's Guide as:

- Unconstrained nonlinear minimization
- Constrained nonlinear minimization including goal attainment problems, minimax problems and semi-infinite optimization problems.
- Quadratic and linear programming
- Non-linear least squares curve fitting
- Non-linear system of equation solving
- Constrained linear least squares
- Sparse and structured large-scale problems.

The specific Matlab® Optimization Toolbox function that is used for this study is `fmincon`, which is developed for the finding a minimum to constrained nonlinear multi variable functions starting with an initial estimate. `fmincon` uses a SQP method, in which an estimate of the Hessian of the Lagrangian is updated at each iteration step using BFGS formula for the solution of the QP subproblem. Although `fmincon` is a very useful tool, like the rest of the Optimization Toolbox, it has some limitations and setbacks. The biggest of these is the local minimization which is a common problem for all the classical methods. This brings the code sensitivity to the initial conditions. One workaround proposed by MathWorks, is to run the `fmincon` with a number of different initial conditions and use the best result of

these runs as the optimal solution, provided that the function to be minimized is continuous and real valued as well as the constraints [26].

CHAPTER 4

DESIGN METHODOLOGY AND TEST CASES

4.1 THE OPTIMIZATION CODE – FMLCAD

The theoretical background of the study is established in Chapter 2 and Chapter 3. As explained in Chapter 1, the aim of the study is to develop a methodology which will be the basis of a code that will be used in the design optimization of the FML models.

The development platform is selected to be Matlab®. Although Matlab® is very powerful when it comes to calculations, the graphical user interface supporting capabilities are limited. Nevertheless, a GUI is designed using the GUIDE tool of Matlab® for easy data input to the code (Figure 4.1). The caller function for the GUI is named as FMLCAD – Flight Mechanics Laboratory Computer Aided Design Tool.

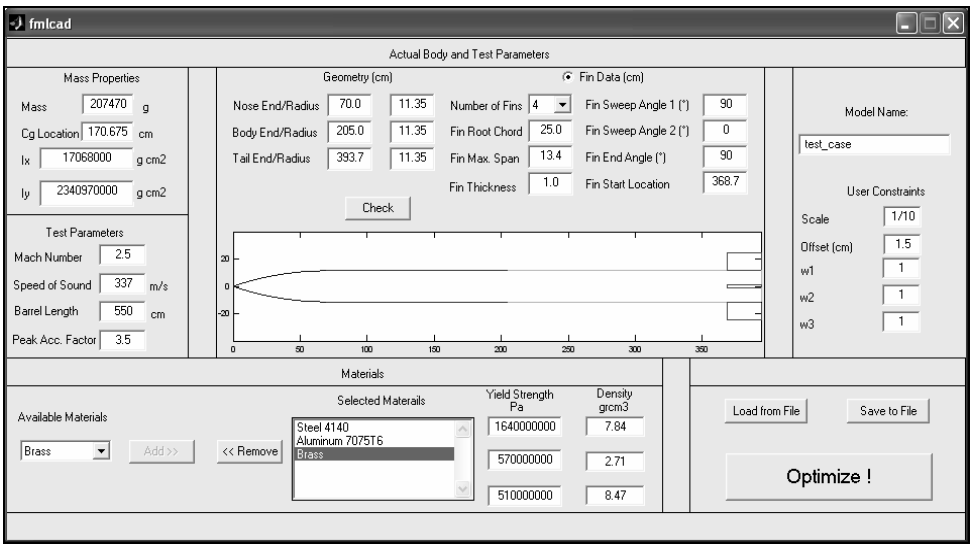

Figure 4.1 User Interface of the FMLCAD

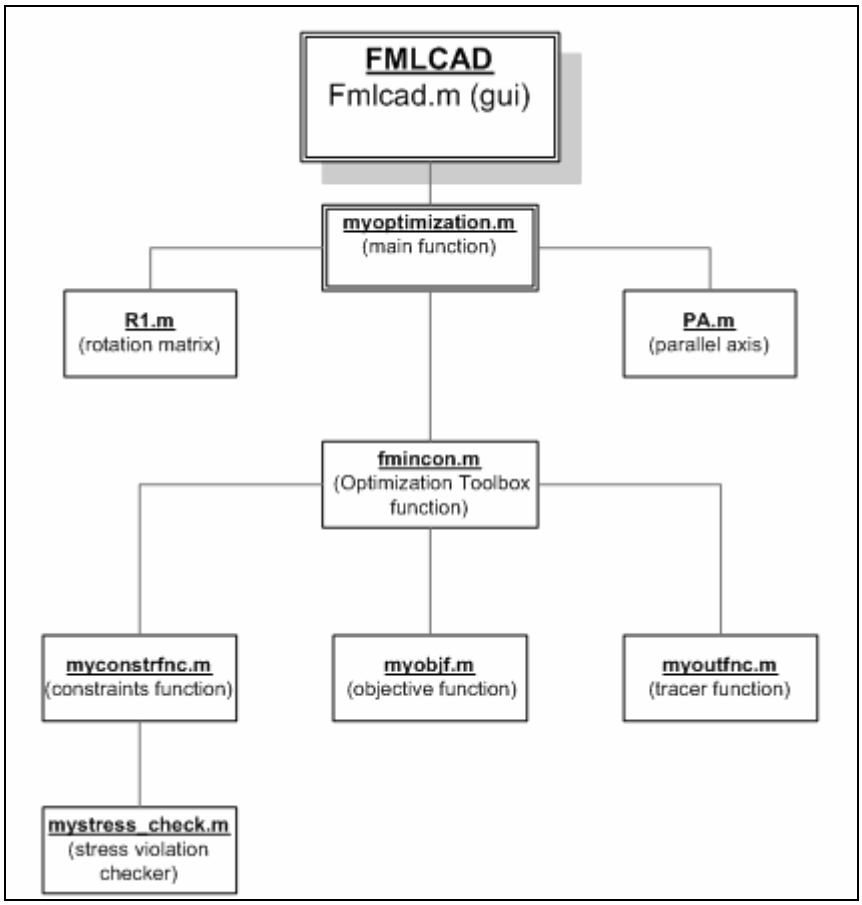

Figure 4.2 FMLCAD hierarchy

FMLCAD is made up of nine functions. The hierarchy of these functions is given in Figure 4.2. All the input entered by the user using the GUI is passed to the main function, myoptimization.m. This function calls all the subfunctions and displays the optimal results at the end. Optimization is carried out by the `fmincon` function of the Optimization Toolbox.

Total length of the functions, excluding `fmincon` and other Optimization Toolbox functions which are called by `fmincon` during optimization, is 3586 lines including the comments. GUI function fmlcad.m is the longest of all with 1768 lines and parallel axis transformation function PA.m is the shortest with 3 lines. Flow chart of FMLCAD is presented in Figure 4.3.

FMLCAD requires the actual munitions' properties together with the test conditions as input from the user and tries to find an optimum design configuration for the FML model. The "optimum configuration" defines the materials set used for the model and the internal configuration (i.e. the parameters of the optimum cylinder described in Chapter 2).

All of the inputs of FMLCAD are listed as:

- Actual munitions' mass properties
    - Weight (grams)
    - Location of the centre of gravity (from the nose - cm)
    - Axial inertia (gr cm^2)
    - Transverse inertia (gr cm^2)
- Actual munitions' geometry
    - Distance of the end of the nose section from the munitions' nose (cm)
    - Radius of the munition at the end of the nose section (cm)
    - Distance of the end of the body section from the munitions' nose (cm)
    - Radius of the munition at the end of the body section (cm)

    - Total length of the munition (cm)
    - Radius of the munition at the base (cm)
- Test and facility parameters:
    - Mach number
    - Speed of sound at the facility (m/s)
    - Length of the barrel (cm)
    - Peak acceleration factor
- Material selection:
    - Up to three different materials
    - Yield strengths (Pa)
    - Densities (gr/cm^3)
- Other inputs that must be provided by the user:
    - Scale factor
    - Weighting factors for the objectives
    - Offset distance (cm)

Once started, the target values are calculated using the actual munition parameters and scale factor. Actual geometry is scaled down using scale factor and geometry matrices are filled for equally distributed 500 axial stations along the model longitudinal axis (x axis). Then, geometrical constraints are generated using this geometry information and offset value input by user.

Next step is to generate the initial conditions set, which defines the starting points for the optimization routine. The formal approach should be to define the minimum and maximum values of the states and generate the initial condition set depending on these values. Thus, for three design variables (x_1, x_2, x_3) there are 27 different initial guesses containing all possible combinations of the minimum, maximum and mean values of the design variables. However, this approach, although very simple and straightforward, can not be applied since for most of the combinations; the initial guess of the design variables violates the geometrical constraints defined in Chapter 2. It is preferred to start the optimization routine with an initial condition set that does not violate the constraints. So, an alternative approach is developed

for the generation of the initial conditions. In this approach, the allowable domain (i.e. the domain defined by the geometrical constraints) for the design variables are swept using a generic formula derived by trial and error method. 8 different initial guess sets are defined, which span the model domain according to the following formula:

$$X_{1_k}{}^0 = \begin{cases} AS(fno) + \dfrac{ns}{7} \times (k-1) \times ds + 5 \times ds & , \ k \le 4 \\ X_{3_{k-4}}{}^0 - X_{1_{k-4}}{}^0 & , \ k > 4 \end{cases}$$

$$X_{2_k}{}^0 = \min\left[Offset(X_{3_k}{}^0 - X_{1_k}{}^0), Offset(X_{3_k}{}^0)\right] - Offset(fno)/2 \qquad (4.1)$$

$$X_{3_k}{}^0 = \begin{cases} x_f - 5 \times ds - \dfrac{ns}{7} \times (k-1) \times ds & , \ k \le 4 \\ X_{3_{k-4}}{}^0 & , \ k > 4 \end{cases}$$

where AS: the matrix that keeps the positions of the axial stations from the nose,
ns: number of stations (500),
ds: the distance between axial stations,
Offset: the matrix that keeps the offset information of the external curve.
fno: (stands for first non-zero offset) denotes the first axial location for which the offset curve has a positive value.

4 additional initial conditions are defined by taking the mirror images of the first 4 with respect to the model half length and modifying the x2 guess in Equation (4.1) if necessary. So a total number of 12 initial conditions are swept for each external geometry configuration. The initial guess matrix is plotted for the geometries of the test cases respectively in Figure 4.4 and Figure 4.5.

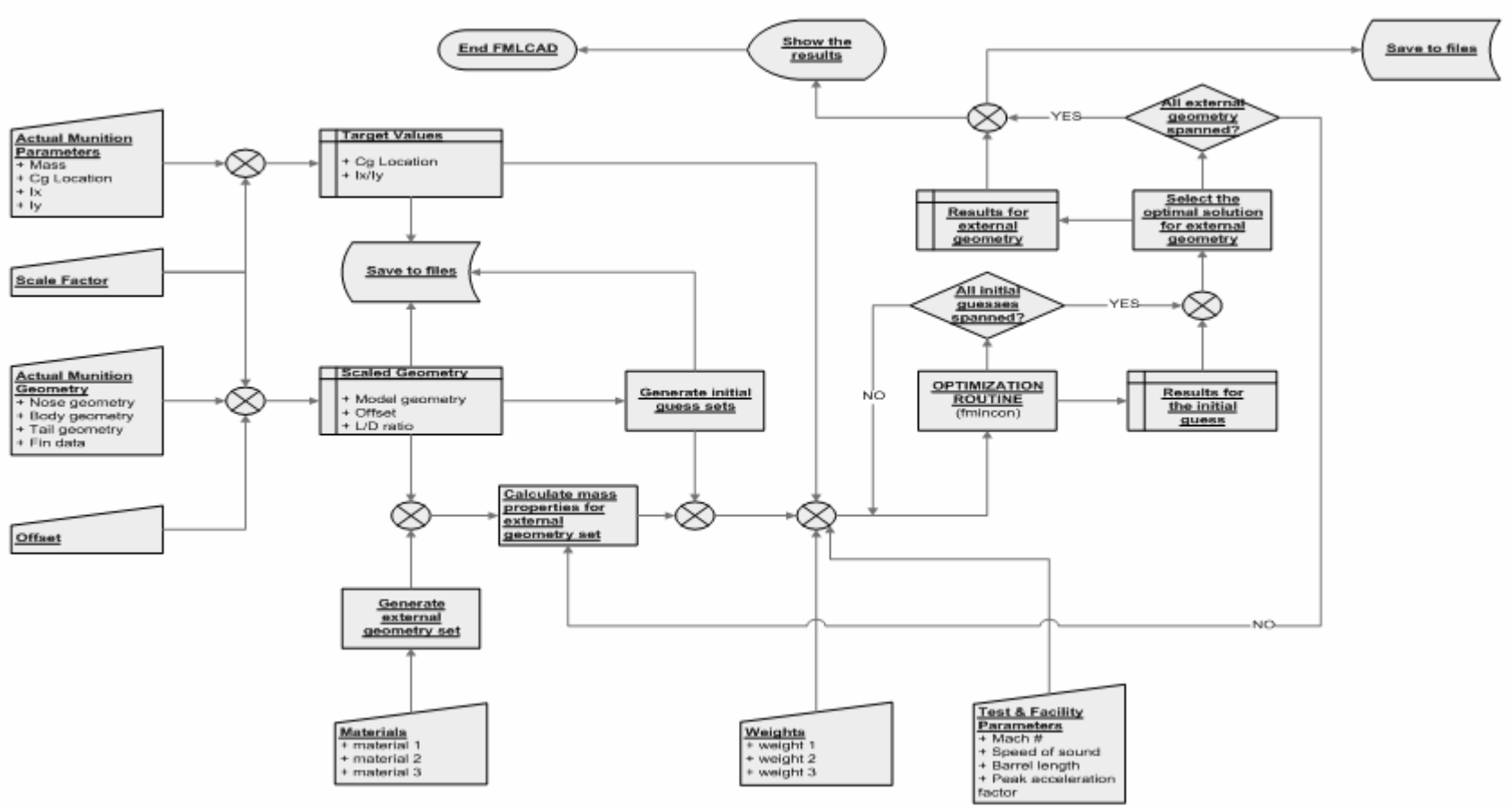

Figure 4.3 FMLCAD Flow chart

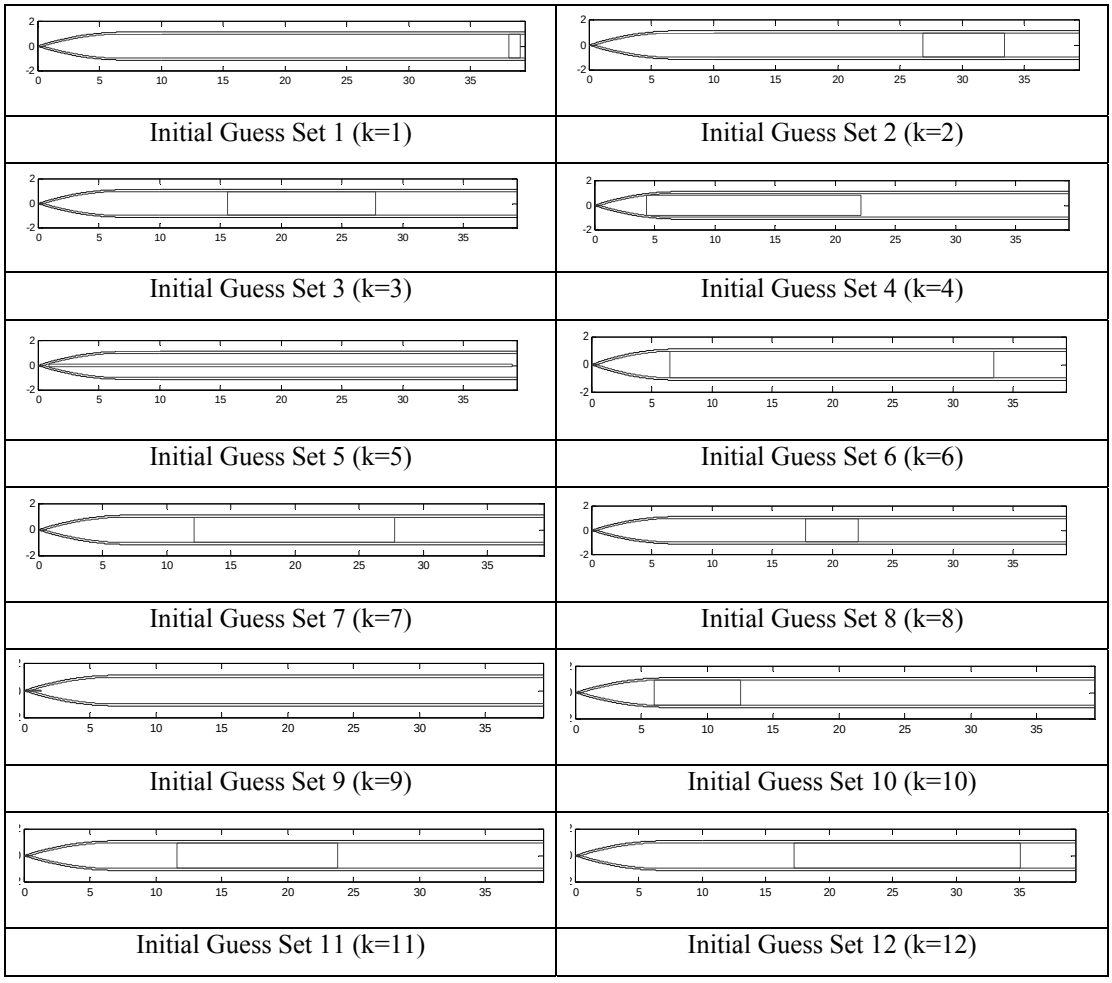

Figure 4.4 Initial guess sets for the geometry of test case 1

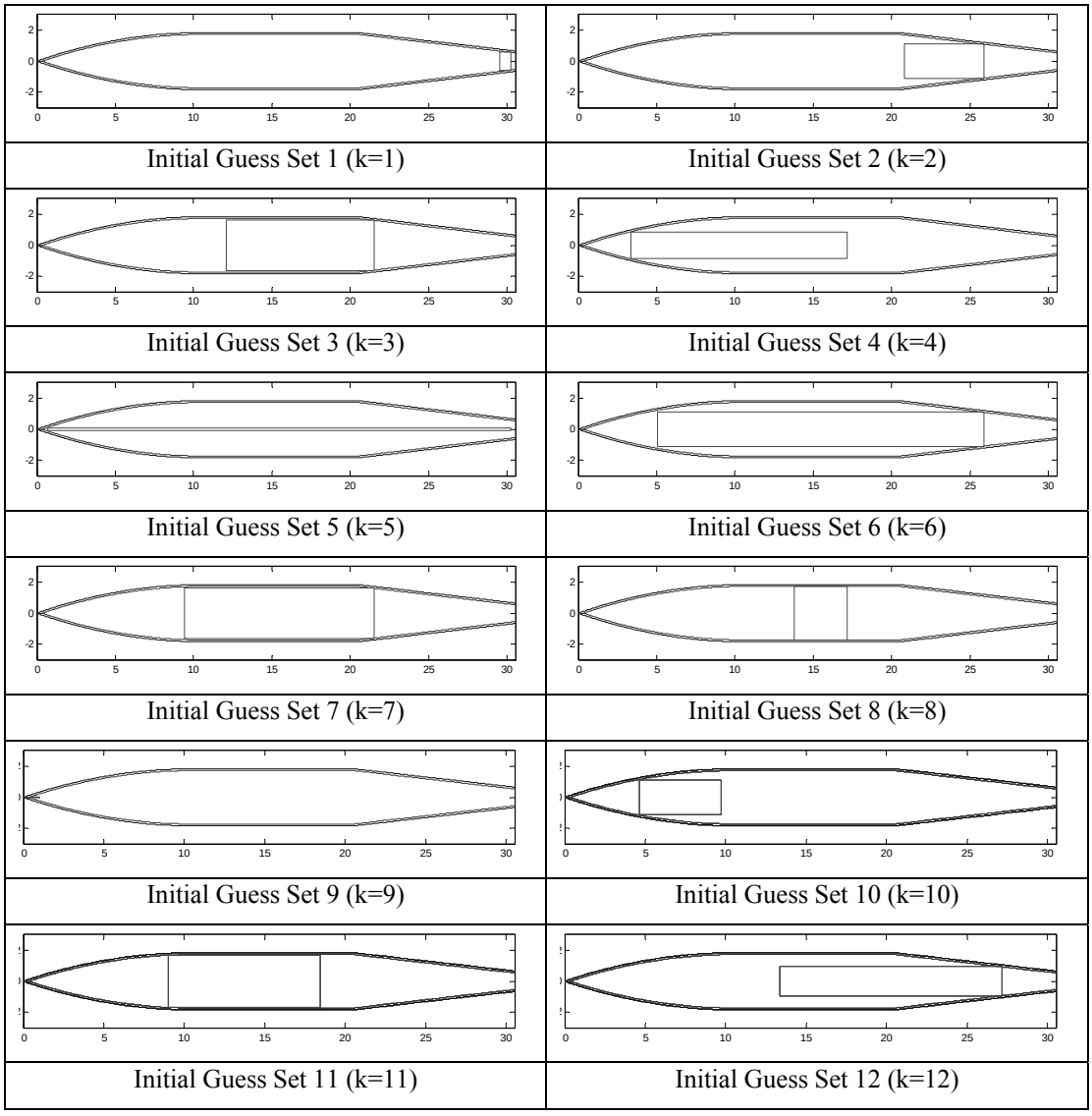

Figure 4.5 Initial guess sets for the geometry of test case 2

Up to 27 different external configurations may be defined depending on the number of different materials selected. For each external configuration case the optimization routine is called for each initial condition and the optimum solution for that case is selected among the results of these runs depending on the weights input by the user. For this purpose a Figure of Merit (FOM) is defined as:

$$FOM = ErrCg \times w_1 + ErrI \times w_2 + \frac{m_{model}}{1000} \times w_3 \tag{4.2}$$

where ErrCg is the error in centre of gravity location, ErrI is the error in inertia ratio, m_{model} is the final weight of the model and w_i is the weighting factors input by user.

Then for each case the following are output:

- Materials for the nose, body and tail sections
- Length of the optimal cylinder
- Radius of the optimal cylinder
- End point of the optimal cylinder from the nose of the model
- Mass of the model
- Centre of gravity location for the model from the nose
- Ratio of the axial inertia to the transverse inertia of the model
- Percent error in centre of gravity location
- Percent error in inertia ratio
- Figure of merit (FOM)
- Exit flag for the case

The optimum solution for the FML model is the one with an exit flag equal to 1 and minimum FOM value (different than zero), where exit flag is an identifier, which can take the values 1, 0 or -1, depending on whether the optimization routine converged to a solution, exceeded the allowed number of iterations or did not converge. The results are saved to files and also to Matlab® workspace.

4.2 TEST CASE – 1: MEDIUM – RANGE UNGUIDED ARTILLERY ROCKET

The first case selected to test the FMLCAD is a medium range unguided artillery rocket.

Table 4-1 shows the mass properties of the medium range unguided artillery rocket selected as the test case – 1. The external geometry of the rocket is given in Table 4-2, Table 4-3 and shown in Figure 4.6.

Scale factor for this rocket is selected to be 0.1 based on the similar models that were tested at FML. This scale factor gives a maximum diameter of 49.5 mm at the fin tips. Maximum Mach number at which the tests will be performed is selected as 2.5. However, to investigate the effect of test velocity on the model design, FMLCAD is run twice using Mach 1.5 and Mach 2.5 as test velocities. Also two sets of weighting factors are used for each Mach number (Table 4-4).

The most common materials used in manufacturing of aeroballistic range models and their properties are given in Table 4-5 [3], [30], [27]. For test case-1 the selected materials are Steel 4140, Aluminum 7075 T6 and Soft Yellow Brass.

Table 4-1 Mass properties for test case - 1

Mass (kg)	207.47
Centre of gravity location (cm – from nose)	170.675
Axial inertia (kg m^2)	1.7068
Transverse inertia (kg m^2)	234.097

Table 4-2 Geometry properties for test case - 1

Section	End location (cm –from nose)	End radius (cm)
Nose	70.0	11.35
Body	205.0	11.35
Tail	393.7	11.35

Table 4-3 Fin data

Number of fins	4
Starting coordinates from the nose (cm)	(368.70,11.35)
Root chord (cm)	25.0
Maximum span length (cm)	13.40
Reference thickness (cm)	1.0
Leading edge sweep angle 1 (°)	90
Leading edge sweep angle 2 (°)	0
Trailing edge sweep angle (°)	90

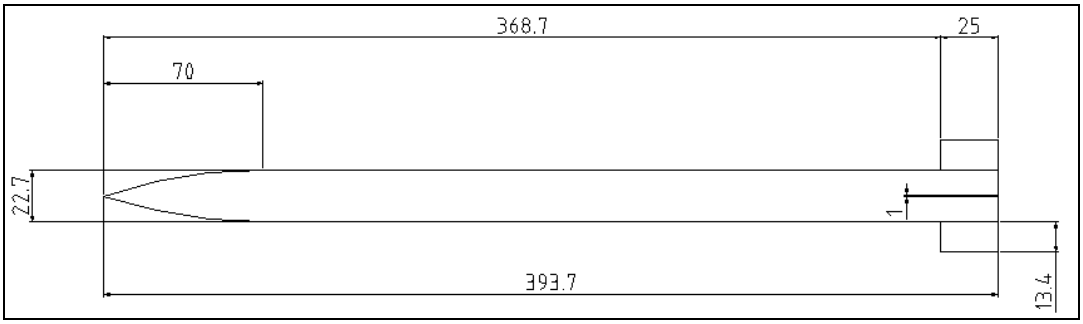

Figure 4.6 External geometry for test case – 1

Table 4-4 Weighting factors for test case - 1

Weighting factor set 1:	[0.3333, 0.3333 , 0.3333]
Weighting factor set 2:	[0.4 ,0.4 , 0.2]

Table 4-5 Common materials for aeroballistic range models

Material	Density (gr/cm^3)	Yield Strength (MPa)
Steel 1040	7.84	593
Steel 4140	7.84	1640
Aluminum 2024T4	2.71	470
Aluminum 7075T6	2.71	570
Soft Yellow Brass	8.47	510
Titanium	4.73	900
Polycarbonate	1.2	850

4.2.1 Results for Mach 1.5

4.2.1.1 Weighting Factor Set 1:

The optimum solution found by FMLCAD for this case is obtained with a brass nose section, steel body section and aluminum tail section. The results are presented in Table 4-6. Details of the results are given in Appendix B as tables. Optimization history for the states, objective function, constraint violation and the gradients of the objective function are given in following figures.

It is seen from the results of Table 4-6 that the optimum solution found by the code is quite satisfactory with a mass of 680 grams and error in center of gravity location of 0.03 %. Error in inertia ratio (2.5%) is also satisfactory, although it is a little high when compared to the error in center of gravity location.

Table 4-6 Details of the optimum solution

Initial Conditions	
Initial x1:	4.36445
Initial x2:	0.98426
Initial x3:	22.10344
Optimization Results	
x1:	37.2172
x2:	0.38686
x3:	39.21252
Objective Function Value:	0.23105
Exit Flag:	1
Number of Iterations:	12
Final Step Size:	1
Optimization Algorithm:	medium-scale: SQP, Quasi-Newton, line-search
Gradient of Objective Function wrt x1:	0.0087
Gradient of Objective Function wrt x2:	0.05163
Gradient of Objective Function wrt x3:	-0.16855
Final Mass (gr):	680.07931
Final Cg Location (cm):	17.07284
Final Ix (grcm2):	501.01643
Final Iy (grcm2):	67018.29672
Final Inertia Ratio:	0.00748
Error in Cg Location (%):	0.0313
Error in Ix/Iy Ratio (%):	2.53492
Figure of Merit:	1.0821

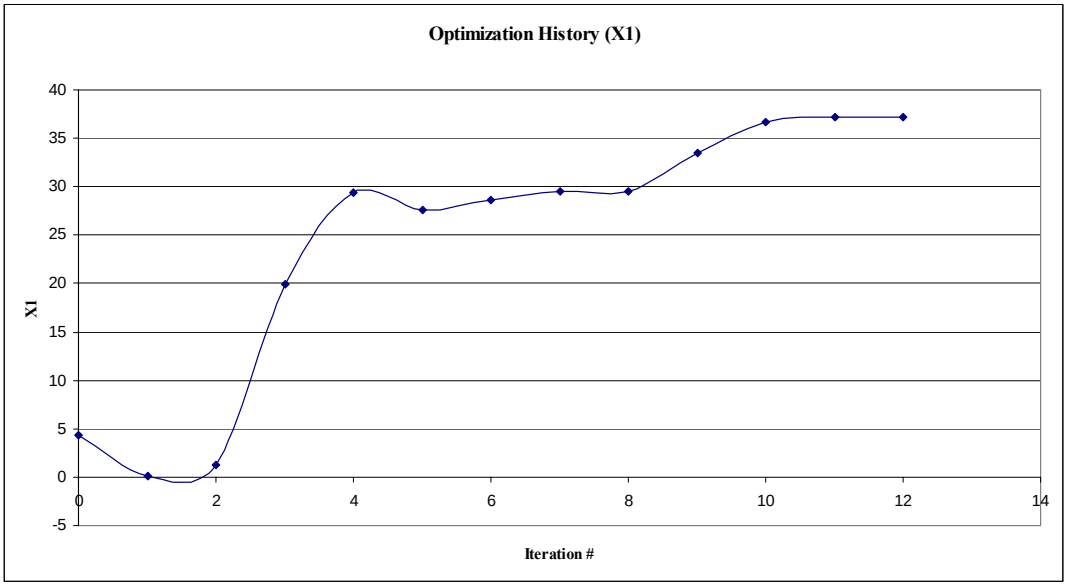

Figure 4.7 Optimization history for x1

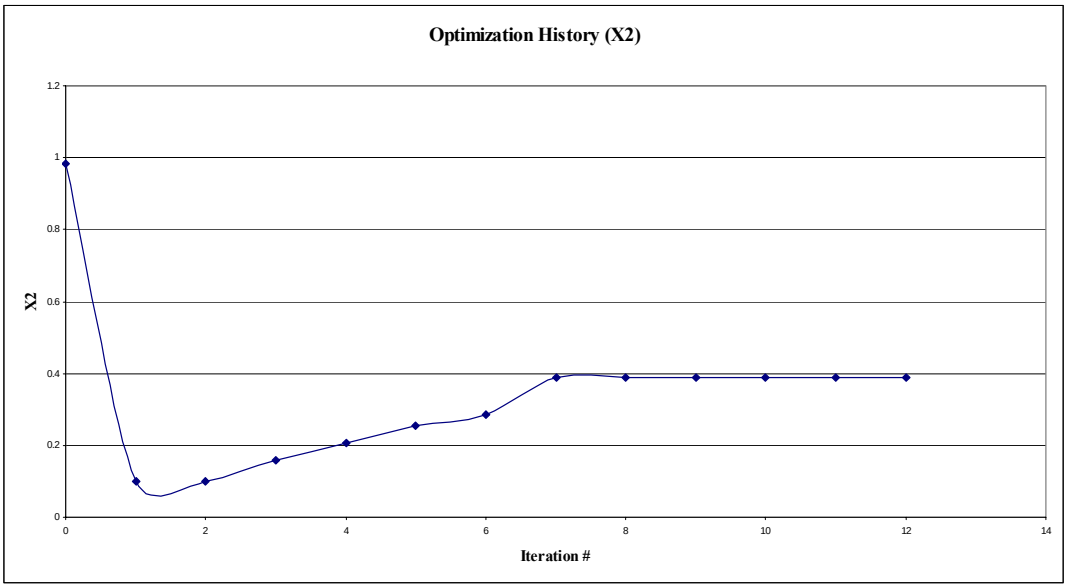

Figure 4.8 Optimization history for x2

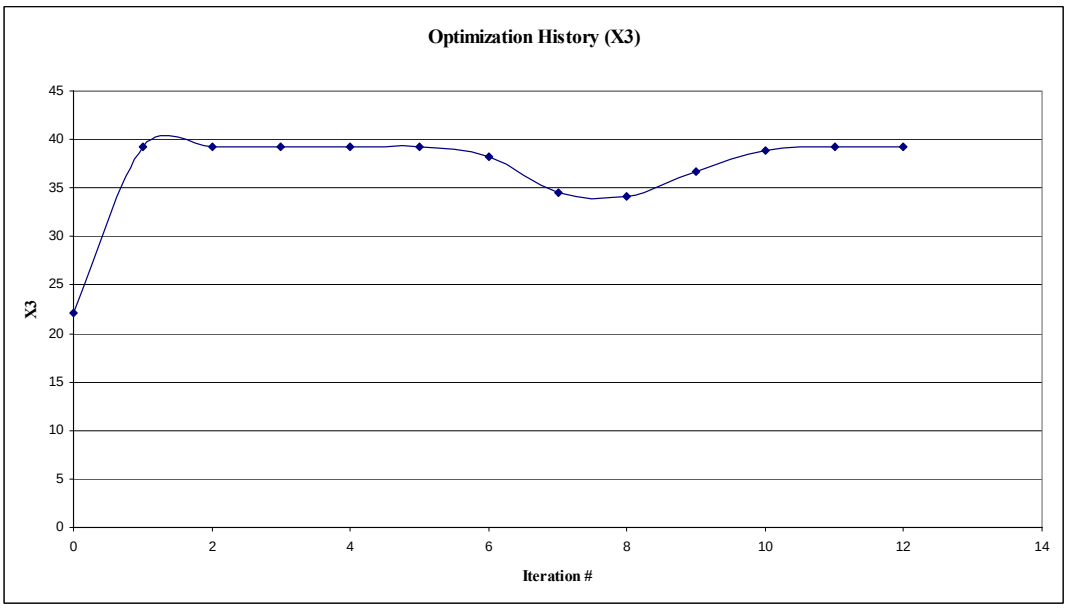

Figure 4.9 Optimization history for x3

It is seen that second state (x2) reaches the vicinity of the optimum solution in less iteration steps when compared to x1 and x3. When the histories of the gradients of the objective function are examined it is noticed that, the final gradient value with respect to third design variable (x3) is higher than the values for x1 and x2. History of the maximum constraint violation indicates that, none of the constraints were violated during the iterations.

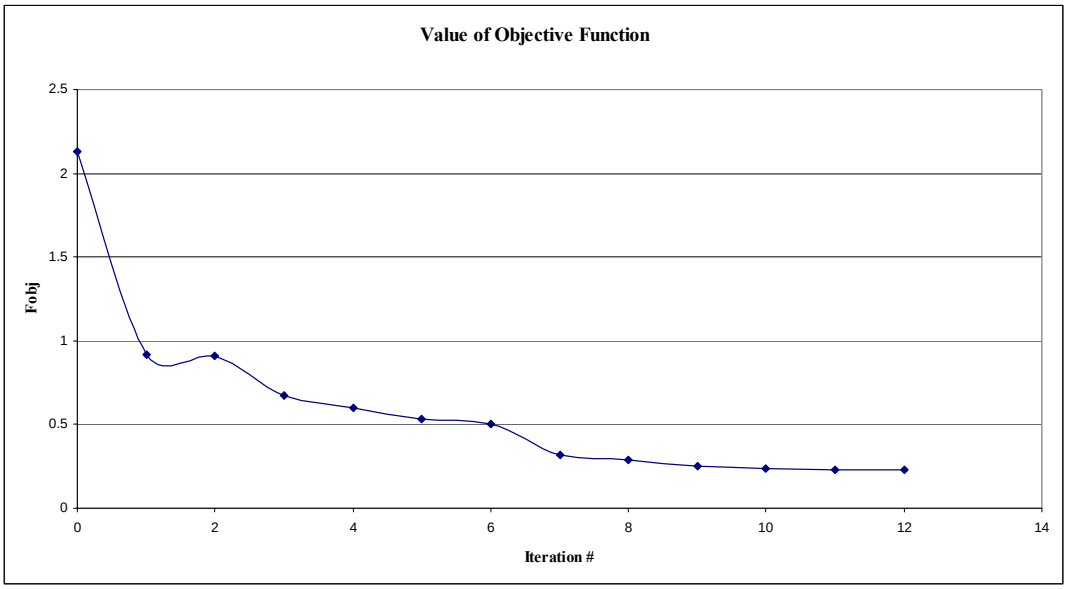

Figure 4.10 Optimization history for objective function

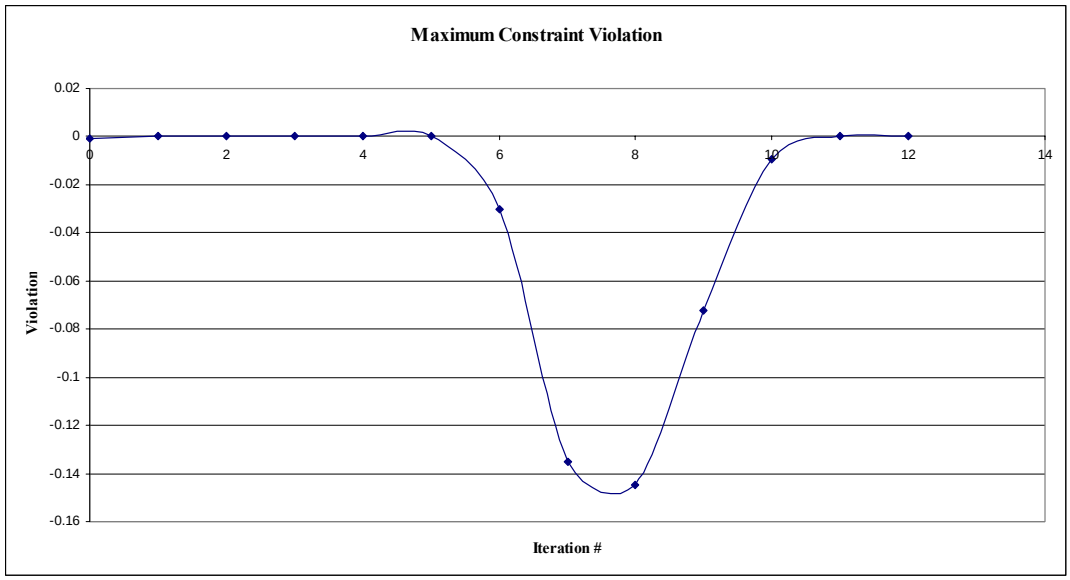

Figure 4.11 Optimization history for constraint violation

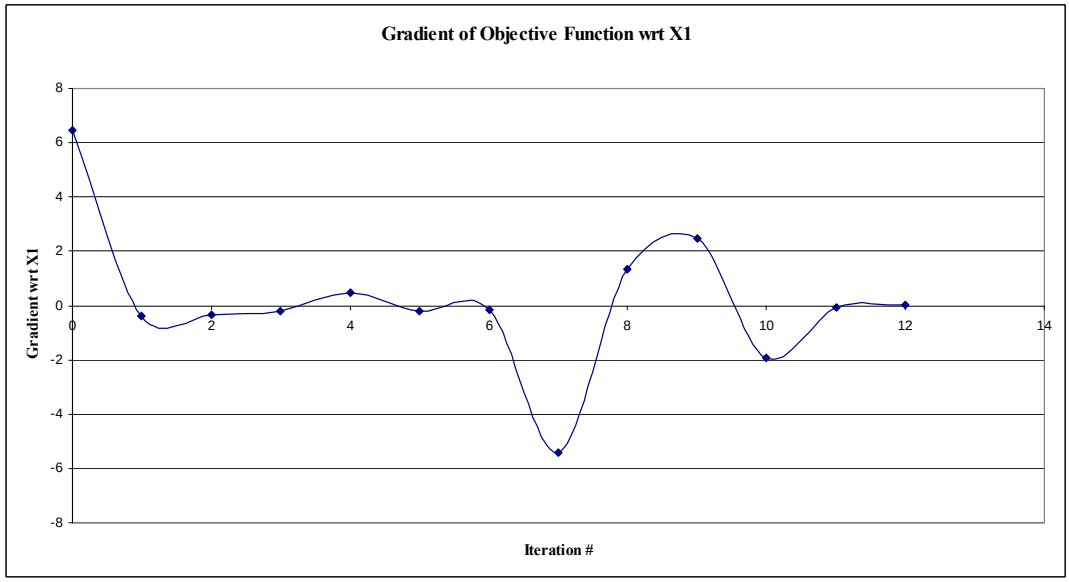

Figure 4.12 Optimization history for the gradient of objective function wrt x1

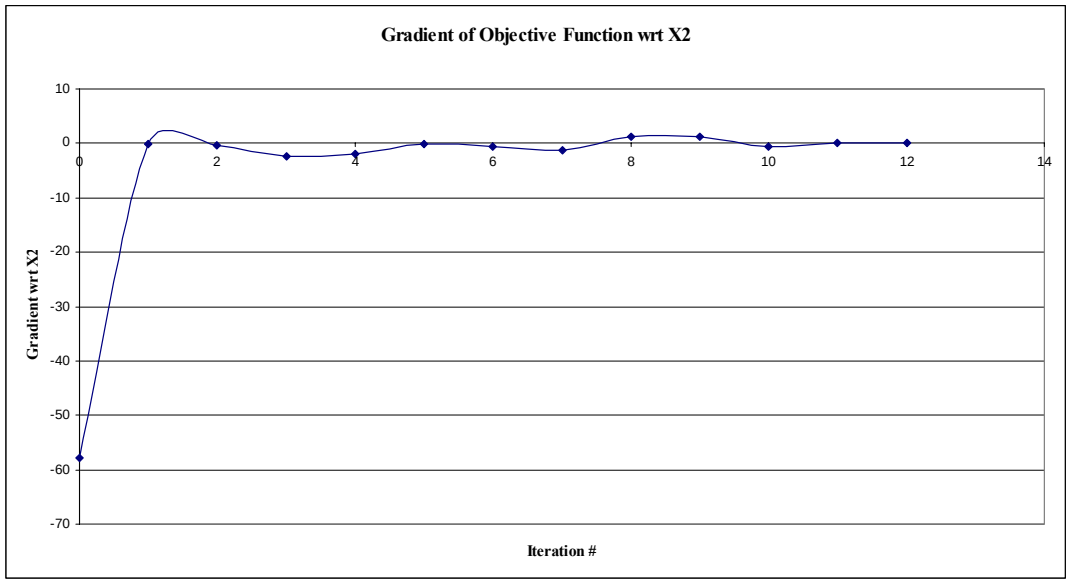

Figure 4.13 Optimization history for the gradient of objective function wrt x2

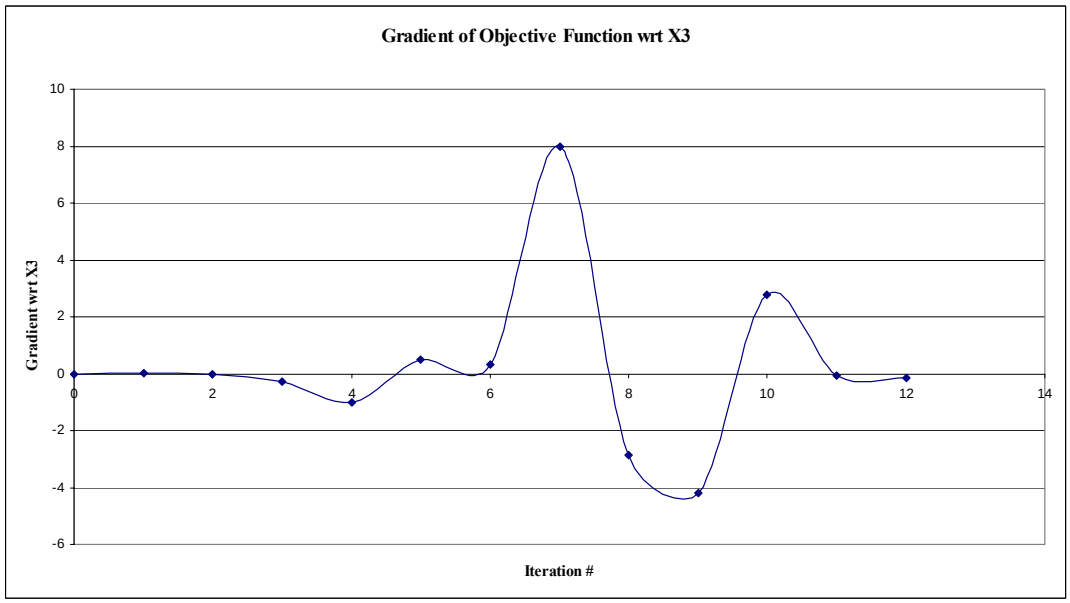

Figure 4.14 Optimization history for the gradient of objective function wrt x3

The optimum internal geometry of the FML model for the medium range unguided artillery rocket of test case 1 is shown in Figure 4.15 together with the plot of the estimated axial compressive stress along the model axis (Figure 4.16).

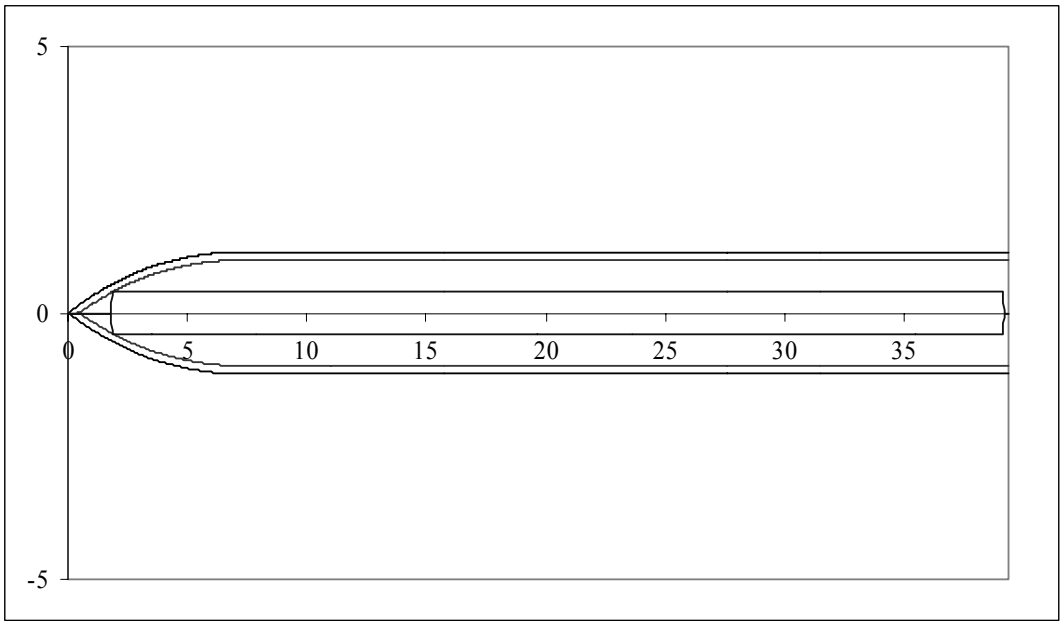

Figure 4.15 Optimum geometry for test case 1 at Mach 1.5 with weighting set 1

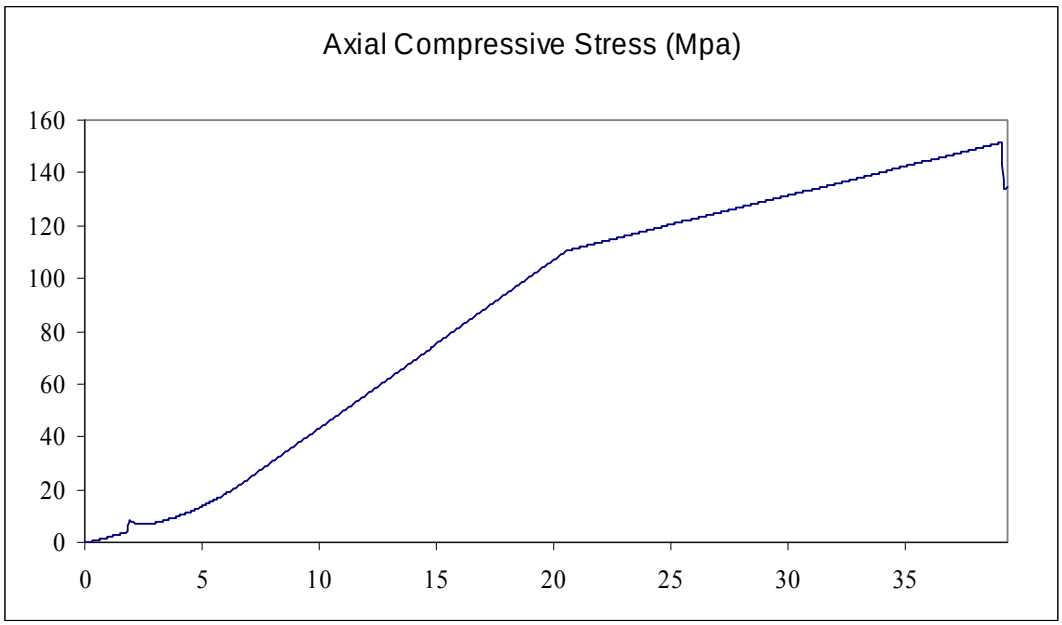

Figure 4.16 Axial compressive stress plot

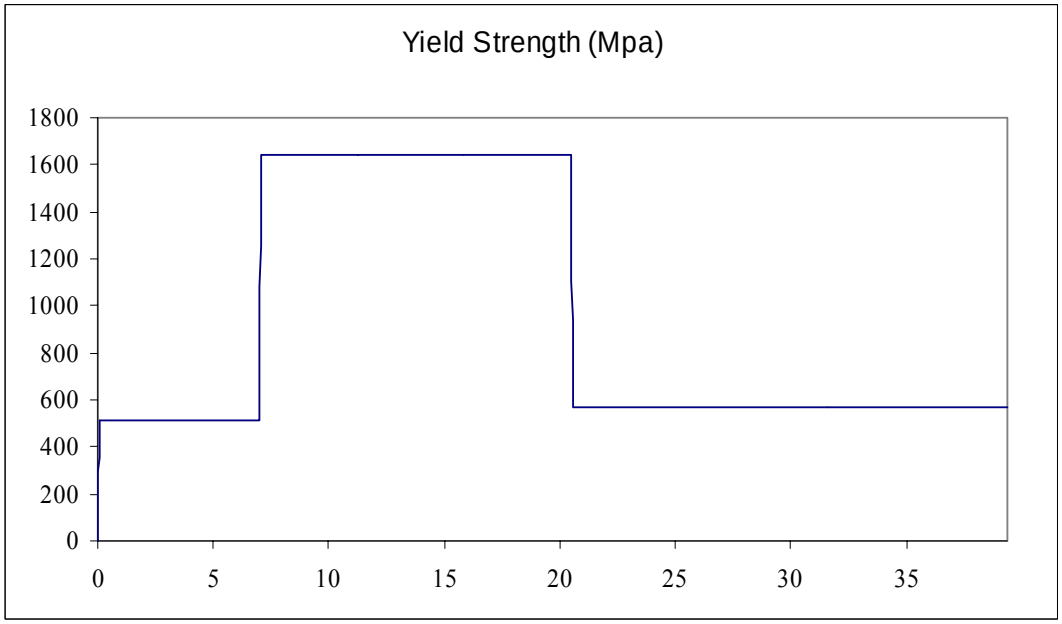

Figure 4.17 Yield strength

4.2.1.2 Weighting Factor Set 2:

The optimum solution found by FMLCAD for this weighting factor set is obtained with a brass nose section, steel body section and aluminum tail section. The results are presented in Table 4-7. Details of the results are given in Appendix B as tables. Optimization history for the states, objective function, constraint violation and the gradients of the objective function are given in following figures.

Table 4-7 Details of the optimum solution

Initial Conditions	
Initial x1:	4.36445
Initial x2:	0.98426
Initial x3:	22.10344
Optimization Results	
x1:	36.45766
x2:	0.3415
x3:	38.22935
Objective Function Value:	0.14116
Exit Flag:	1
Number of Iterations:	38
Final Step Size:	1
Optimization Algorithm:	medium-scale: SQP, Quasi-Newton, line-search
Gradient of Objective Function wrt x1:	0.52119
Gradient of Objective Function wrt x2:	0.30093
Gradient of Objective Function wrt x3:	-0.86957
Final Mass (gr):	701.30238
Final Cg Location (cm):	17.07313
Final Ix (grcm^2):	503.80847
Final Iy (grcm^2):	69375.06476
Final Inertia Ratio:	0.00726
Error in Cg Location (%):	0.033
Error in Ix2Iy Ratio (%):	0.39634
Figure of Merit:	0.312

It is seen from the results of Table 4-7 that the optimum solution found by the code is quite good with a mass of 701 grams, error in center of gravity location of 0.03 % and error in inertia ratio of 0.3 %. Although the number of iterations made by `fmincon` is 38, the optimal solution is obtained at 18th step. When the optimization histories are examined, the reason becomes obvious: the states at the 18th iteration step give the minimum objective function value while satisfying the constraints.

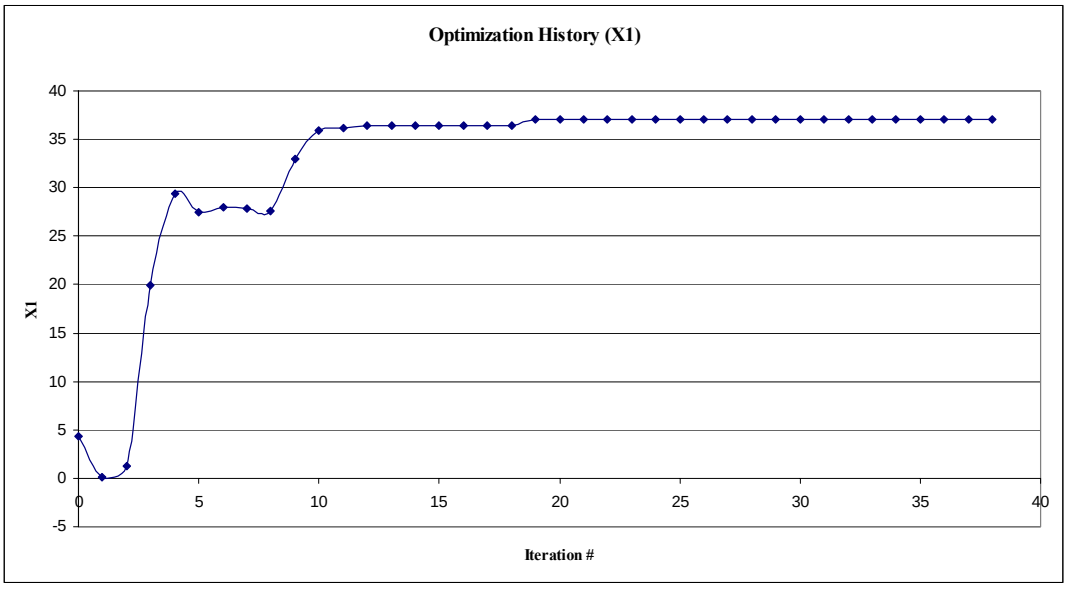

Figure 4.18 Optimization history for x1

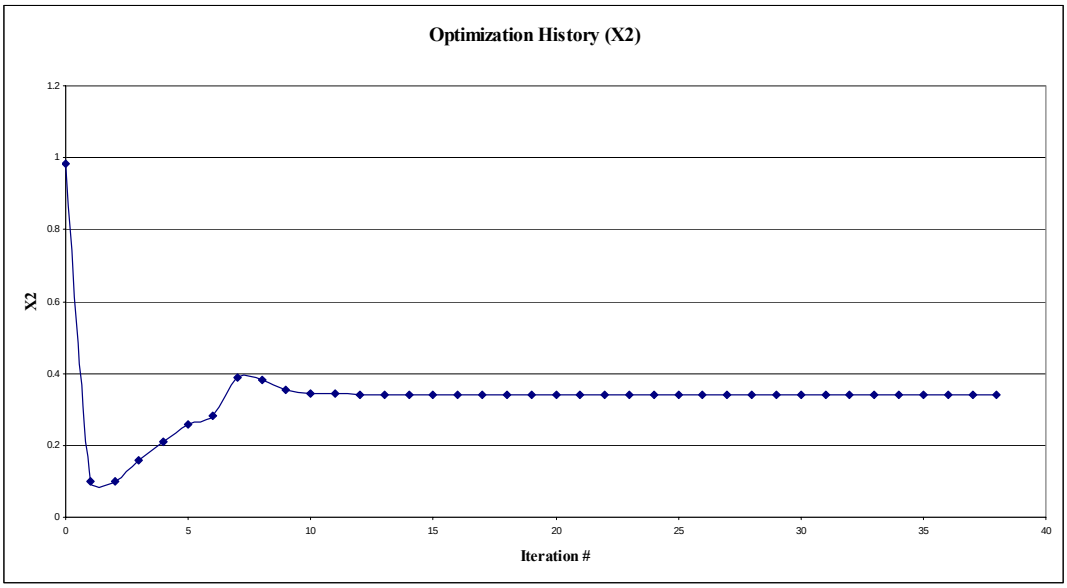

Figure 4.19 Optimization history for x2

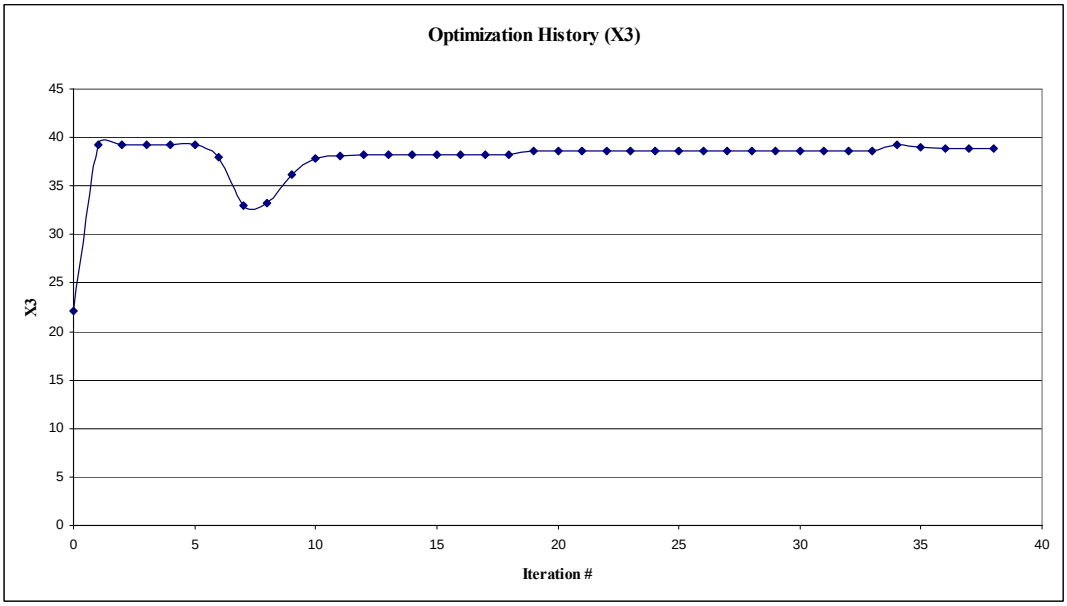

Figure 4.20 Optimization history for x3

It is seen that while the value of the objective function remains almost constant for the iterations after the 18th step, the gradient of the objective function tend to go to zero. However, because of the constraint violation no valid solution can be reached as a result of the iterations after step 18. So the optimum solution is the one that gives the minimum objective function value with no constraint violation, which is obtained at step 18.

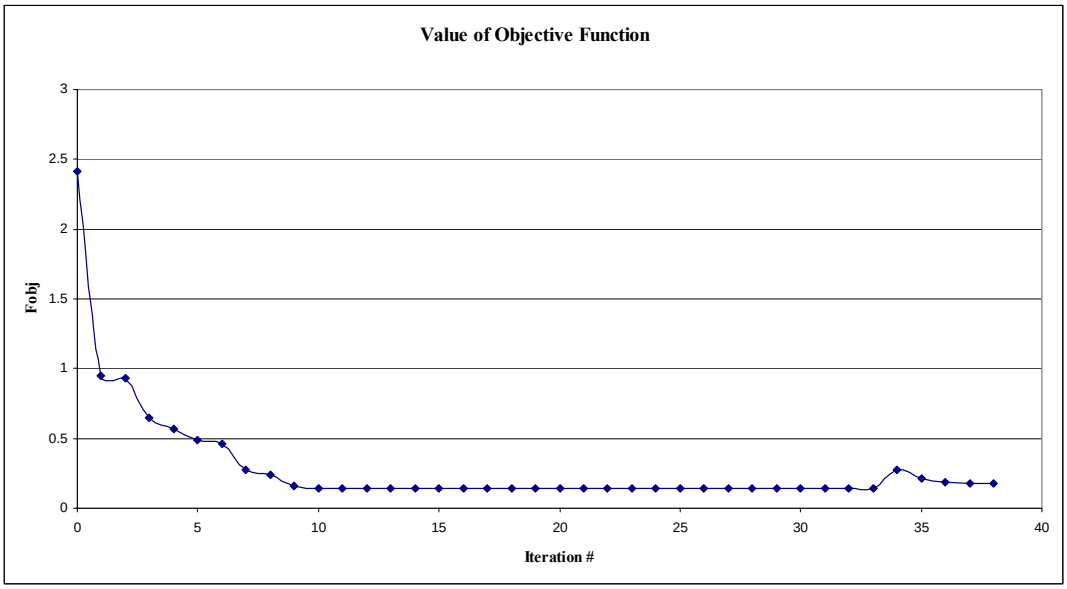

Figure 4.21 Optimization history for objective function

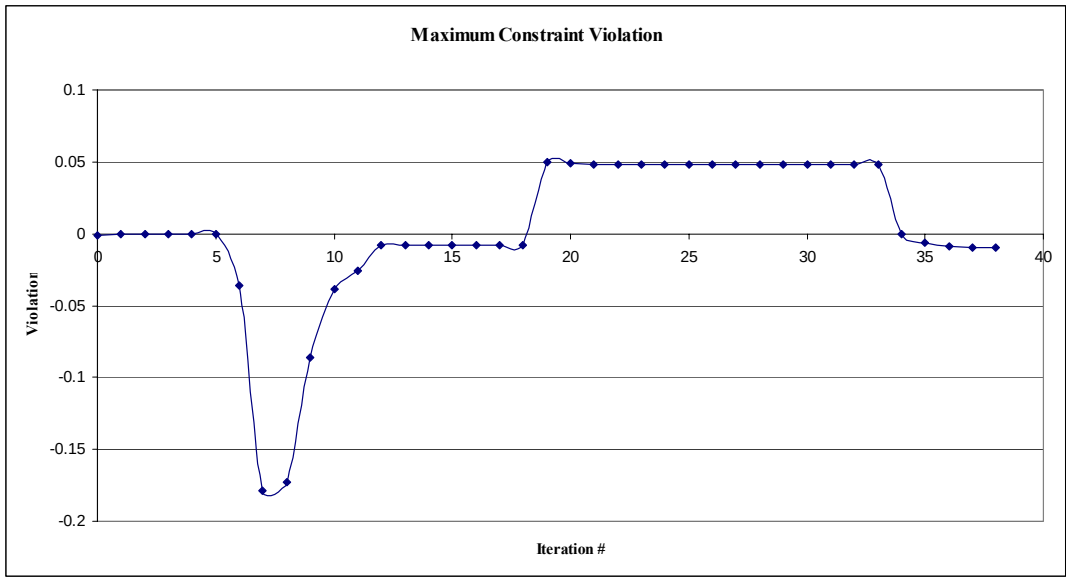

Figure 4.22 Optimization history for constraint violation

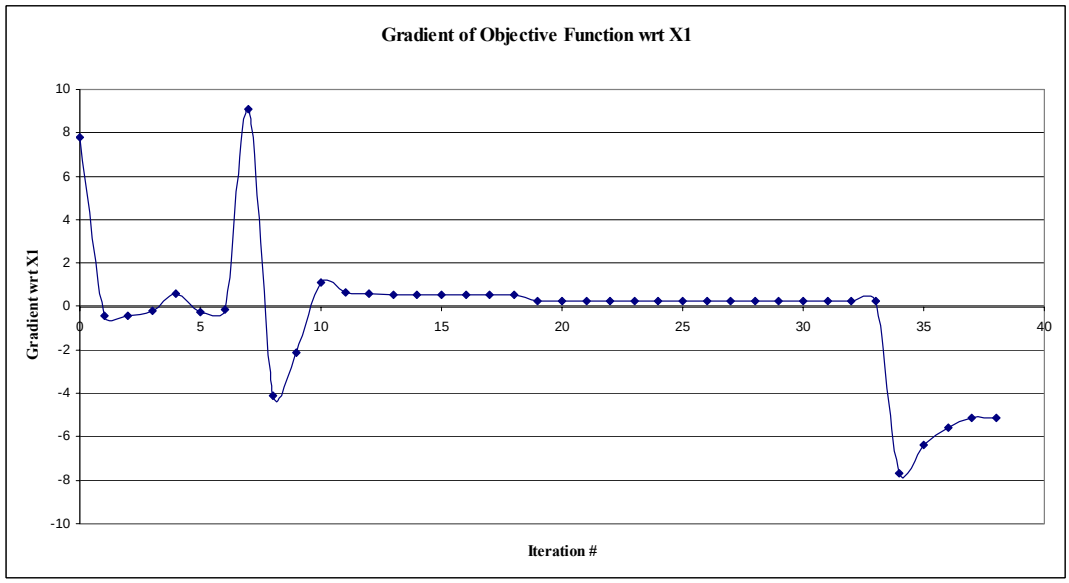

Figure 4.23 Optimization history for the gradient of objective function wrt x1

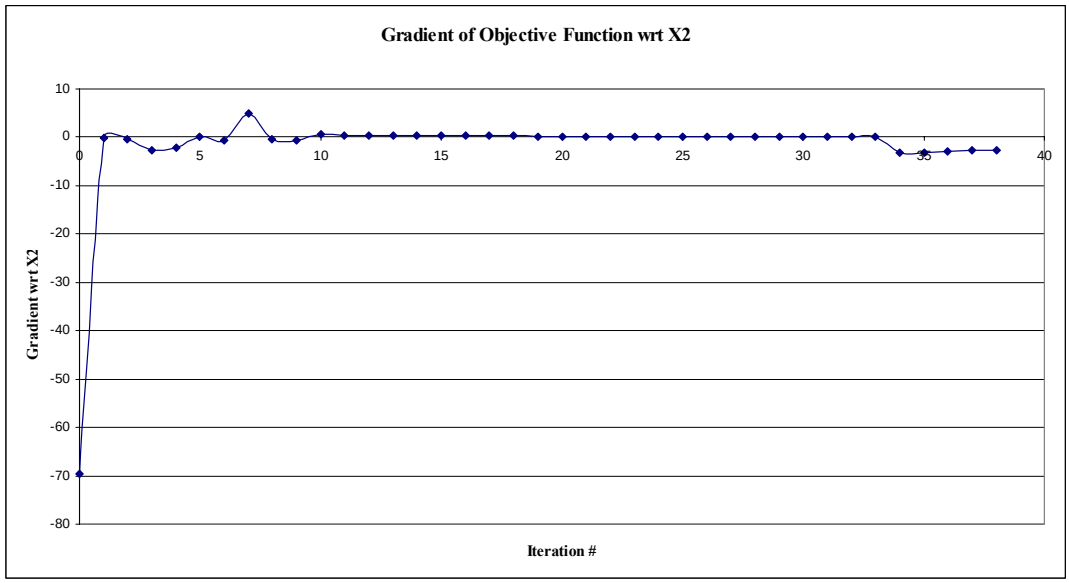

Figure 4.24 Optimization history for the gradient of objective function wrt x2

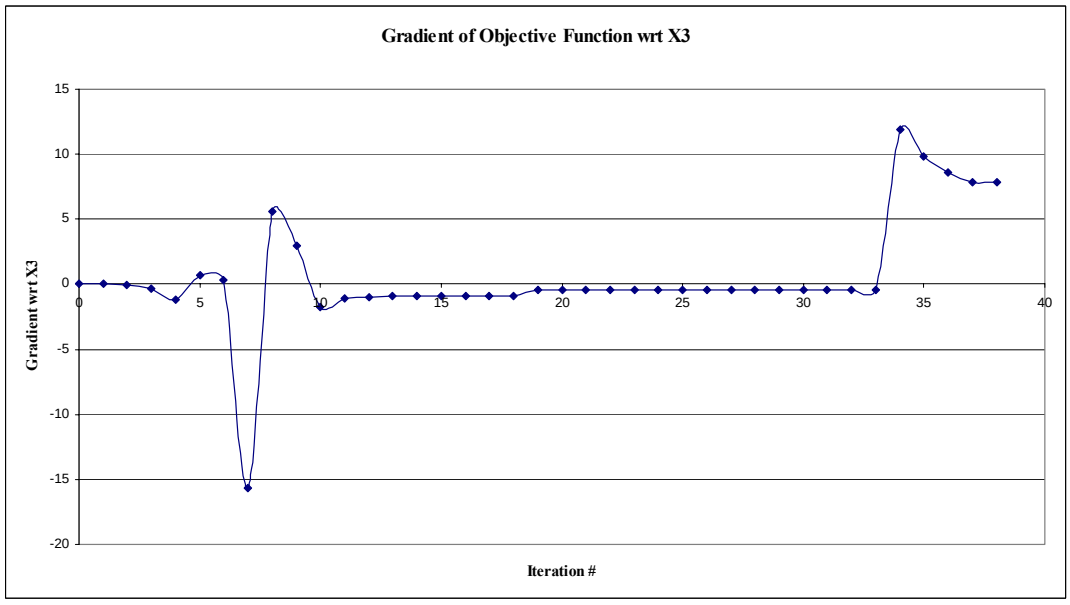

Figure 4.25 Optimization history for the gradient of objective function wrt x3

The final inner geometry of the FML model for weighting factor set 2 is given in Figure 4.26.

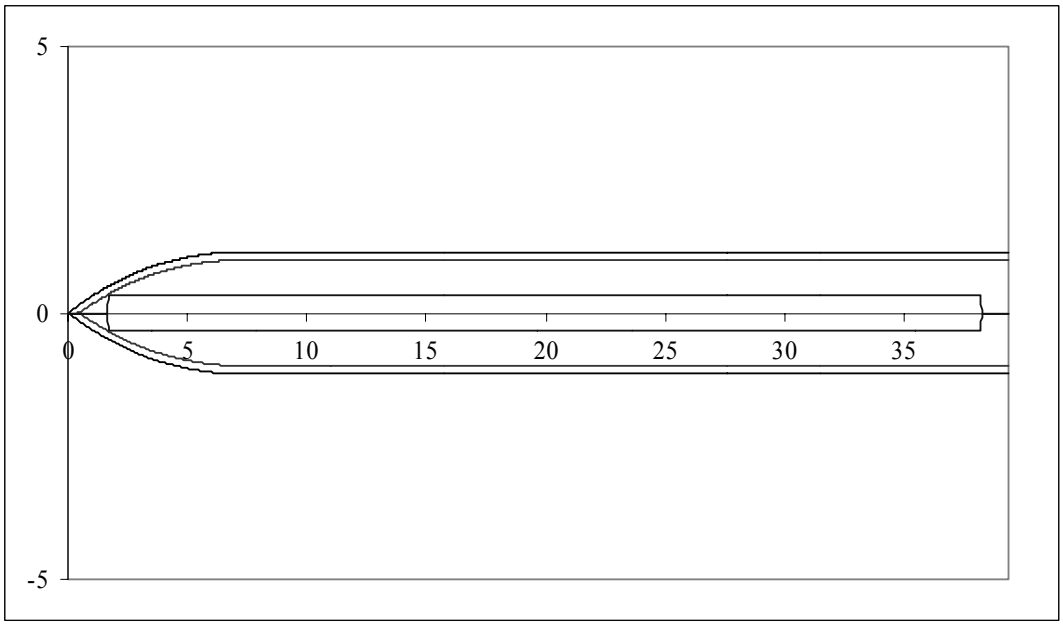

Figure 4.26 Optimum geometry for test case 1 at Mach 1.5 with weighting set 2

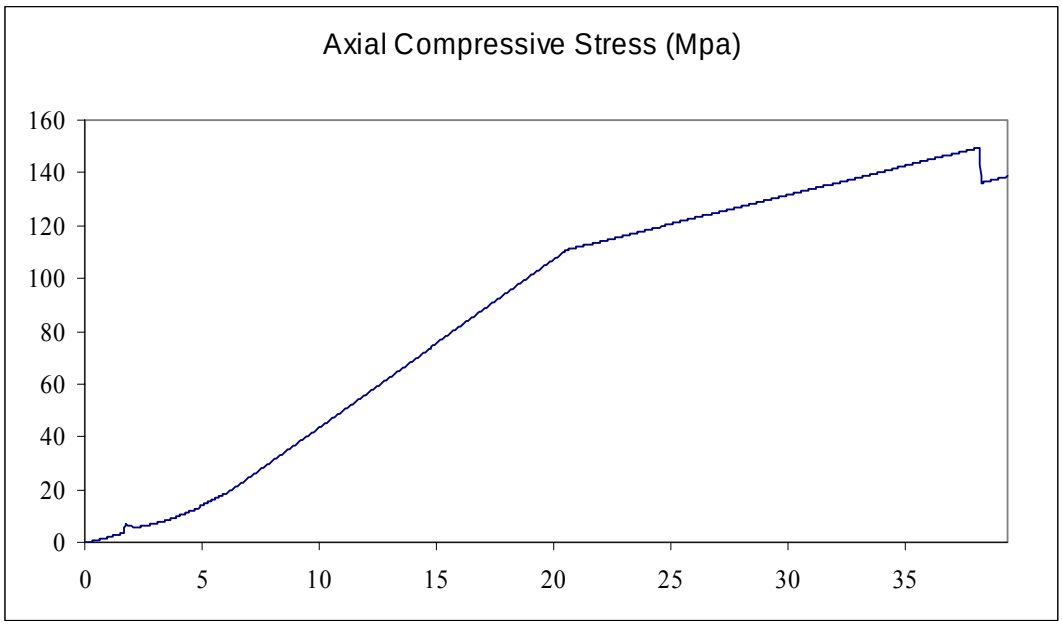

Figure 4.27 Axial compressive stress plot

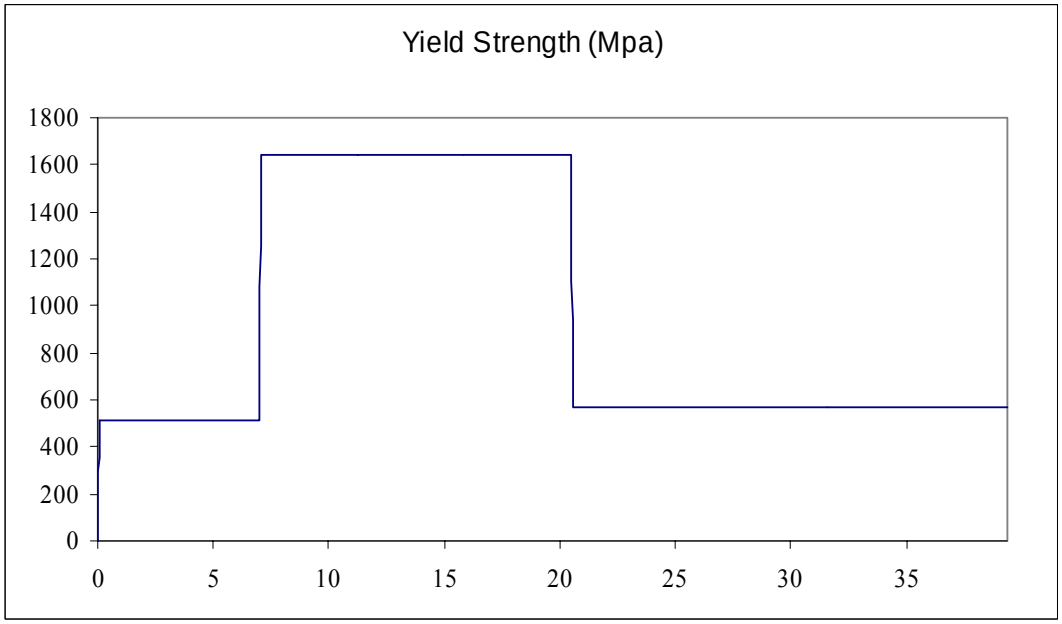

Figure 4.28 Yield strength

4.2.2 Results for Mach 2.5

4.2.2.1 Weighting Factor Set 1:

Once again, the optimum solution found by FMLCAD is obtained with a brass nose section, steel body section and aluminum tail section. The results are presented in Table 4-8. Details of the results are given in Appendix B as tables.

Table 4-8 Details of the optimum solution

Initial Conditions	
Initial x1:	4.36445
Initial x2:	0.98426
Initial x3:	22.10344
Optimization Results	
x1:	37.2172
x2:	0.38686
x3:	39.21252
Objective Function Value:	0.23105
Exit Flag:	1
Number of Iterations:	12
Final Step Size:	1
Optimization Algorithm:	medium-scale: SQP, Quasi-Newton, line-search
Gradient of Objective Function wrt x1:	0.0087
Gradient of Objective Function wrt x2:	0.05163
Gradient of Objective Function wrt x3:	-0.16855
Final Mass (gr):	680.07931
Final Cg Location (cm):	17.07284
Final Ix (grcm^2):	501.01643
Final Iy (grcm^2):	67018.29672
Final Inertia Ratio:	0.00748
Error in Cg Location (%):	0.0313
Error in Ix/Iy Ratio (%):	2.53492
Figure of Merit:	1.0821

When the results given in Table 4-8 are compared to those given in Table 4-6, it is seen that only difference between the optimizations at Mach 1.5 and Mach 2.5 is the maximum constraint violation at the initial guess.

The optimum internal geometry of the FML model for the medium range unguided artillery rocket of test case 1 is shown in Figure 4.29 together with the plot of the estimated axial compressive stress along the model axis (Figure 4.30).

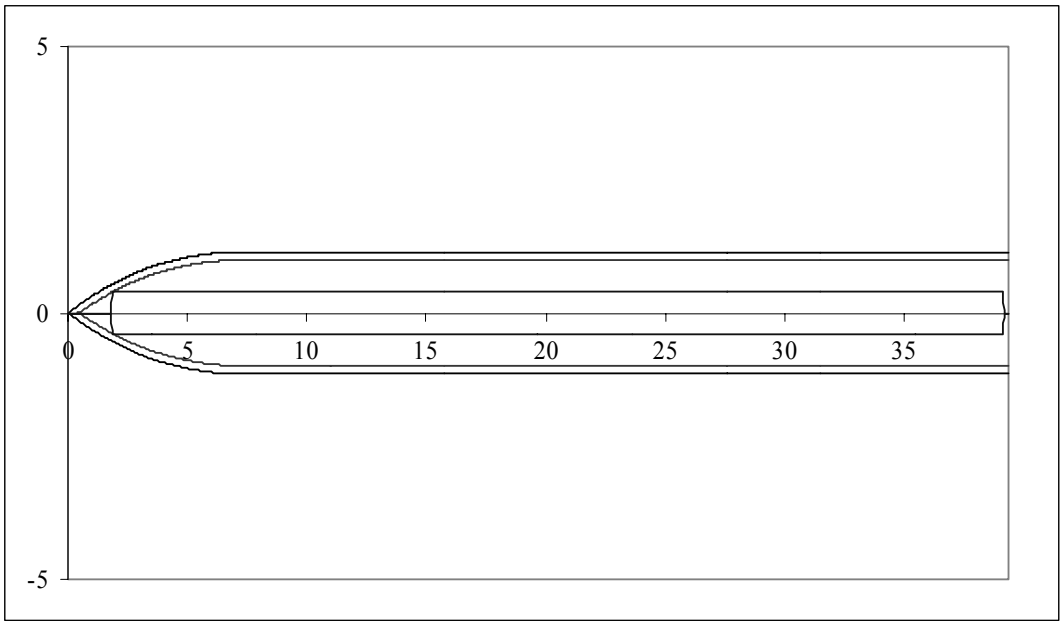

Figure 4.29 Optimum geometry for test case 1 at Mach 2.5 with weighting set 1

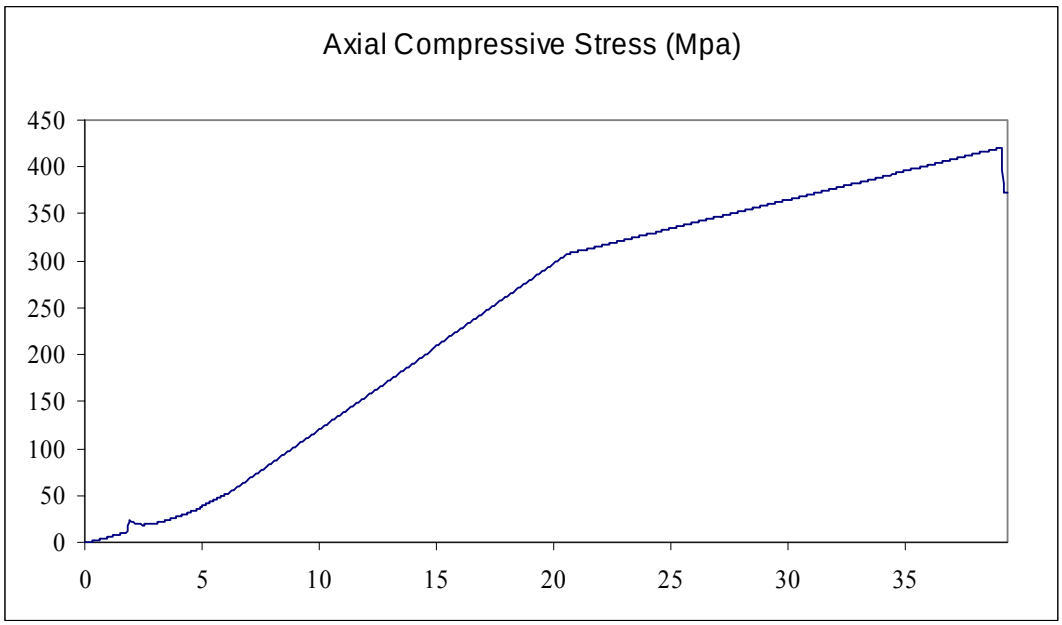

Figure 4.30 Axial Compressive stress plot

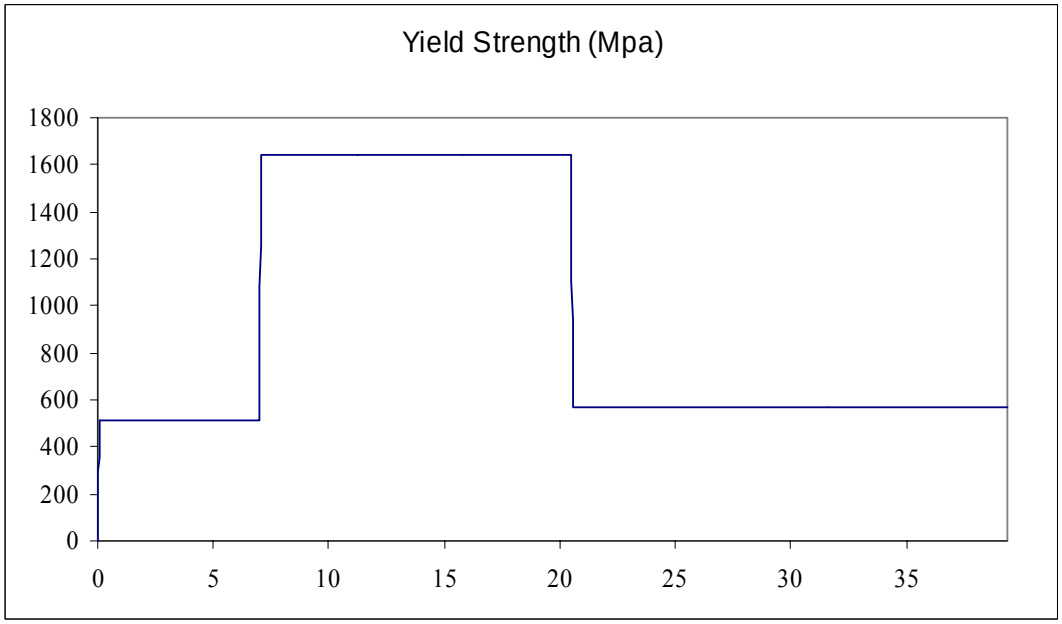

Figure 4.31 Yield strength

4.2.2.2 Weighting Factor Set 2:

Once again, the optimum solution found by FMLCAD for this case is obtained with a brass nose section, steel body section and aluminum tail section (Table 4-9). Details of the results are given in Appendix B.

Table 4-9 Details of the optimum solution

Initial Conditions	
Initial x1:	4.36445
Initial x2:	0.98426
Initial x3:	22.10344
Optimization Results	
x1:	36.45766
x2:	0.3415
x3:	38.22935
Objective Function Value:	0.14116
Exit Flag:	1
Number of Iterations:	38
Final Step Size:	1
Optimization Algorithm:	medium-scale: SQP, Quasi-Newton, line-search
Gradient of Objective Function wrt x1:	0.52119
Gradient of Objective Function wrt x2:	0.30093
Gradient of Objective Function wrt x3:	-0.86957
Final Mass (gr):	701.30238
Final Cg Location (cm):	17.07313
Final Ix (grcm^2):	503.80847
Final Iy (grcm^2):	69375.06476
Final Inertia Ratio:	0.00726
Error in Cg Location (%):	0.033
Error in Ix2Iy Ratio (%):	0.39634
Figure of Merit:	0.312

When the results of Table 4-9 are compared to those given in Table 4-7, it is seen that significant difference between the optimizations at Mach 1.5 and Mach 2.5 is the maximum constraint violation at the initial guess.

The final inner geometry of the FML model for weighting factor set 2 is given in Figure 4.32.

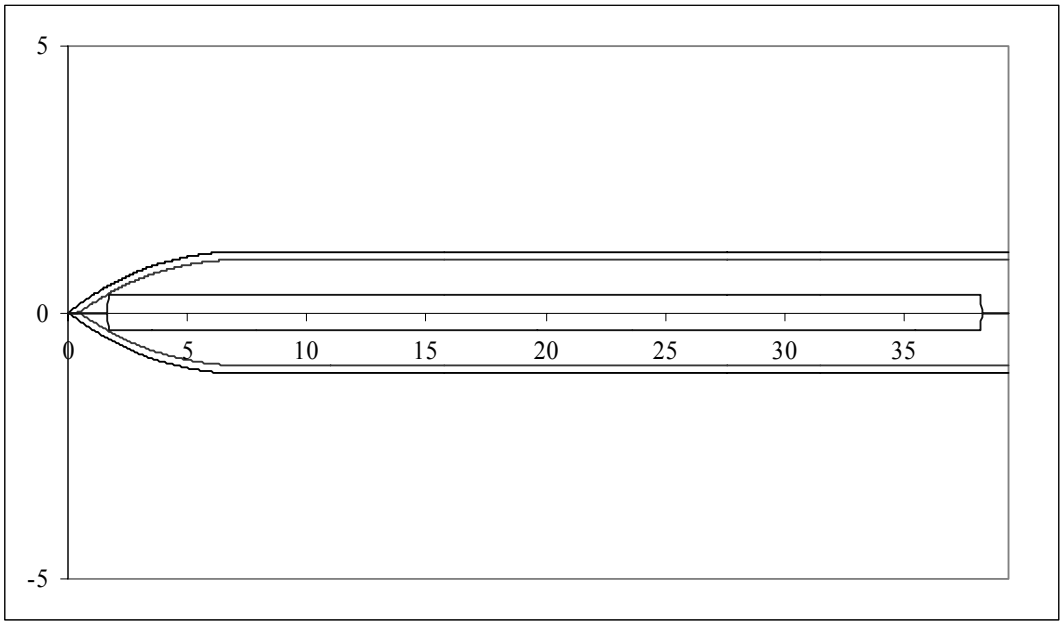

Figure 4.32 Optimum geometry for test case 1 at Mach 2.5 with weighting set 2

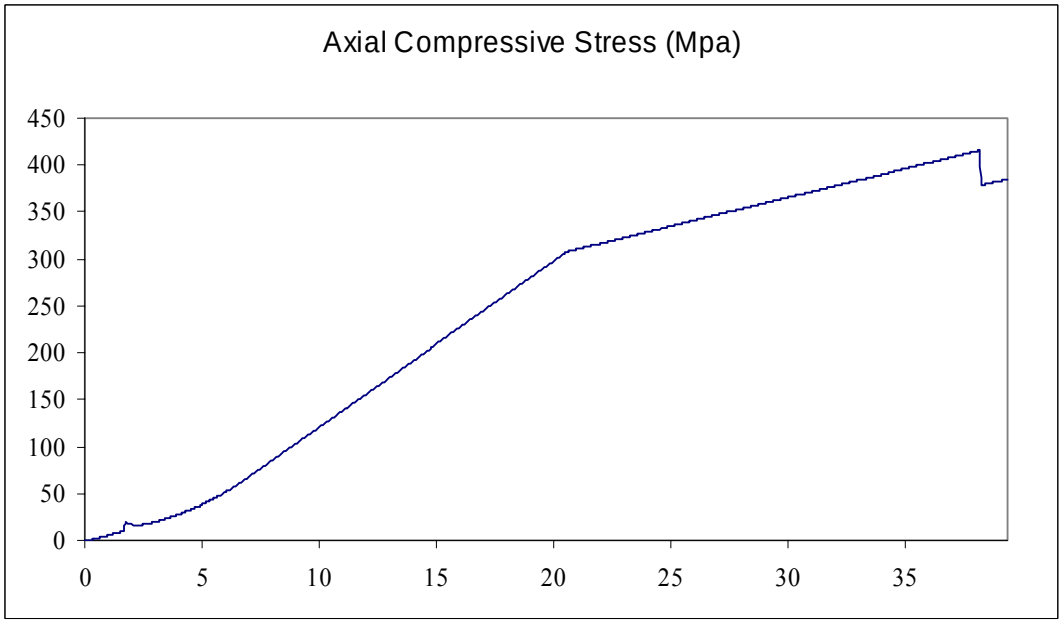

Figure 4.33 Axial compressive stress plot

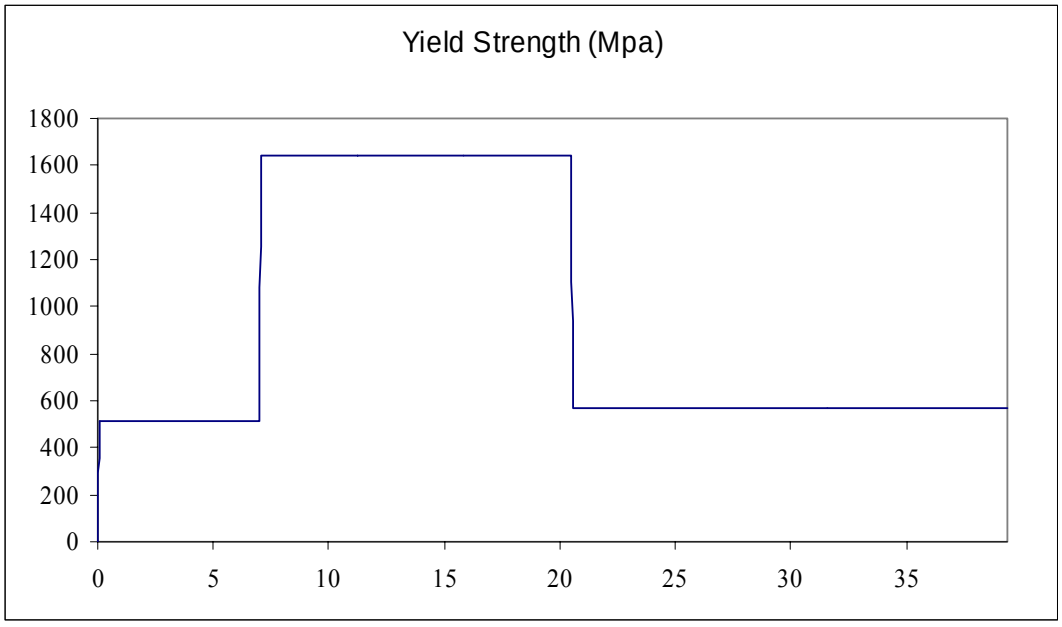

Figure 4.34 Yield strength

4.3 TEST CASE – 2: LOW DRAG GENERAL PURPOSE AIRCRAFT BOMB

The second case selected to test the FMLCAD is a low drag general purpose aircraft bomb.

Table 4-10 shows the mass properties of the LDGP aircraft bomb selected as the test case – 2. The external geometry of the bomb is given in Table 4-11, Table 4-12 and shown in Figure 4.35.

Table 4-10 Mass properties for test case - 1

Mass (kg)	910
Centre of gravity location (cm – from nose)	160.0
Axial inertia (kg m^2)	22.33332
Transverse inertia (kg m^2)	536.976

Table 4-11 Geometry properties for test case - 1

Section	**End location (cm –from nose)**	**End radius (cm)**
Nose	132.46	22.85
Body	256.26	22.85
Tail	381.5	8.138

Table 4-12 Fin data

Number of fins	4
Starting coordinates from the nose (cm)	(334.00, 13.70)
Root chord (cm)	45.31
Maximum span length (cm)	26.37
Reference thickness (cm)	2.5
Leading edge sweep angle 1 (°)	52
Leading edge sweep angle 2 (°)	6.7
Trailing edge sweep angle (°)	83.18

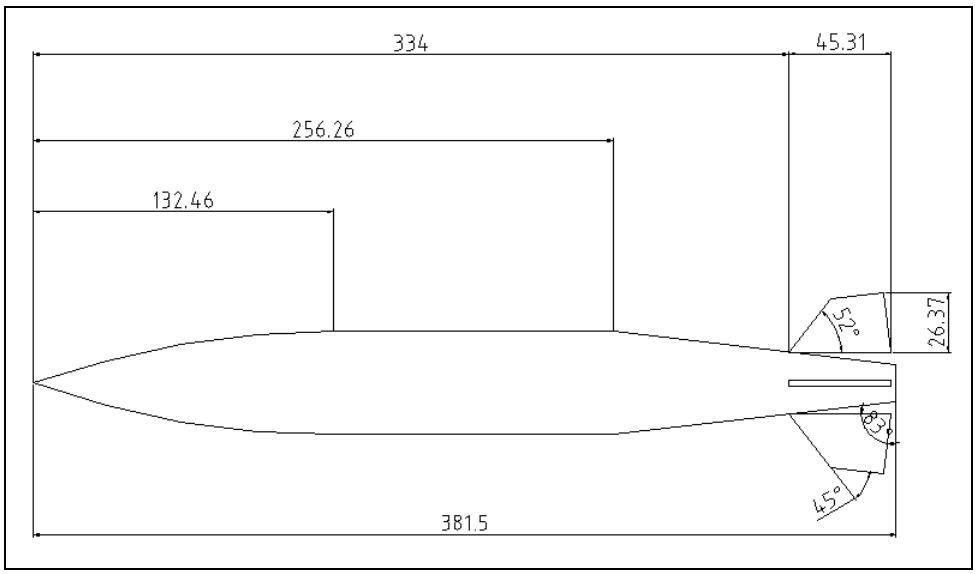

Figure 4.35 External geometry for test case - 2

When the geometry of the test case is examined (Figure 4.35), it is seen that the fins are modeled parallel to the longitudinal axis of the munition. Although this approach introduces a small error in inertia calculations, its effect is negligible. This approach is also used in modeling fins by commercial software packages used in aeroballistics such as PRODAS (Projectile Design and Analysis Software) and APC 2002 (Aero Prediction Code 2002) [28].

Scale factor for this rocket is selected to be 0.08 based on the similar models that were tested at FML. This scale factor gives a maximum diameter of 52 mm at the fin tips. Maximum Mach number at the tests will be performed is selected as 1.2. However, to investigate the effect of test velocity on the model design, FMLCAD is run twice using Mach 0.6 and Mach 1.2 as test velocities. Also two sets of weighting factors are used for each Mach number (Table 4-13).

Table 4-13 Weighting factors for test case - 2

Weighting factor set 1:	[1,1,1]
Weighting factor set 2:	[0.4,0.4,0.2]

Like test case-1, Steel 4140, Aluminum 7075 T6 and Soft Yellow Brass are selected as materials for this case.

4.3.1 Results for Mach 0.6

4.3.1.1 Weighting Factor Set 1:

The optimum solution found by FMLCAD for this case is obtained with a steel nose section, brass body section and aluminum tail section. The results are presented in Table 4-14. Details of the results are given in Appendix C as tables. Optimization history for the states, objective function, constraint violation and the gradients of the objective function are given in following figures.

Table 4-14 Details of the optimum solution

Initial Conditions	
Initial x1:	29.54336
Initial x2:	0.08621
Initial x3:	30.2148
Optimization Results	
x1:	16.44918
x2:	1.2911
x3:	24.14132
Objective Function Value:	0.43893
Exit Flag:	1
Number of Iterations:	47
Final Step Size:	1
Optimization Algorithm:	medium-scale: SQP, Quasi-Newton, line-search
Gradient of Objective Function wrt x1:	0.00349
Gradient of Objective Function wrt x2:	-0.65202
Gradient of Objective Function wrt x3:	-0.0067
Final Mass (gr):	911.00062
Final Cg Location (cm):	13.60652
Final Ix (grcm^2):	1851.69856
Final Iy (grcm^2):	45222.23794
Final Inertia Ratio:	0.04095
Error in Cg Location (%):	6.30097
Error in Ix/Iy Ratio (%):	1.54907
Figure of Merit:	2.92035

It is seen from the results of Table 4-14 that the optimum solution found by the code is acceptable with a mass of 911 grams and error in inertia ratio of 1.5 % although error in centre of gravity location is higher than 5%.

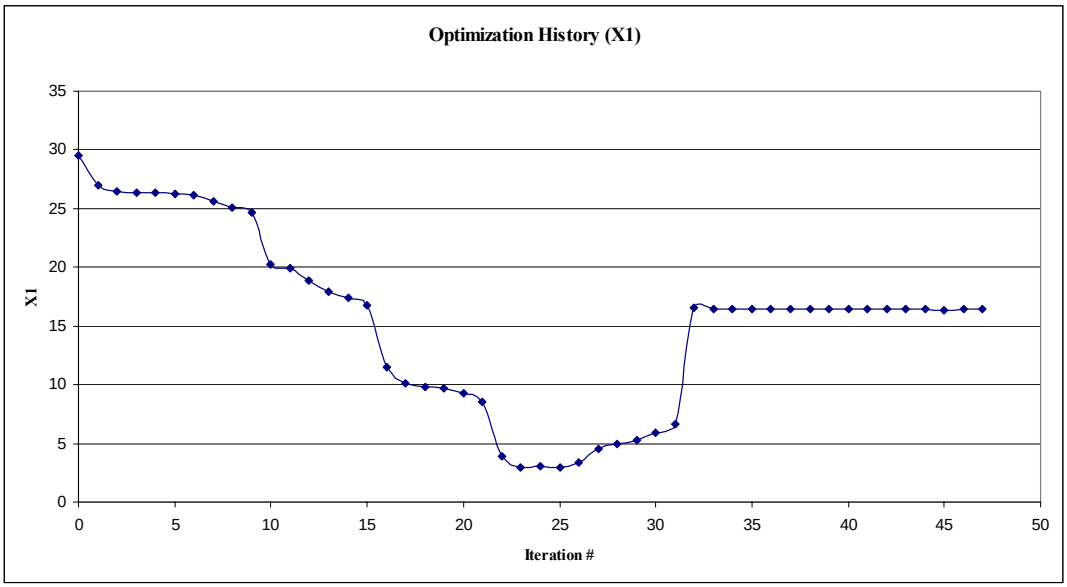

Figure 4.36 Optimization history for x1

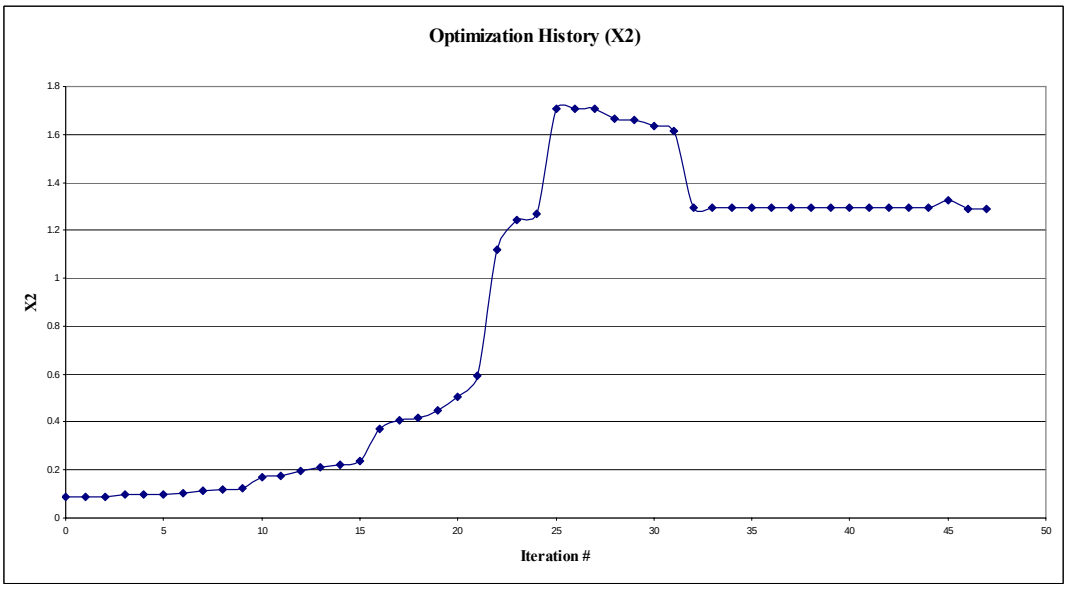

Figure 4.37 Optimization history for x2

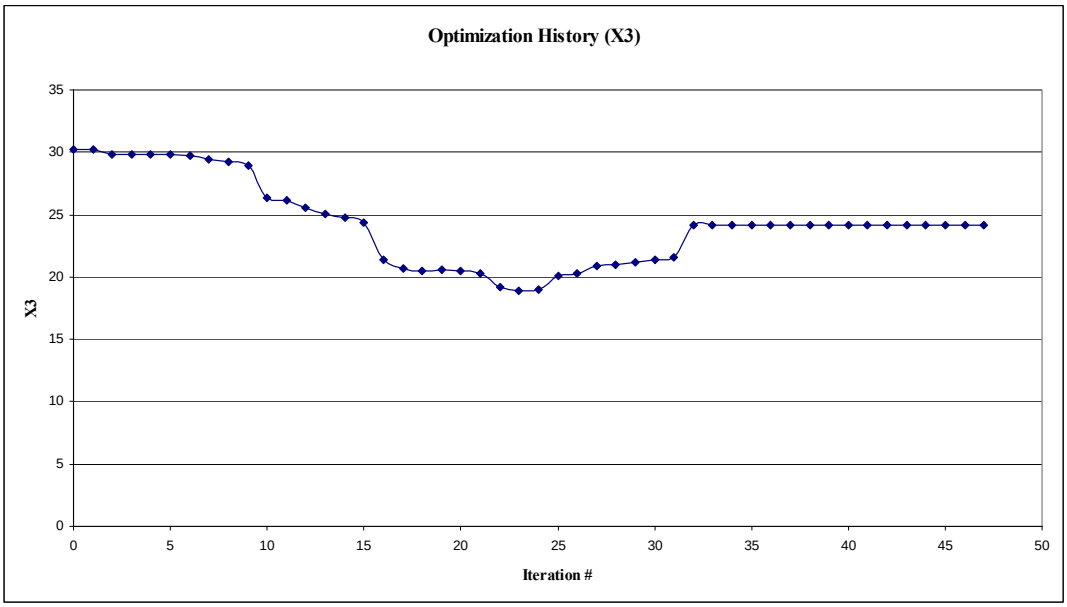

Figure 4.38 Optimization history for x3

It is seen that it takes the optimization routine to reach a solution 47 iteration steps. However, when the results are examined it is seen that the value of the objective function is almost constant for iterations after step 31. This is also true for the value of the design variables. When the histories of the gradients are examined, it is seen that up to the 31st iteration step, value of the gradient with respect to x3 is relatively high when compared to the other two gradients. However, after step 31, both the values of the gradients of the objective function with respect top x1 and x3 decrease while gradient with respect to x2 increase. Although, the improvement in the objective function value is very slow after step 32, at the end the gradients of the objective function with respect to x1 and x3 are almost zero. Also it is noted that there is constraint violation starting from 26th step until 46th step. However the final solution satisfies the constraints (no constraint violation).

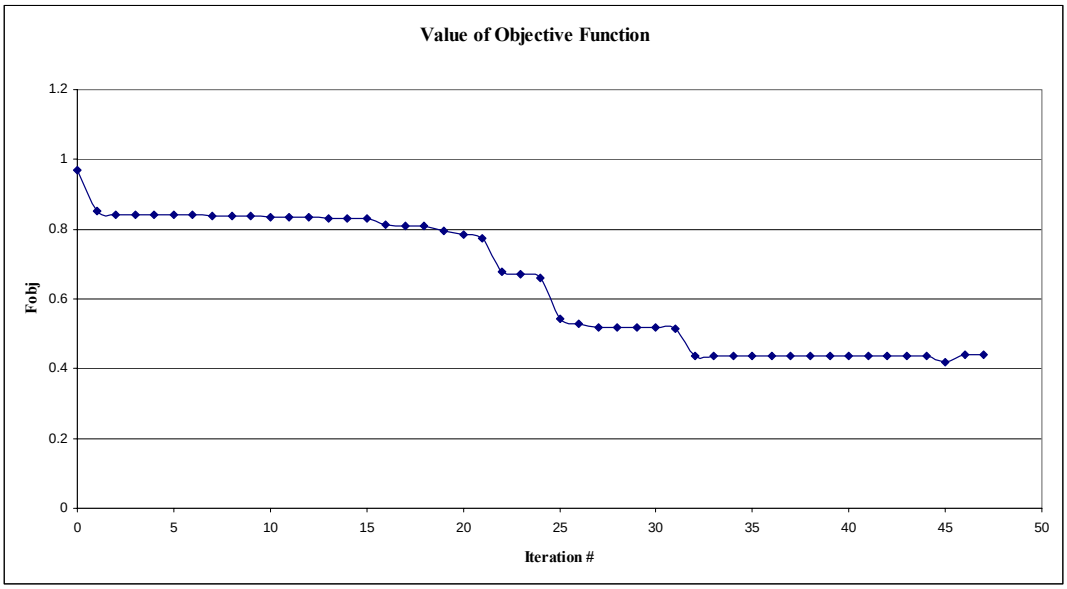

Figure 4.39 Optimization history for objective function

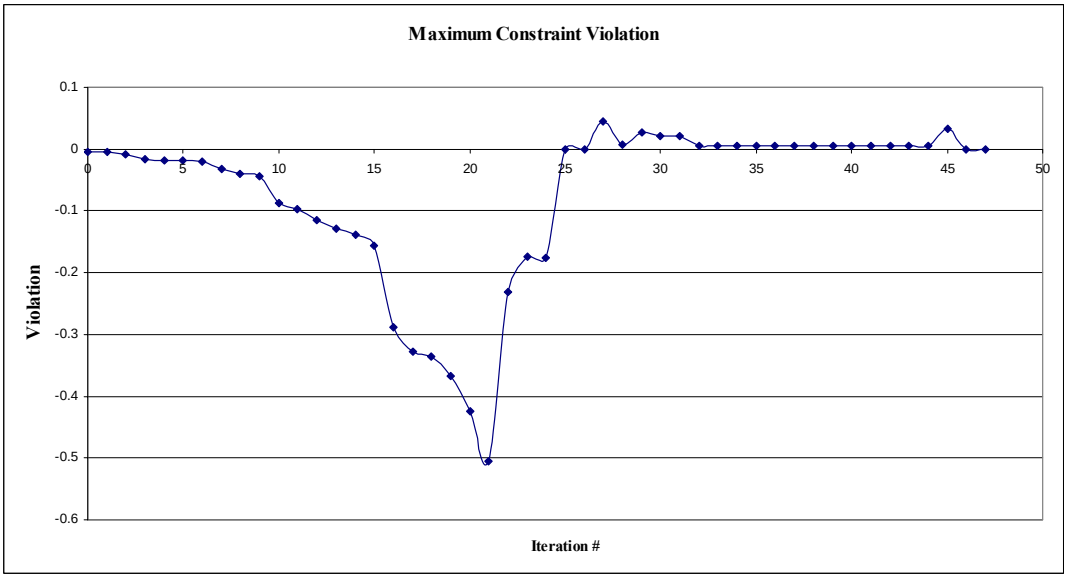

Figure 4.40 Optimization history for constraint violation

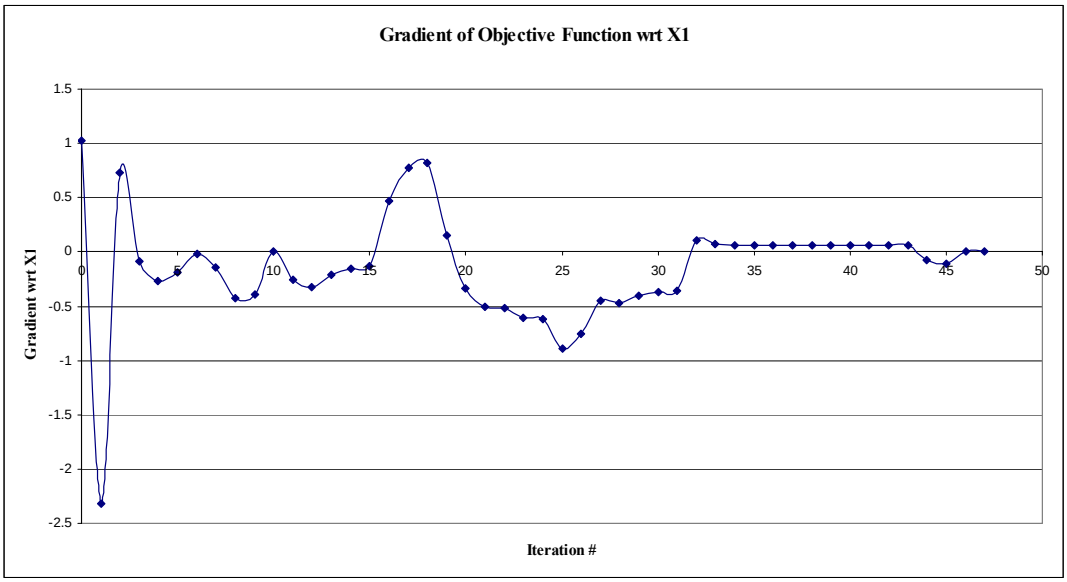

Figure 4.41 Optimization history for the gradient of objective function wrt x1

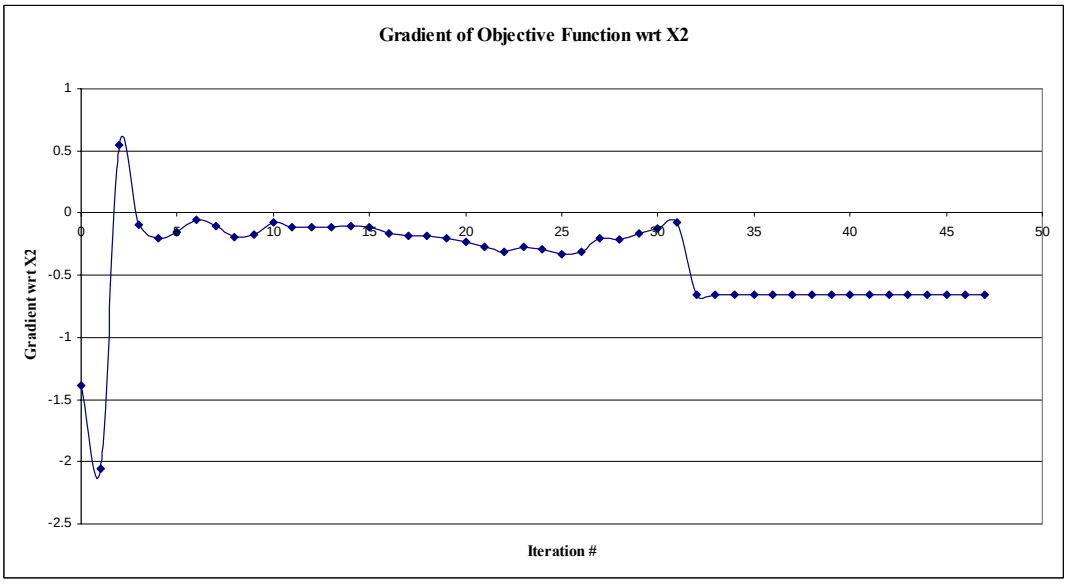

Figure 4.42 Optimization history for the gradient of objective function wrt x2

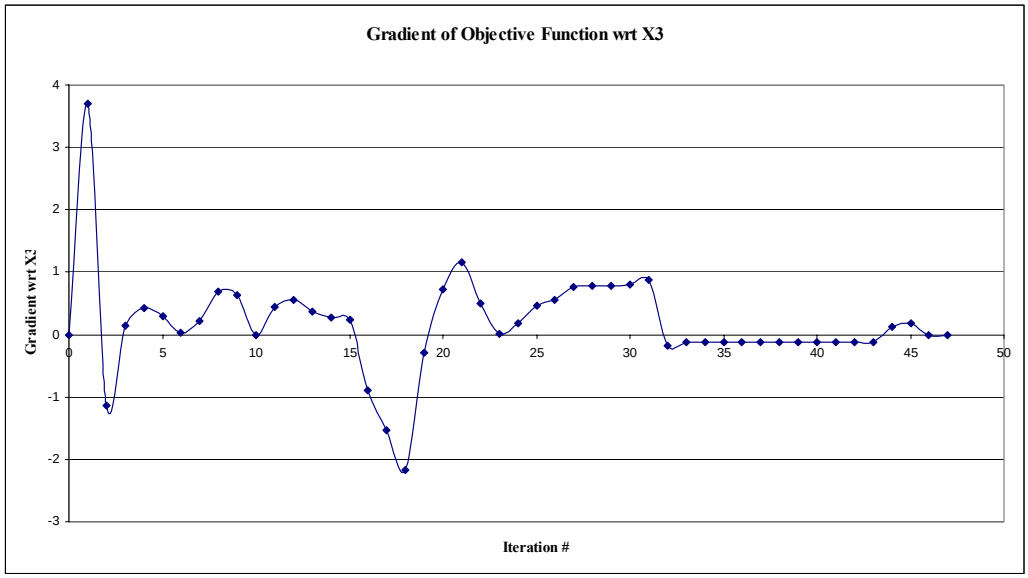

Figure 4.43 Optimization history for the gradient of objective function wrt x3

The optimum internal geometry of the FML model for the LDGP aircraft bomb of test case 2 is shown in Figure 4.44 together with the plot of the estimated axial compressive stress along the model axis (Figure 4.45).

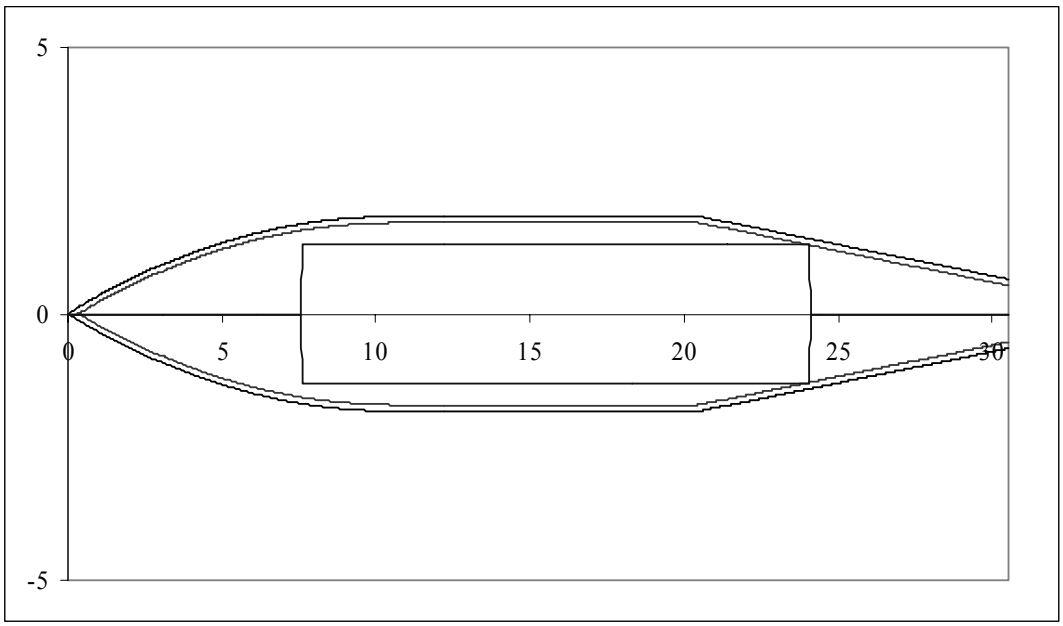

Figure 4.44 Optimum geometry for test case 2 at Mach 0.6 with weighting set 1

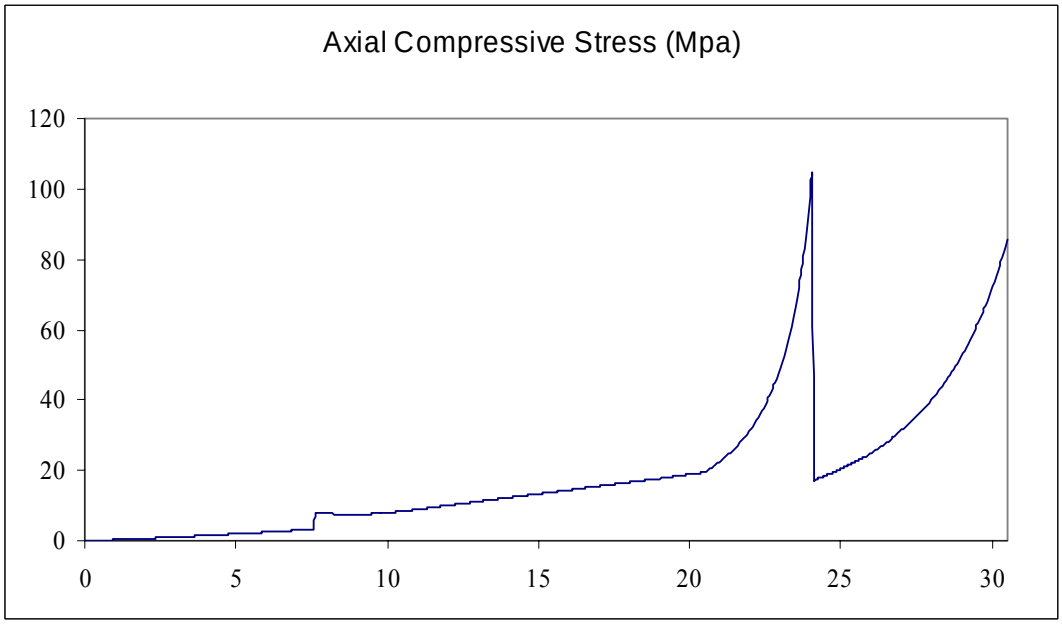

Figure 4.45 Axial compressive stress

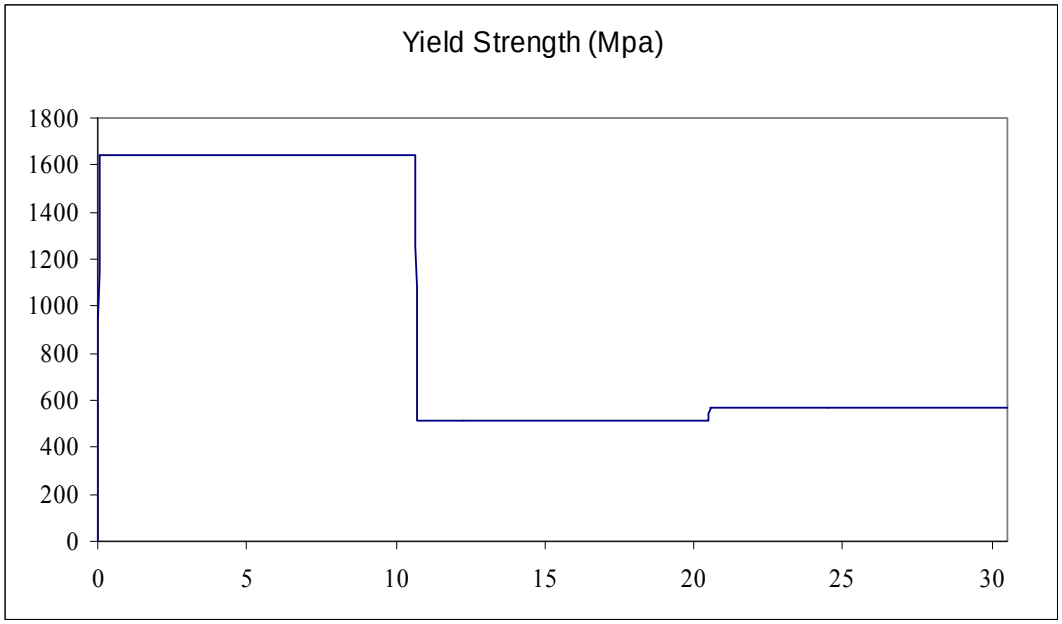

Figure 4.46 Yield strength

4.3.1.2 Weighting Factor Set 2:

The optimum solution found by FMLCAD for this case is obtained with a brass nose section and body section and aluminum tail section. The results are presented in Table 4-15 and following figures. Details of the results are given in Appendix C as tables. Optimization history for the states, objective function, constraint violation and the gradients of the objective function are given in following figures.

Table 4-15 Details of the optimum solution

Initial Conditions	
Initial x1:	5.03144
Initial x2:	1.07931
Initial x3:	25.8548
Optimization Results	
x1:	9.89645
x2:	1.08316
x3:	20.5008
Objective Function Value:	0.42098
Exit Flag:	1
Number of Iterations:	10
Final Step Size:	1
Optimization Algorithm:	medium-scale: SQP, Quasi-Newton, line-search
Gradient of Objective Function wrt x1:	-0.06787
Gradient of Objective Function wrt x2:	-0.52214
Gradient of Objective Function wrt x3:	0.14423
Final Mass (gr):	1252.40588
Final Cg Location (cm):	13.5347
Final Ix (grcm^2):	2229.73693
Final Iy (grcm^2):	55206.79715
Final Inertia Ratio:	0.04039
Error in Cg Location (%):	5.73983
Error in Ix2Iy Ratio (%):	2.89029
Figure of Merit:	3.70253

It is seen from the results of Table 4-15 that the optimum solution found by the code is acceptable with a mass of 1252 grams and error in inertia ratio of 2.9% although the error in center of gravity location is higher than 5%.

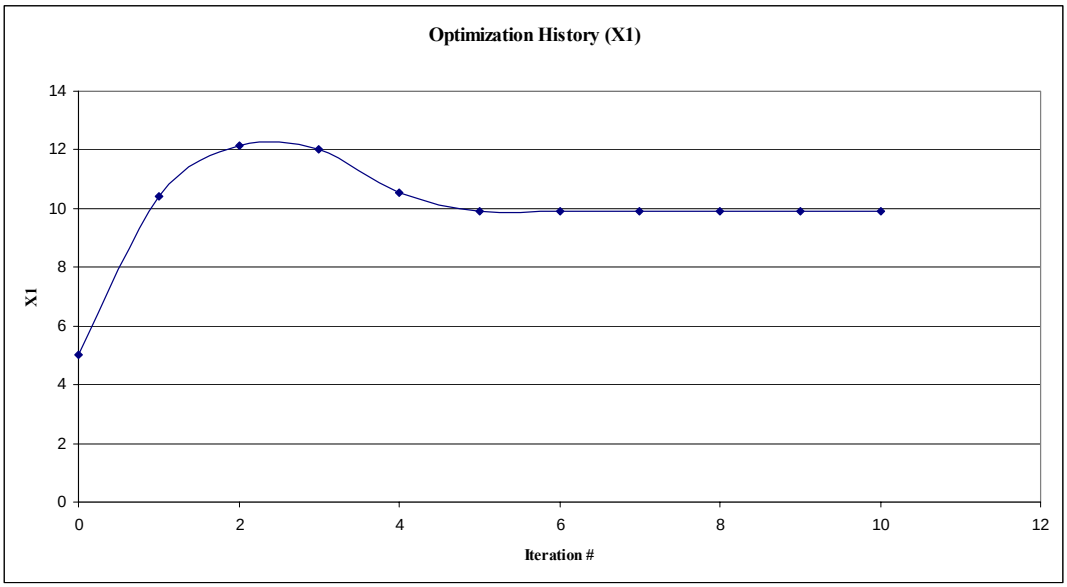

Figure 4.47 Optimization history for x1

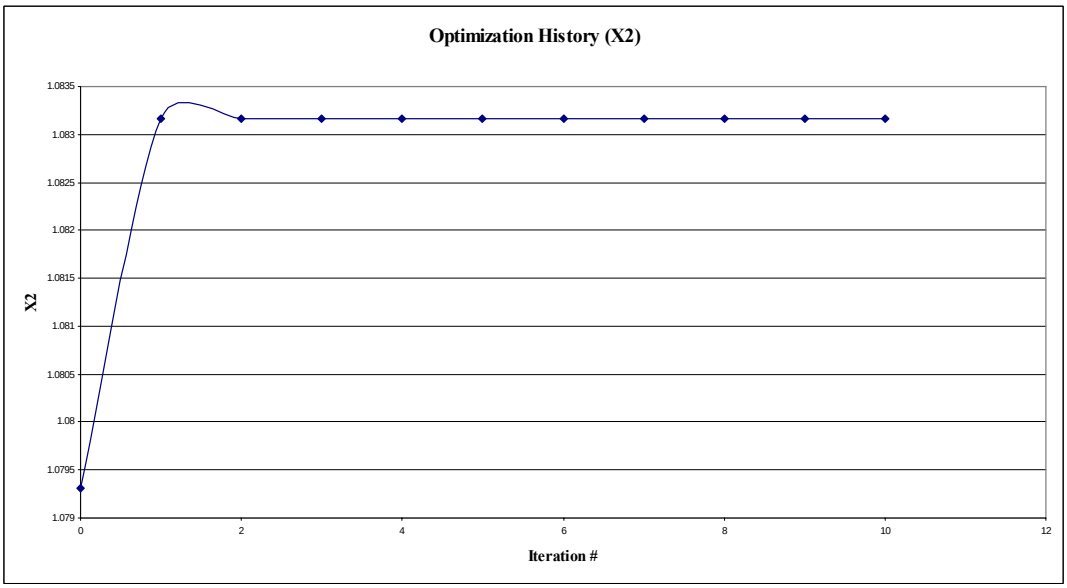

Figure 4.48 Optimization history for x2

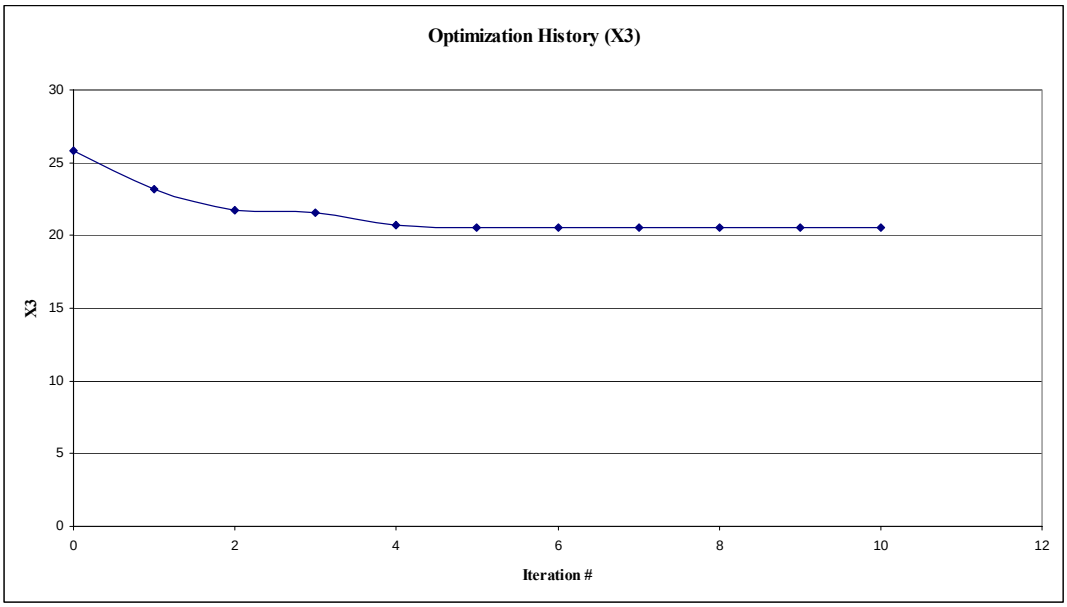

Figure 4.49 Optimization history for x3

It is seen that the value of the objective function and the design variables remain almost constant after 5th iteration. However, it takes the code to reach the optimum solution 10 steps, since the gradients of the objective function are improved although at the final solution the gradient with respect to x2 is relatively high when compared to gradients with respect to x1 and x3.

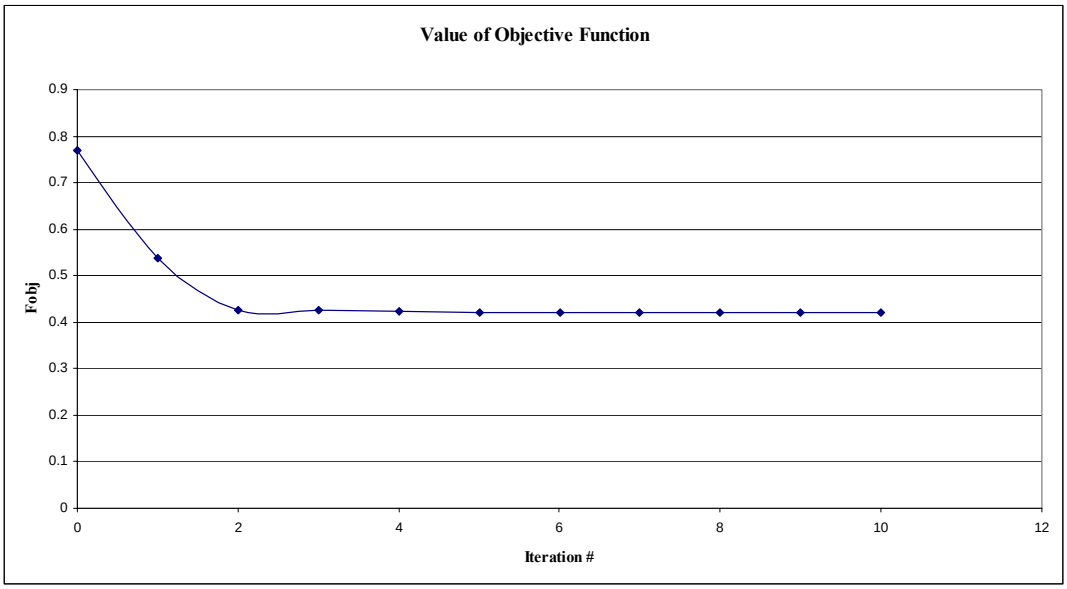

Figure 4.50 Optimization history for objective function

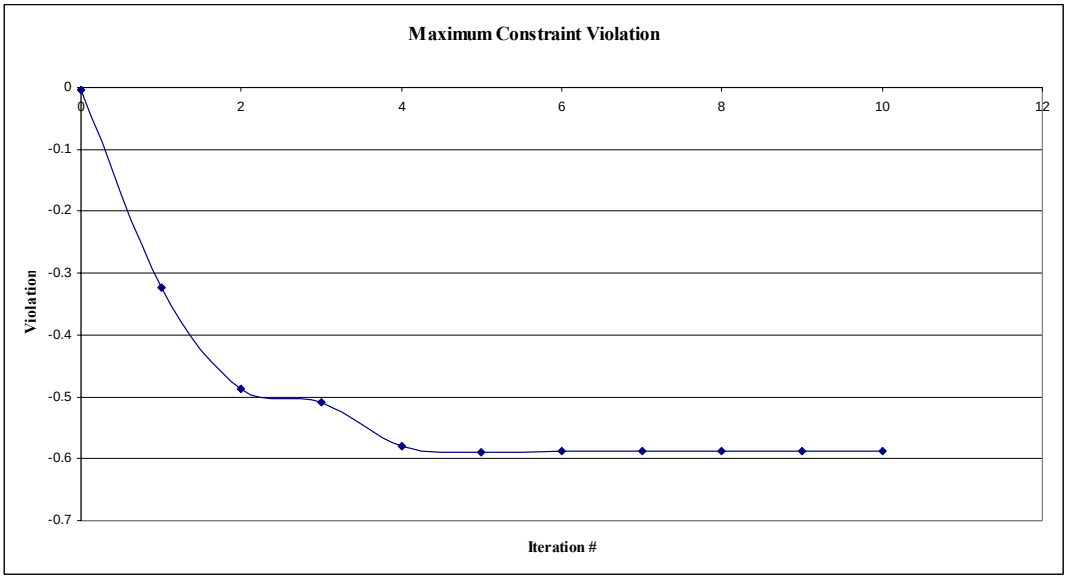

Figure 4.51 Optimization history for constraint violation

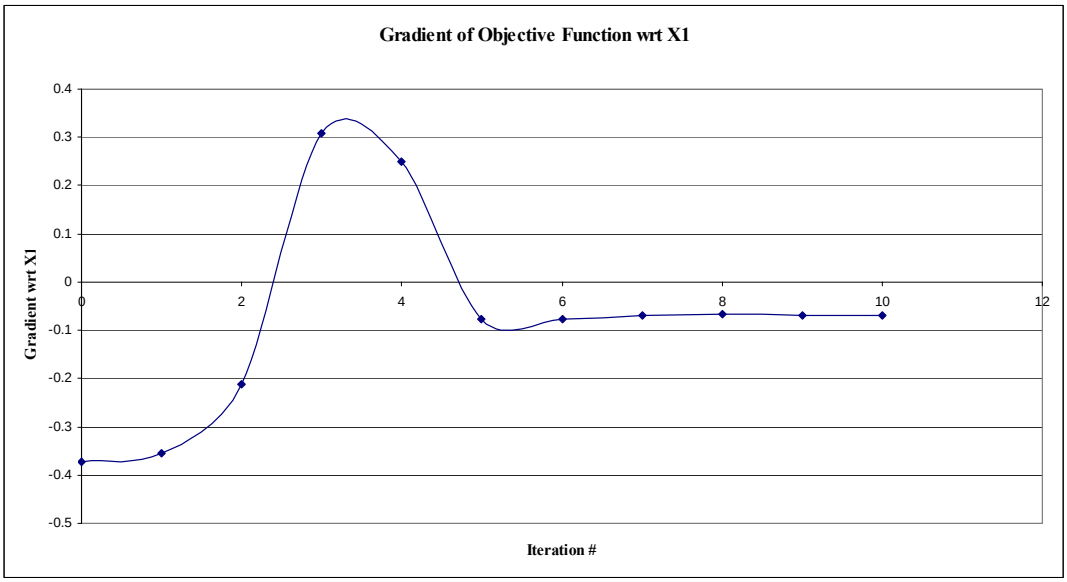

Figure 4.52 Optimization history for the gradient of objective function wrt x1

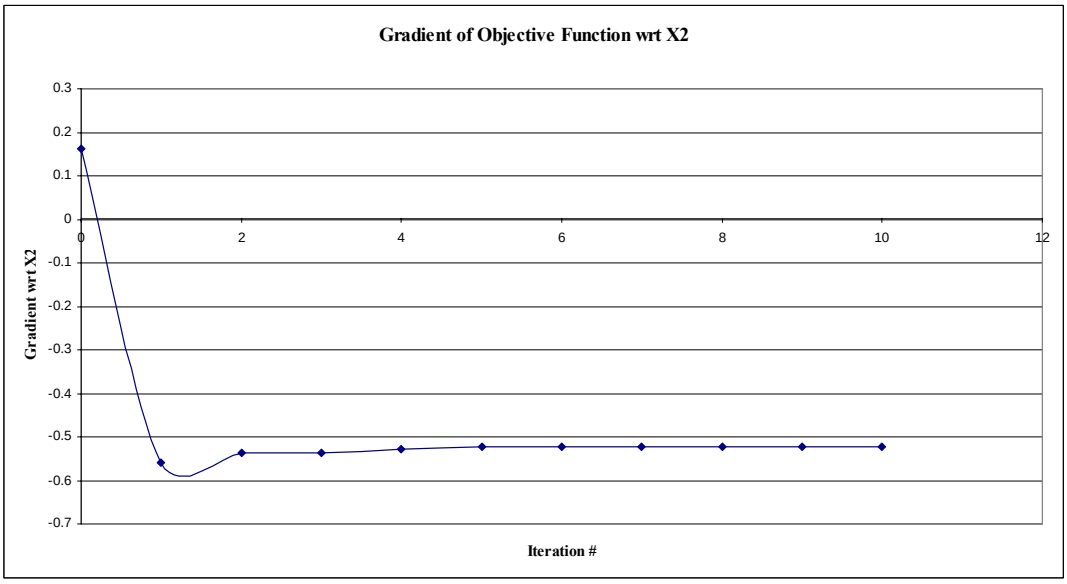

Figure 4.53 Optimization history for the gradient of objective function wrt x2

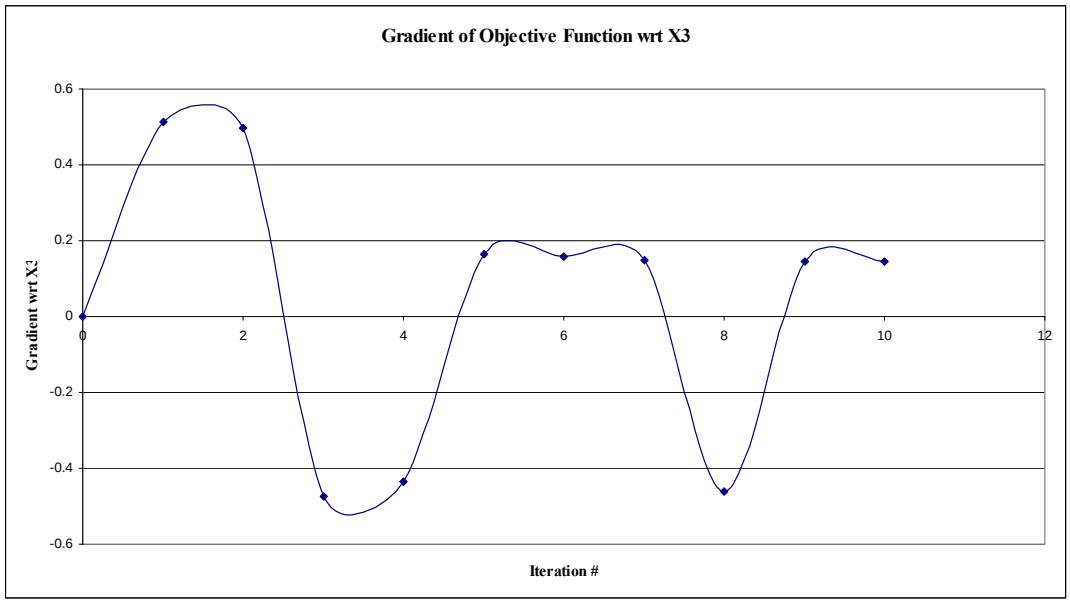

Figure 4.54 Optimization history for the gradient of objective function wrt x3

The final inner geometry of the FML model for weighting factor set 2 is given in Figure 4.55.

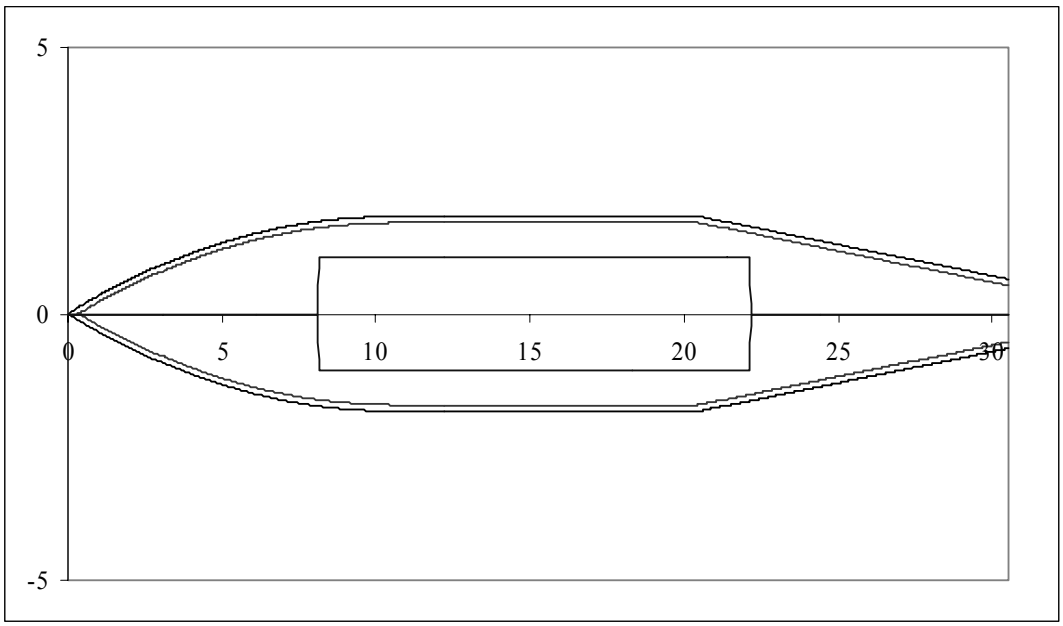

Figure 4.55 Optimum geometry for test case 2 at Mach 0.6 with weighting set 2

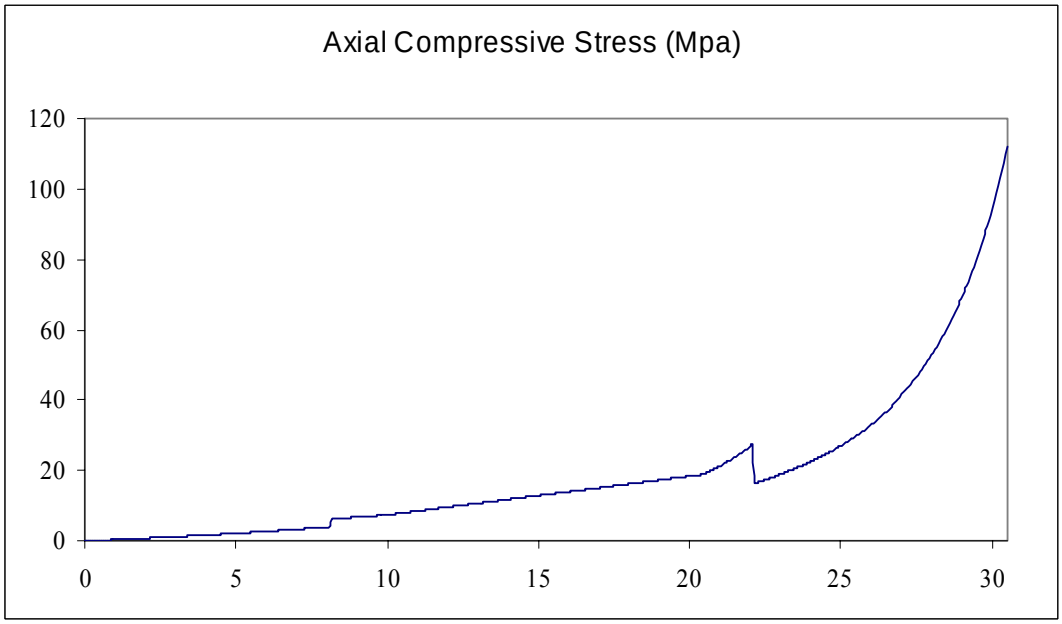

Figure 4.56 Axial compressive stress

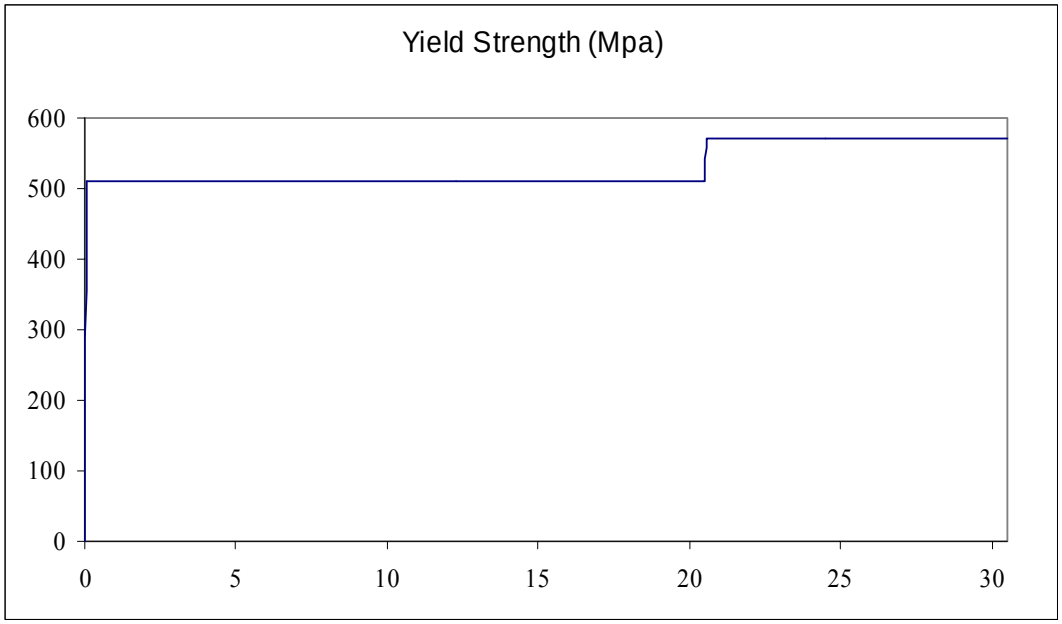

Figure 4.57 Yield strength

4.3.2 Results for Mach 1.2

4.3.2.1 Weighting Factor Set 1:

The optimum solution found by FMLCAD for this case is obtained with a brass nose section, steel body section and aluminum tail section. The results are presented in Table 4-16. Details of the results are given in Appendix C as tables.

It is seen from the results of Table 4-16 that the optimum solution found by the code is acceptable with a mass of 1041 grams and error in inertia ratio of 1.9% although error in the center of gravity location is higher than 5%. When the results presented in Table 4-16 are compared to the results in Table 4-14, it is seen that with increasing test speeds the FOM values increase too. Also the optimum solutions for two test velocities are different.

Table 4-16 Details of the optimum solution

Initial Conditions	
Initial x1:	5.03144
Initial x2:	1.07931
Initial x3:	25.8548
Optimization Results	
x1:	17.81258
x2:	1.09852
x3:	24.9131
Objective Function Value:	0.54863
Exit Flag:	1
Number of Iterations:	32
Final Step Size:	1
Optimization Algorithm:	medium-scale: SQP, Quasi-Newton, line-search
Gradient of Objective Function wrt x1:	-0.18778
Gradient of Objective Function wrt x2:	-0.63444
Gradient of Objective Function wrt x3:	0.43021
Final Mass (gr):	1041.58151
Final Cg Location (cm):	13.55742
Final Ix (grcm^2):	2027.51682
Final Iy (grcm^2):	47856.07561
Final Inertia Ratio:	0.04237
Error in Cg Location (%):	5.91733
Error in Ix/Iy Ratio (%):	1.86593
Figure of Merit:	2.94162

The optimization histories for the states, objective function, constraints and the gradients of the objective function are given in the following figures.

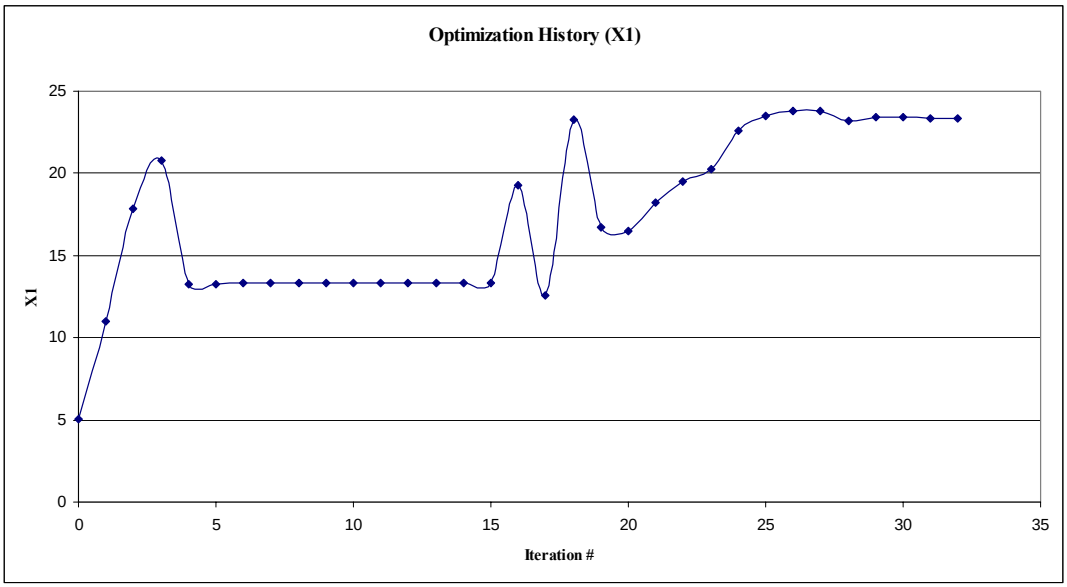

Figure 4.58 Optimization history for x1

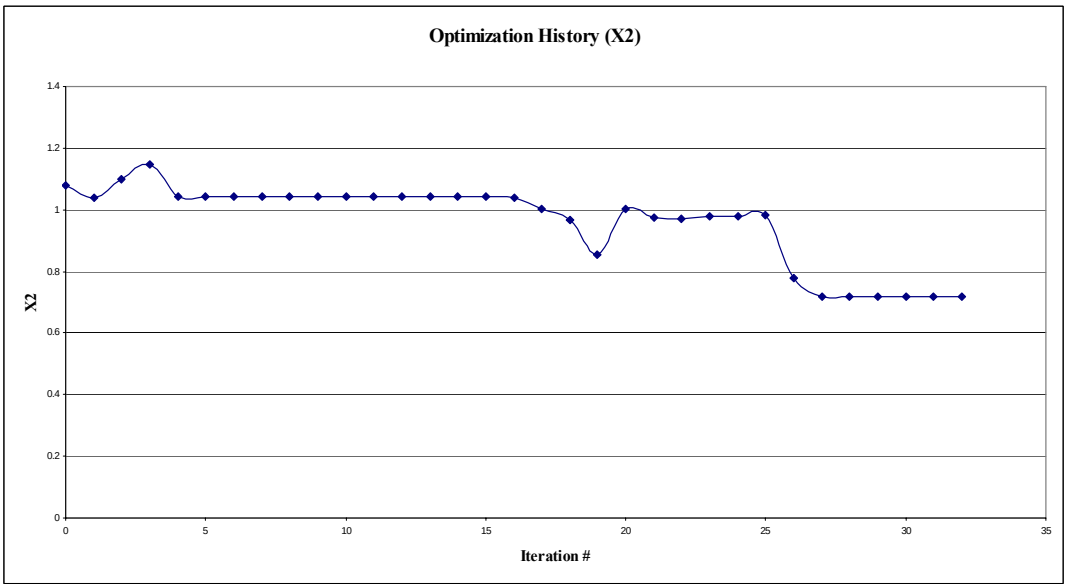

Figure 4.59 Optimization history for x2

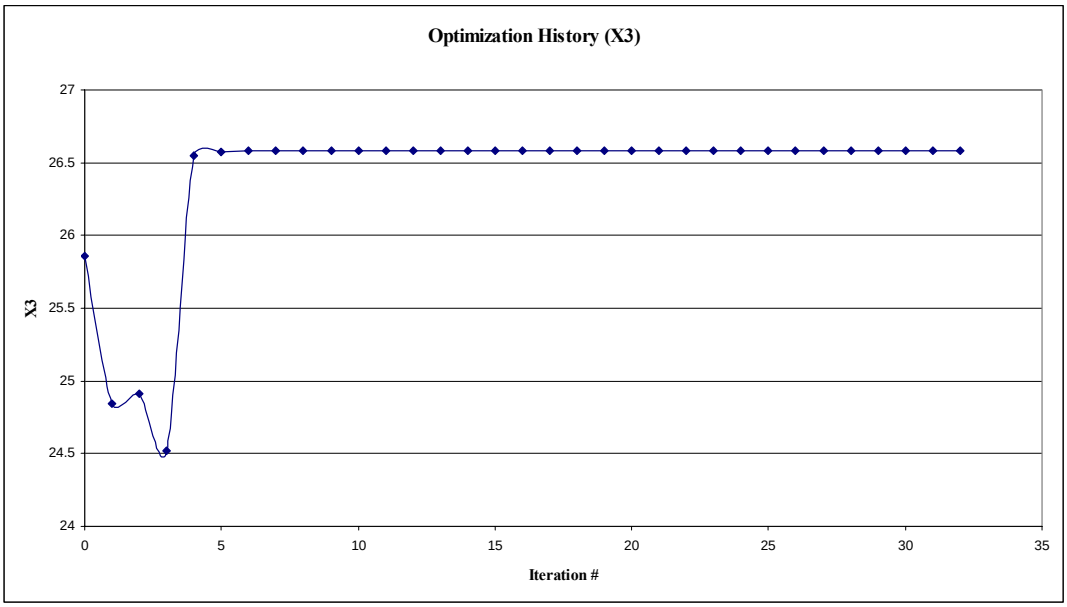

Figure 4.60 Optimization history for x3

Although the number of iterations made by `fmincon` is 32, the optimal solution is obtained at 2nd step. When the results are examined, the reason is obvious: the states at the 2nd iteration step give the minimum objective function value while satisfying the constraints. Also it is noticed that, for most of the optimization steps the violated constraint is the strength constraint.

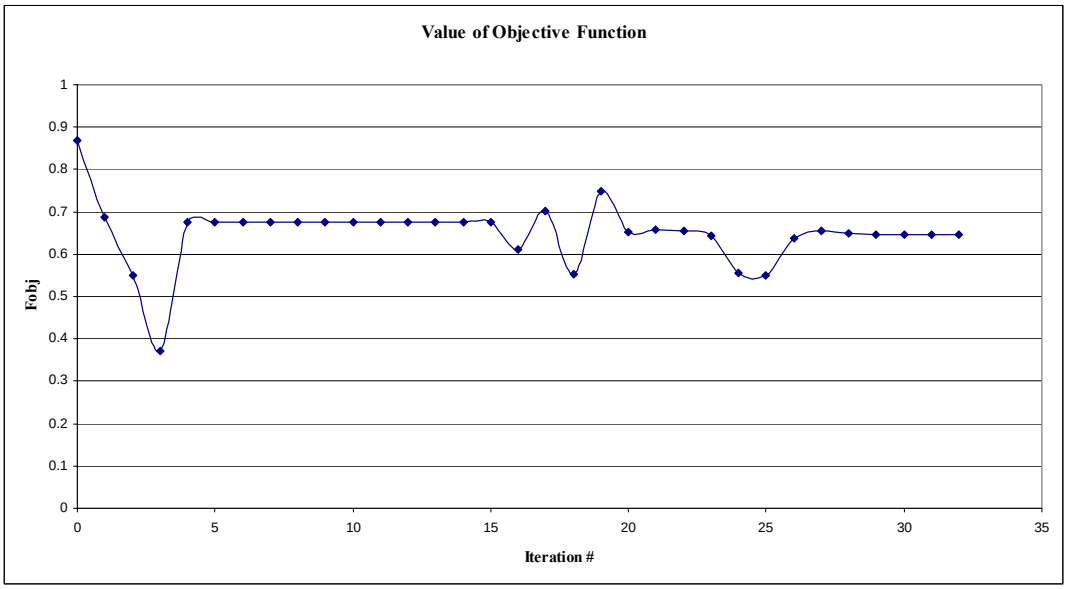

Figure 4.61 Optimization history for objective function

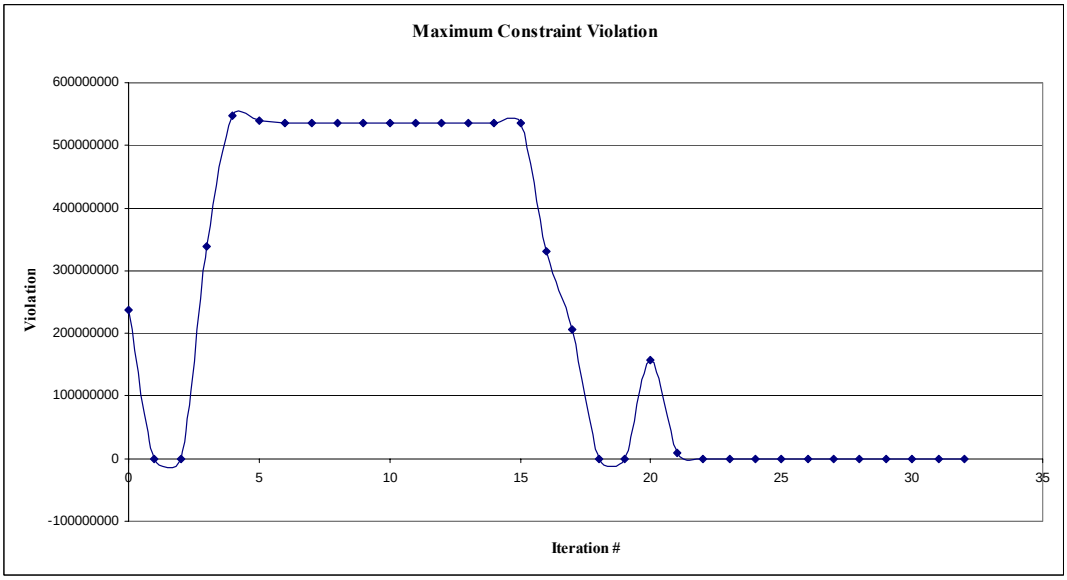

Figure 4.62 Optimization history for constraint violation

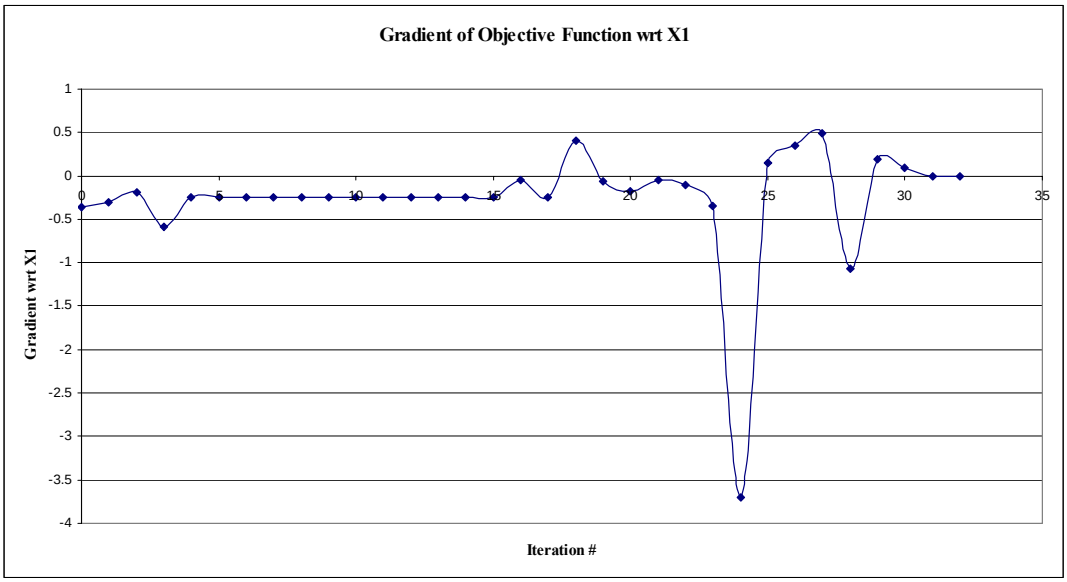

Figure 4.63 Optimization history for the gradient of objective function wrt x1

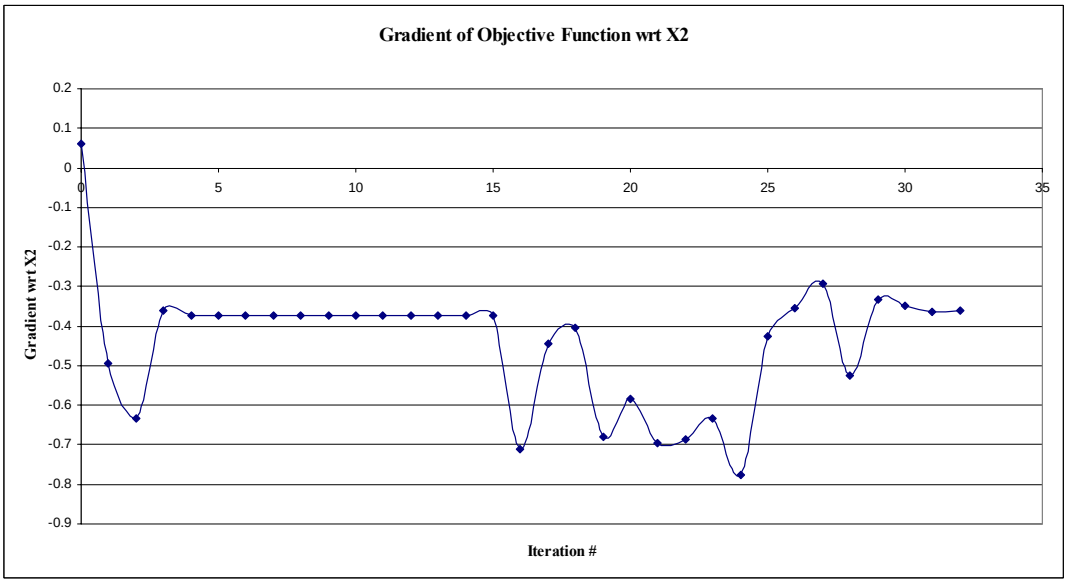

Figure 4.64 Optimization history for the gradient of objective function wrt x2

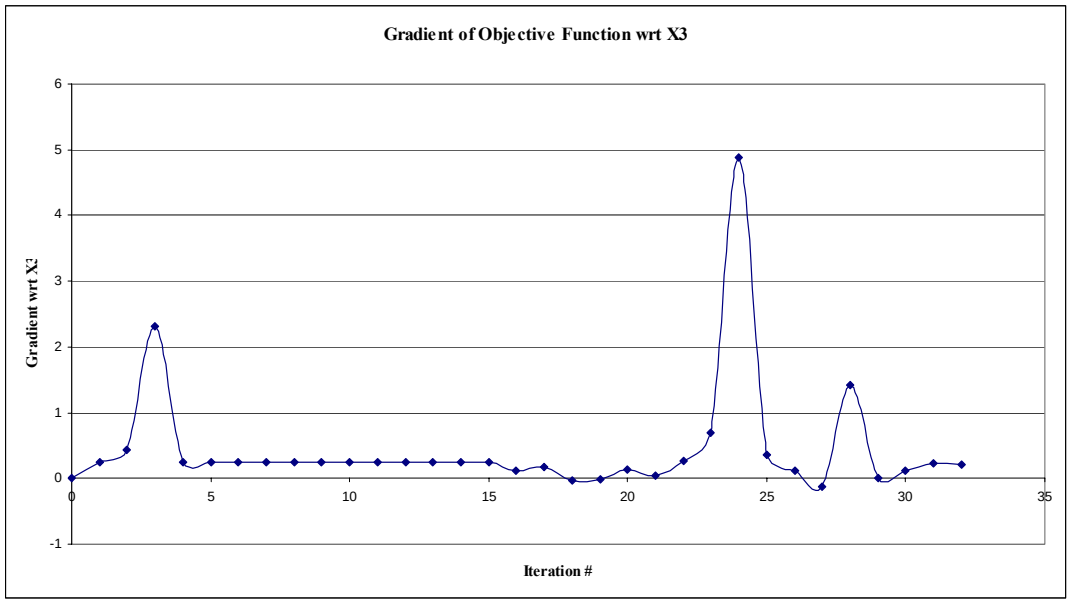

Figure 4.65 Optimization history for the gradient of objective function wrt x3

The optimum internal geometry of the FML model for the LDGP aircraft bomb of test case 2 is shown in Figure 4.66 together with the plot of the estimated axial compressive stress along the model axis (Figure 4.67).

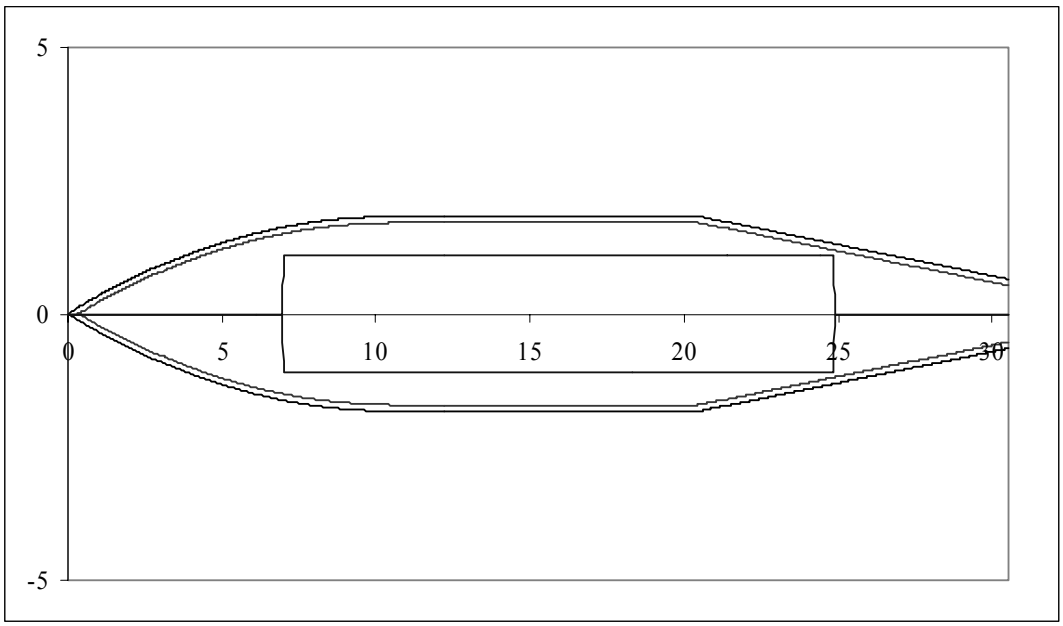

Figure 4.66 Optimum geometry for test case 1 at Mach 2.5 with weighting set 1

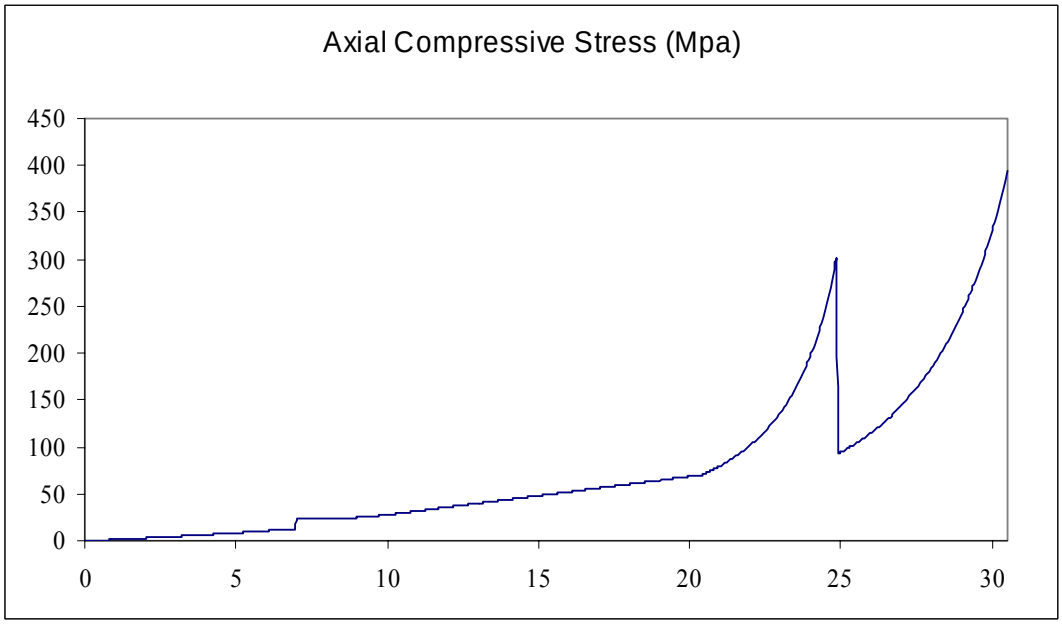

Figure 4.67 Axial compressive stress

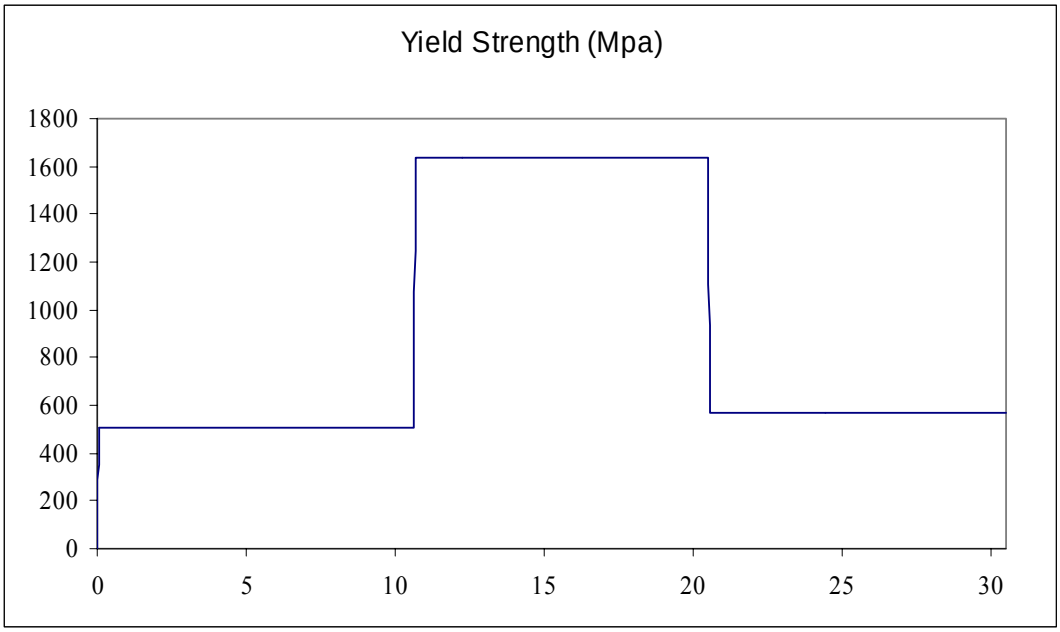

Figure 4.68 Yield strength

4.3.2.2 Weighting Factor Set 2:

The optimum solution found by FMLCAD for this case is obtained with a brass nose and body section and aluminum tail section. The results are presented in Table 4-17. Details of the results are given in Appendix C as tables.

Table 4-17 Details of the optimum solution

Initial Conditions	
Initial x1:	5.03144
Initial x2:	1.12619
Initial x3:	9.69664
Optimization Results	
x1:	13.87875
x2:	1.05182
x3:	22.13745
Objective Function Value:	0.54842
Exit Flag:	1
Number of Iterations:	50
Final Step Size:	1
Optimization Algorithm:	medium-scale: SQP, Quasi-Newton, line-search
Gradient of Objective Function wrt x1:	6.40102
Gradient of Objective Function wrt x2:	-0.61126
Gradient of Objective Function wrt x3:	-11.01969
Final Mass (gr):	1183.29488
Final Cg Location (cm):	13.70533
Final Ix (grcm^2):	2201.89888
Final Iy (grcm^2):	53094.5771
Final Inertia Ratio:	0.04147
Error in Cg Location (%):	7.07293
Error in Ix2Iy Ratio (%):	0.28769
Figure of Merit:	3.18091

It is seen from the results of Table 4-17 that the optimum solution found by the code is acceptable with a mass of 1183 grams and error in inertia ratio of 0.29% although the error in center of gravity location is higher than 5%. The optimization histories for the states, objective function, constraints and the gradients of the objective function are given in the following figures.

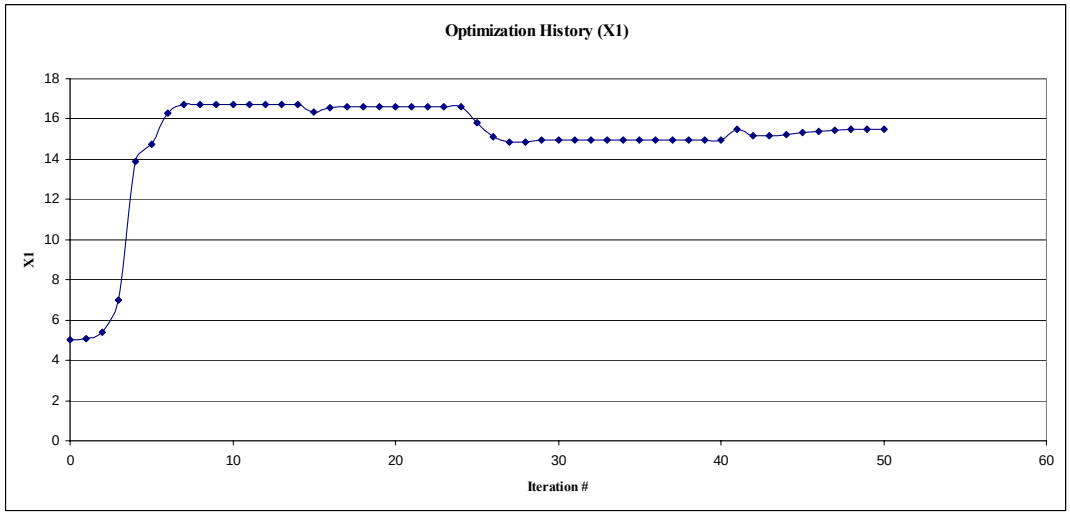

Figure 4.69 Optimization history for x1

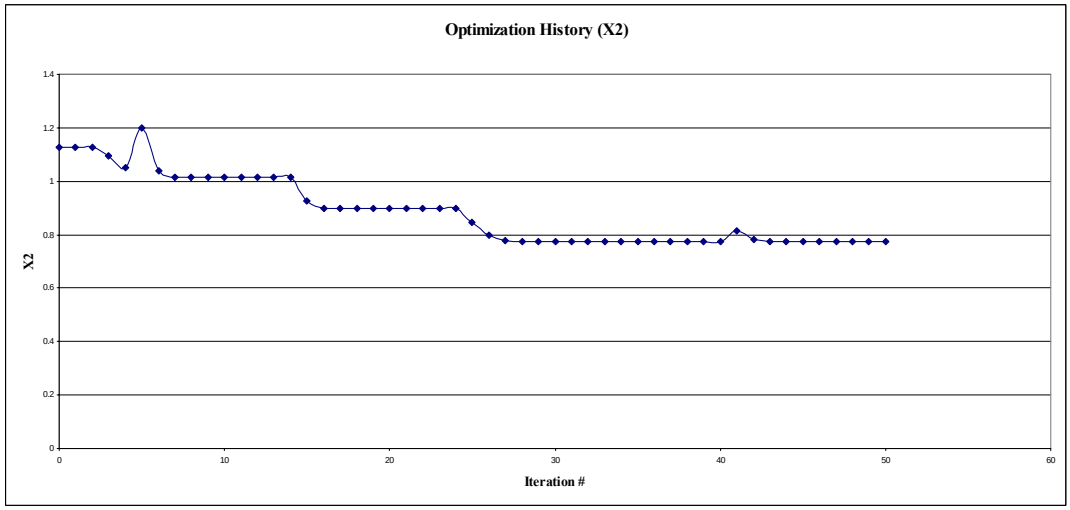

Figure 4.70 Optimization history for x2

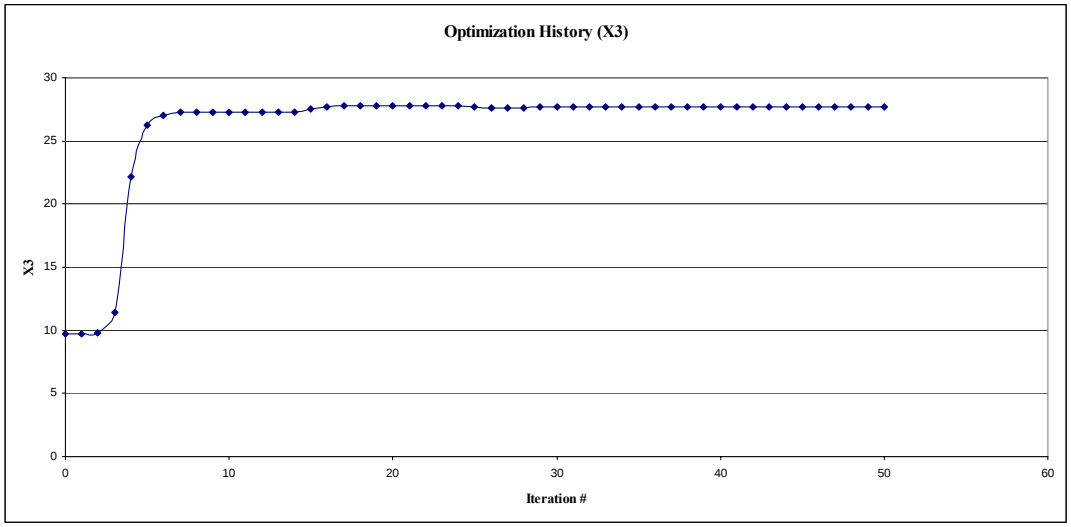

Figure 4.71 Optimization history for x3

It is seen that although the total number of iterations is 50, the optimum solution is obtained at the step 4. The reason is obvious, the minimum value of the objective function with no constraint violation is obtained at this step. However, when the histories of the gradients of the objective function is examined it is seen that values of gradients are quite high.

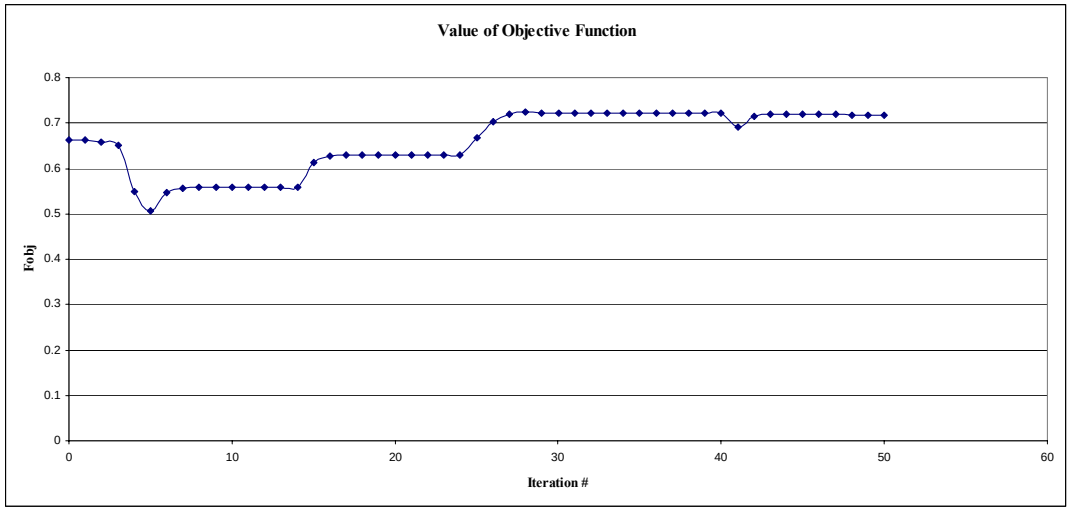

Figure 4.72 Optimization history for objective function

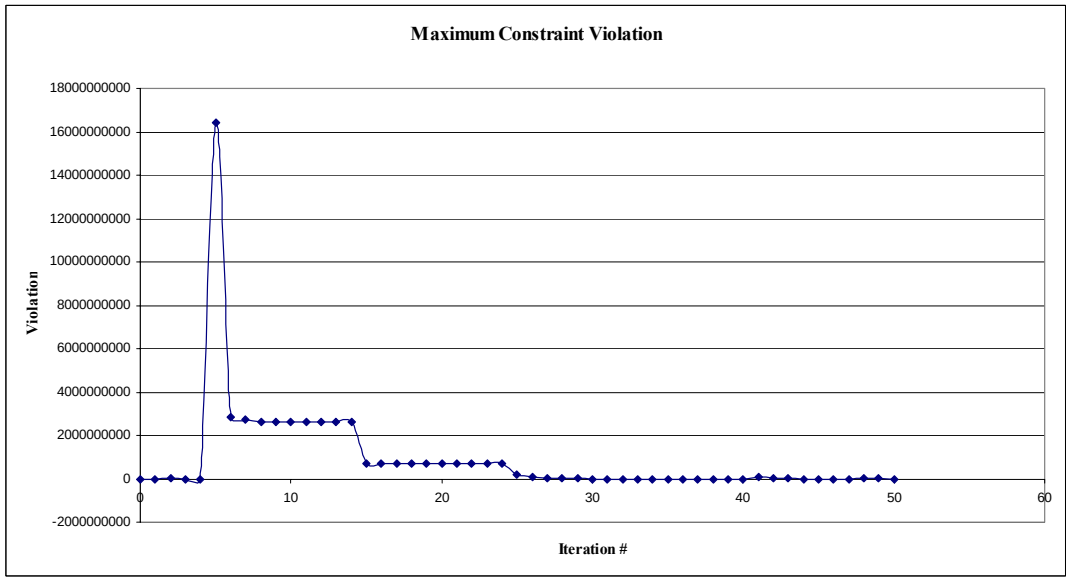

Figure 4.73 Optimization history for constraint violation

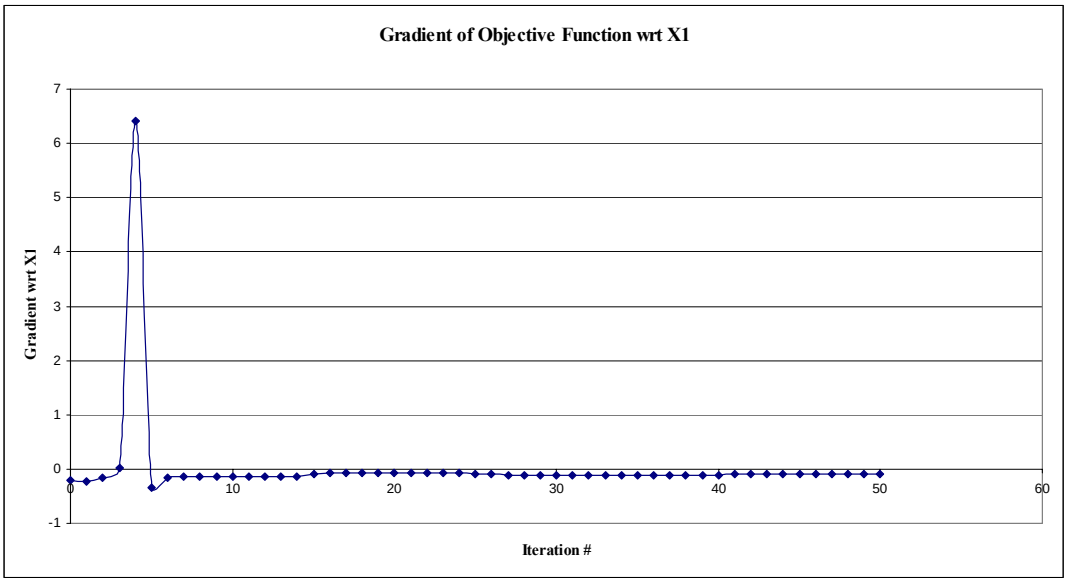

Figure 4.74 Optimization history for the gradient of objective function wrt x1

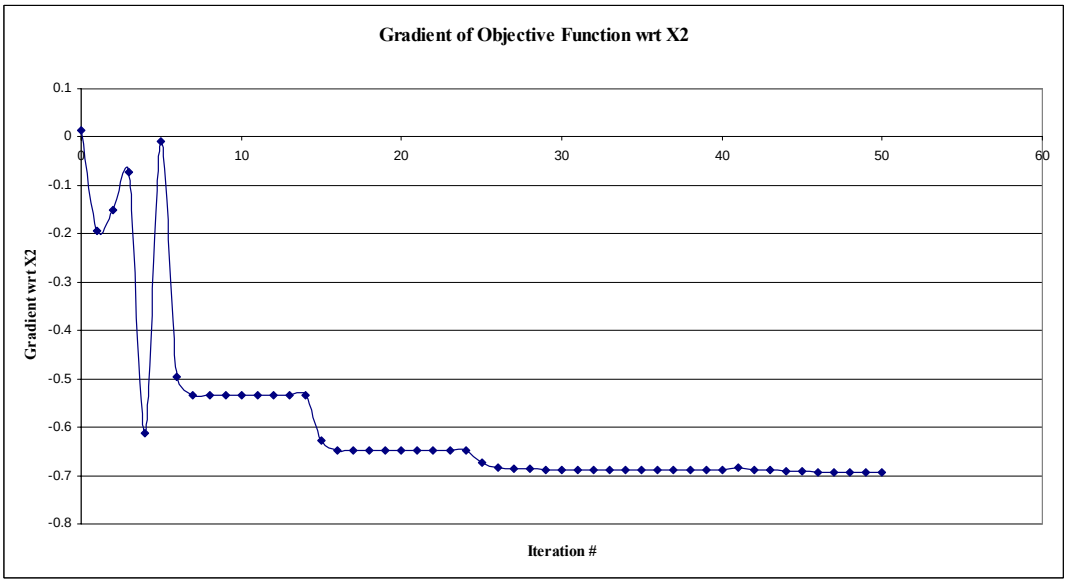

Figure 4.75 Optimization history for the gradient of objective function wrt x2

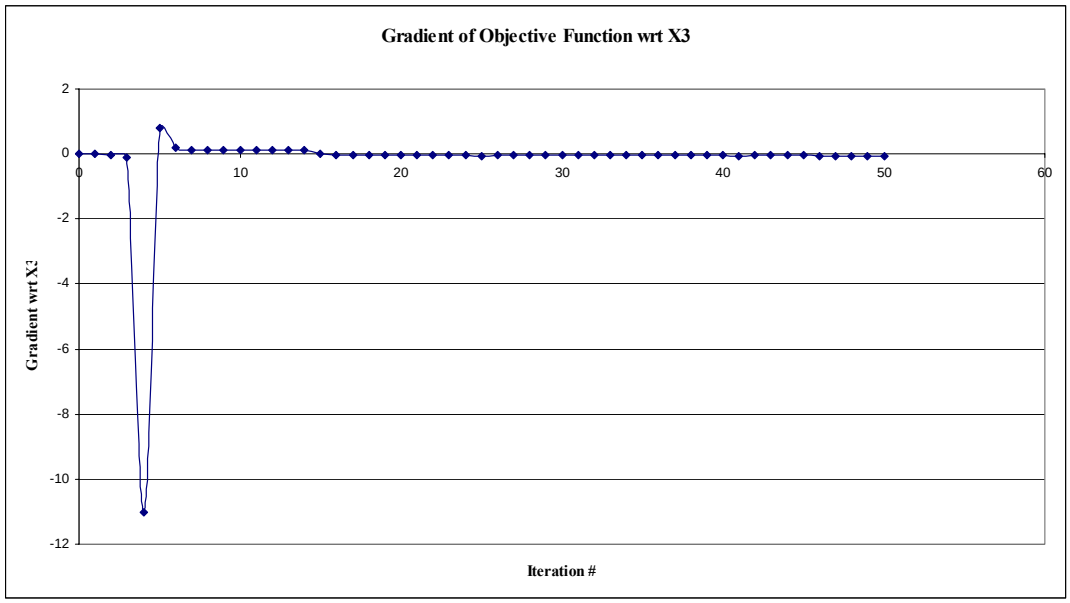

Figure 4.76 Optimization history for the gradient of objective function wrt x3

The final inner geometry of the FML model for weighting factor set 2 is given in Figure 4.77.

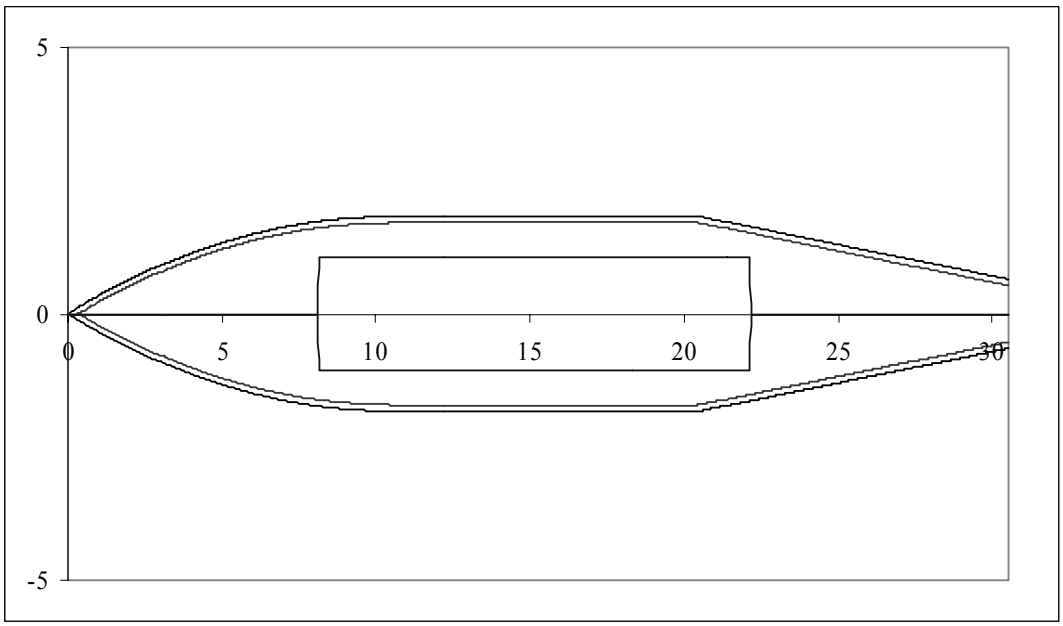

Figure 4.77 Optimum geometry for test case 2 at Mach 1.2with weighting set 2

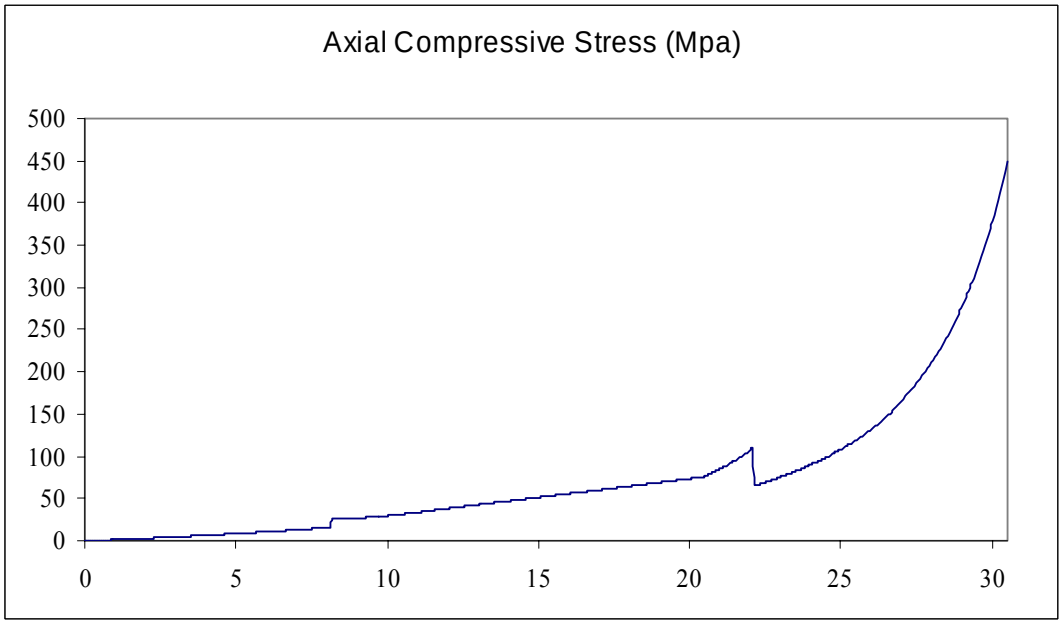

Figure 4.78 Axial compressive stress plot

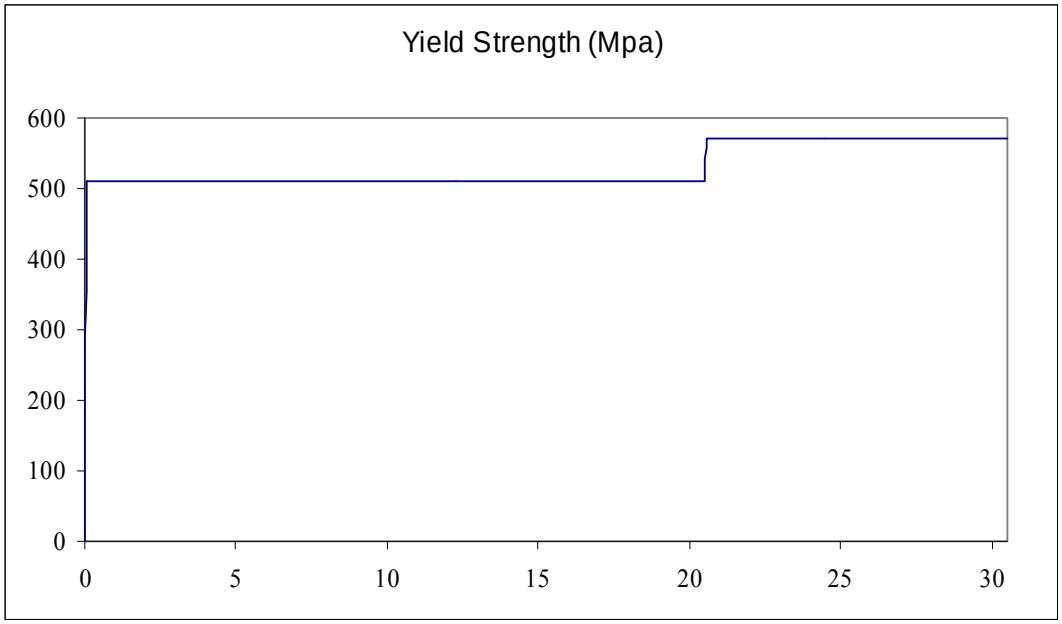

Figure 4.79 Yield strength

4.4 SUMMARY OF THE RESULTS

The results of the test cases are summarized in Table 4-18. It is seen that, for test case 1, medium range unguided artillery rocket, the optimum solutions found by FMLCAD are quite good. For weighting factor set 2 ($w_1 = 0.4$, $w_2 = 0.4$, $w_3 = 0.2$), percent error in centre of gravity location between the targeted value and the resulting value is 0.03% and percent error in inertia ratio is 0.4%. The model weights are less than 750 gr for both weighting factor sets, which is almost half of the weight of similar aeroballistic range models designed and tested at the FML in the past. However, for test case 2, the percent errors in centre of gravity location and inertia ratio are higher than those found for test case 1, although they are still acceptable.

Table 4-18 Summary of Results

Test Case	Weighting Factor	Mach #	Error in Cg Location (%)	Error in Inertia Ratio (%)	Mass (gr)
1	Set 1	1.5	0.03	2.53	680.1
		2.5	0.03	2.53	680.1
	Set 2	1.5	0.03	0.40	701.3
		2.5	0.03	0.40	701.3
2	Set 1	0.6	6.30	1.55	911.0
		1.2	5.92	1.87	1041.6
	Set 2	0.6	7.07	0.29	1183.3
		1.2	7.07	0.29	1183.3

The computation time spent by FMLCAD during optimization is given in Table 4-19. The test cases were solved on an AMD Athlon ThunderBird 1.2 GHz computer with 512 MB of RAM, which is a low-end system for today. When the test cases are solved on an Intel Centrino 1.6 GHz computer with 1 GB of RAM, a high end system for today, it is seen that the computation time is shortened by 50% for all of the test cases.

Table 4-19 Computation time for the test cases

Test Case	Weighting Factor	Mach #	Total Computation Time (minutes)
1	Set 1	1.5	27
		2.5	28
	Set 2	1.5	26
		2.5	28
2	Set 1	0.6	23
		1.2	30
	Set 2	0.6	23
		1.2	30

CHAPTER 5

DISCUSSION AND CONCLUSION

5.1 DISCUSSION

In this study, a computer aided design tool, based on the devised design methodology, is developed which will be used in the actual design optimization of aeroballistic range models.

The optimization code, which is named as FMLCAD, takes the actual munition parameters as input from the user and tries to find the optimum aeroballistic range model configuration (materials selection and internal geometry) which satisfies the geometrical as well as test conditions imposed constraints.

FMLCAD is intended to be used by a trained user who has some knowledge about aeroballistic range model design beforehand. Although the graphical user interface, which is very simple in appearance, provides easy access to the design variables and also save/load functionality for the model files, a trained designer is needed to enter the correct and error free inputs expected by the computational routines. The results of the code are not to be used directly for manufacturing purposes, but they are starting points for the detailed mechanical design process. After the results are obtained, the designer should work on material interfaces, fin connection details and make fine tuning on the final configuration before generating technical drawings for the manufacturing.

Objective function used in the optimization is derived in Chapter 2. Each time the weighting factors of this objective function are changed, a new optimization problem is defined. Thus, for each different weighting factor set, the optimum solution is different. Then, appropriate selection of the weighting factors is a critical issue in optimization of the aeroballistic range model design. Test cases are solved with two different sets of weighting factors and the results are compared in Table 4-18; the effects of the weighting factors are obvious. Model weight is smaller for set 1 ($w_1 = 0.3333$, $w_2 = 0.3333$, $w_3 = 0.3333$) when compared to set 2 ($w1 = 0.4$, $w_2 = 0.4$, $w_3 = 0.2$). But the percent errors in the other two objectives are usually smaller for set 2 when compared to set 1.

One notice about the weighting factors is that, they should be selected carefully, considering the requirements for the specific test. For example, when the aeroballistic range model being designed is a non-spinning one, the second objective, i.e. matching the inertia ratio, is not very important. Then in such a case, FMLCAD can be run with a weighting factor set like ($w_1 = 0.5$, $w_2 = 0.0$, $w_3 = 0.5$) and centre of gravity location can be matched with a very small error.

The `fmincon` function of the Optimization Toolbox of Matlab®, which is the optimization routine that runs under FMLCAD, uses a classical method (SQP and line search). Although this function works fine for most of the time, there is no guarantee that it will converge to a global extremum of the objective function. In fact, this is a common problem in optimization as long as the classical methods are applied. This is the reason behind the initial condition sensitivity of the design methodology derived in Chapter 4 and shown as flow chart in Figure 4.3. To overcome this problem, a set of initial conditions are generated, which span the entire solution domain (i.e. the region defined by the geometrical constraints) and for each external configuration all of these initial conditions are swept. Only way to overcome the initial guess sensitivity problem is to use methods that guarantee global optima. Currently there are two methods commonly used as global optimization techniques: simulated annealing and genetic algorithm. However, both of these methods take very long computational times to reach the solution.

For the test case 1, medium range unguided artillery rocket, the optimum solutions found are quite good. In fact, for the second weighting factor set, the results are even better than the similar aeroballistic range models that were actually designed and tested at FML. However, for test case 2, the percent errors in centre of gravity location and inertia ratio are relatively high when compared to test case 1. The reason behind this is the shape of the LDGP aircraft bomb. For the bomb to be carried externally, radius of the aft section must be decreased so that the bomb fits under the wing. However, this decreasing tail cross-section brings a big trouble to the aeroballistic range model design. During launch, the axial compressive stresses acting on the base of the model (i.e. the tail section) are so great that this section fails under the loading and in order to prevent this, the tail section is usually designed without any holes, which makes it almost impossible to match the required similarity parameters exactly.

This is a well – known problem about the LDGP bomb geometry and only way to overcome this problem is to increase the effective sabot contact area which is used to accelerate the model. Alternative sabot designs have been proposed to be used with the aeroballistic range models of LDGP bombs, some of which "pull" the model from the maximum cross-section [13], [14] and some push the model by enclosing the tail cone instead of the base [2]. However, FMLCAD, currently, only works for traditional pusher type sabots and the best that can be obtained without any modification of the acceleration area are the results presented in Table 4-18.

FMLCAD, being the first version of its kind, has some limitations. These can be listed as:

- To run FMLCAD, Matlab® should be installed with the Optimization Toolbox.
- FMLCAD stress routine assumes that, a traditional pusher type sabot is used to accelerate the model.
- Sabot design is not included in the optimization routine.
- Static loading assumed.

- Material interfaces are not modeled.
- Fins are always modeled as parallel the longitudinal axis of the model.

5.2 CONCLUSION

In conclusion, the major objective of this thesis, which is to develop a code that will be used for actual design of aeroballistic range models, is achieved successfully. For this purpose, a design methodology which provides a successful approach to the aeroballistic range model design problem is derived. Developed code (FMLCAD) is tested with two test cases, which are taken from real life experiences. Both test cases are similar to the models that were tested at FML in the past and the results are highly satisfactory; for the first test case, even better than the actual models that were tested.

Although it has some limitations as stated above, FMLCAD is a very useful tool and will satisfy the needs of the Flight Mechanics Division of TUBITAK-SAGE. By using this code, the aeroballistic range models will be designed in shorter time when compared to manual design. Currently, it takes an experienced designer about 60 hours to design an aeroballistic range model from scratch, where most of the time is spent on selecting materials and deciding on internal geometry. However, by the use of FMLCAD, this design time will be reduced by at least 50%. Also for most cases, the code will provide better solutions than that can be reached by manual design. Furthermore, possible errors that may be caused by designers will be eliminated.

5.3 FUTURE WORK

As first future work, a version of the FMLCAD may be coded that uses the newly introduced Genetic Algorithm Toolbox of Matlab® Release 14 (Matlab® 7) and the results obtained using Optimization Toolbox and Genetic Algorithm Toolbox may be compared. However, this work should involve some modifications to the Genetic Algorithm Toolbox functions since in its current form Genetic Algorithm

Toolbox does not support constrained optimization. Next step in this future work should be to develop a code that decides on which method, i.e. classical or global, to use without user intervention.

Some or all of the above mentioned limitations may be overcome in the future work, since the foundations of the design methodology is derived successfully in this thesis.

First limitation, need to use Matlab, can be removed by coding FMLCAD on a different development platform and making it a stand alone application. However, this would require development of an optimization routine that will solve the problem instead of `fmincon`. Other functions of FMLCAD can be directly used or modified depending on the selected development platform. The development platform would be a high level language such as Delphi or Visual Basic. Also, an integration of the Mechanical Desktop environment can be done in this stand alone version, so that the technical drawings of the resulting optimum geometries may be generated automatically.

Optimization of sabot design is a complex subject and may be examined in a future M.Sc. study.

Another future work may be an improvement on the stress routine. It would not be feasible to use a finite difference approach at each iteration step in terms of CPU time, but a FEA may be applied to the final solution. This would eliminate the need to use another software for final strength analysis.

The error introduced by modeling fins parallel to the longitudinal axis is very small and negligible. Even commercial software packages used in aeroballistics such as PRODAS and APC 2002 model the fins as always parallel. So it will not be necessary to make any additional work on this limitation in the future.

Another future work may be the addition of a module to find an optimum model configuration for a range of different test Mach numbers specified by user. Currently, FMLCAD only searches for the optimum result for only one test Mach number input by the user. However, based on the results of the test cases, it is seen that sometimes the optimum solution is different for different test Mach numbers. Then, it would be better if a future version of the code is developed which makes optimization for a range of Mach numbers and decides on the best possible configuration for that Mach number range. This approach would eliminate the need to use different model designs for different test Mach numbers and also shorten the time needed for design work.

If the proposed future works are carried out, someday, FMLCAD may even become a complete design tool for aeroballistic range testing.

REFERENCES

[1]. Mahmutyazıcıoğlu, G., Tanrıkulu, Ö., "**Aeroballistic Research Laboratory (ARL) Project**", 47th ARA Meeting, (1996)

[2]. Kutluay, Ü., Aytar-Ortaç, S., "**Design Optimization for Aeroballistic Range Models of a Low Drag Aircraft Bomb**", 55th ARA Meeting, (2004)

[3]. "**Ballistic Range Technology**"; AGARDograph No138

[4]. Daniel, D.C., Boudreau, A.H., "**Trends in International Aerospace Ground Test Facilities**", AIAA Paper, AIAA-93-0348, (1993)

[5]. Morgan, J.A., "**A Brief History of Cannon Launch**", AIAA Paper, AIAA-97-3138, (1997)

[6]. Dayanç, K., Mahmutyazıcıoğlu G., Yazgan, A.E., "**Open Air Ballistic Range Experience**", 49th ARA Meeting, (1998)

[7]. Mahmutyazıcıoğlu, G., Ekütekin, V., Korkmaz, Ş, Aytar, S., "**TÜBİTAK-SAGE Flight Mechanics Laboratory**", Mühendis ve Makina, (Aralık 2000)

[8]. Mahmutyazıcıoğlu, G., et. al., "**Flight Mechanics Laboratory Project Report**", TÜBİTAK-SAGE Report, (2000)

[9]. Neihouse, A.I., Pepoon, P.W., "**Dynamic Similitude Between a Model and a Full-Scale Body for Model Investigation at Full-Scale Mach Number**", NACA TN-2062, (1950)

[10]. Anderson, J.D., "**Fundamentals of Aerodynamics**", McGraw-Hill, (1991)

[11]. Wolowicz, C.H., Bowman, J.S., Gilbert, W.P., "**Similitude Requirements and Scaling Relationships as Applied to Model Testing**", NASA TP-1435, (1979)

[12]. Dupuis, A., "**Aerodynamic Characteristics and Analysis of a MK82 Bomb Configuration from Free Flight Tests**", AIAA Paper, AIAA-2001-4325, (2001)

[13]. Dupuis, A., Boivin, M., "**Model, Sabot Design and Free-Flight Tests of the DRDC-ISL A1, A2 and A3 Models**", DRDC Valcartier, TM 2003-077, (2003)

[14]. Dupuis, A., Boivin, M., "**Sabot Performance for Gun Launched Scaled Models of MK83-CF, MK83-BSU85 LD; MK-84CF and GBU-16 Bombs**", DRDC Valcartier, TM 2002-212, (2002)

[15]. Nanlcin, S.L., "**High Velocity Model and Sabot Design**", 1st ARA Meeting, (1961)

[16]. Gothe, K.K., "**A New Stress Routine for the Projectile Design Analysis System (PRODAS)**", 40th ARA Meeting, (1989)

[17]. Korkmaz, Ş., Sular Ç., "**Solmod Software Requirements Document**", TÜBİTAK-SAGE Report, (2002)

[18].Hicks, J.B., "**Computer Calculation of Sabot-Model Launch Stresses Using the Finite Element Method**", 25th ARA Meeting, (1974)

[19]. Cable, A.J., "**An Examination of Failing Loads in Model Launching Experiments**", 7th ARA Meeting, (1964)

[20]. Williams, A.E., Pritz, K.J., "**An Evaluation of Sabot Designs from Static Tests**", 29th ARA Meeting, (1979)

[21]. Kutluay, Ü., Karbancıoğlu, İ.M., Esi, M.A., "**H Project FML Model Design Report**", TÜBİTAK-SAGE Report, (2003)

[22]. Aytar, S., "**Optimal External Configuration Design of Missiles**", M.Sc. Thesis, METU, (2002)

[23]. Tanrıkulu Ö., Ercan V., "**Optimal External Configuration Design of Unguided Missiles**", AIAA Paper, AIAA-97-3725, (1997)

[24]. Venkataraman, P., "**Applied Optimization with MATLAB® Programming**", John Wiley & Sons, (2002)

[25]. "**Optimization Toolbox User's Guide**", Mathworks, (2003)

[26]. "**MathWorks Technical Solutions, Solution Number: 1-19HX9**", Mathworks, (2004)

[27]. Shigley, J.E., "**Mechanical Engineering Design**", McGraw-Hill, (1989)

[28]. Moore, F.G., Hymer, T.C., "**The 2002 Version of the Aeroprediction Code: Users Guide**", Dahlgren Division, NSWC, (2002)

[29]. Beer, F.P., Johnston Jr., E.R., "**Vector Mechanics for Engineers**", McGraw-Hill, (1990)

[30]. Beer, F.P., Johnston Jr., E.R., "**Mechanics of Materials**", McGraw-Hill, (1992)

[31]. Neuhaus, J.R., "**Modeling Mass Properties in an Object Oriented Simulation",** AIAA Paper, AIAA-2004-5166, (2004)

[32]. Baruh, H., "**Analytical Dynamics**", McGraw Hill, (1999)

[33]. Chapra, S.C., Canale, R.P., "**Numerical Methods for Engineers**", McGraw Hill,(2002)

APPENDIX A

INERTIA FORMULATIONS

The external geometries of the components of an aeroballistic range model are defined in Chapter 2.2 . Here, the equations to calculate the mass, centre of gravity, axial and transverse moment of inertia are given.

A.1 MASS PROPERTIES OF AN ARBITRARY GEOMETRY

For a continuous function *y(x)*, defined in the interval [x_0, x_1], the volume formed by a rotation of 360° around x axis is defined by:

$$V = \pi \int_{x_0}^{x_1} y(x)^2 \, dx \tag{A.1}$$

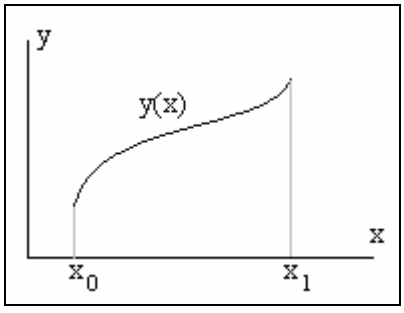

Figure A-1 A general function y(x)

Then the mass of the solid geometry formed by this volume is given by:

$$m = \rho V = \pi\rho \int_{x_0}^{x_1} y(x)^2 \, dx \tag{A.2}$$

The centre of gravity of this solid can be calculated by [29]:

$$CM = \frac{\int_{dm_0}^{dm_1} x \, dm}{m} \tag{A.3}$$

where dm is obtained for a disc of *dx* thickness and *y(x)* radius (Figure A-2) as:

$$dm = \pi\rho \; y(x)^2 \, dx \tag{A.4}$$

Thus, centre of gravity takes the following form:

$$CM = \frac{\pi\rho \int_{x_0}^{x_1} x \cdot y(x)^2 \, dx}{m} \tag{A.5}$$

The axial inertia of a thin disc is given by [29]:

$$I_x = \frac{m_{disc} \cdot r^2}{2} \tag{A.6}$$

The axisymmetric body of revolution given in Figure A-2 can be considered as made up of infinitesimally thin discs. Then the axial inertia becomes:

$$I_x = \int_{dm_0}^{dm_1} \frac{r^2}{2} dm \tag{A.7}$$

Since *r=y(x)* Equation (A.7) becomes as follows after substituting Equation (A.4):

$$I_x = \frac{1}{2}\pi\rho \int_{x_0}^{x_1} y(x)^4 dx \tag{A.8}$$

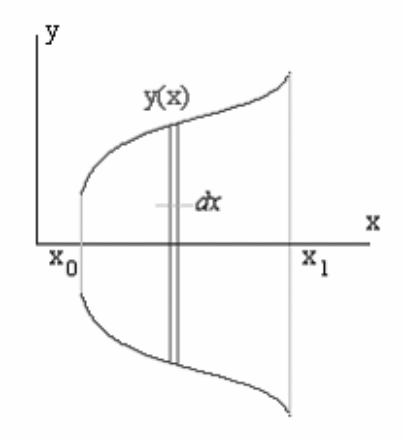

Figure A-2 Body of revolution (axisymmetric body)

The transverse inertia of a thin disc is given by [29]:

$$I_y = \left(\frac{r^2}{4} + x^2\right) m_{disc} \tag{A.9}$$

Similar to the derivation of Equation (A.8), total transverse inertia is obtained as:

$$I_y = \pi\rho \int_{x_0}^{x_1} \left(\frac{y(x)^2}{4} + x^2 \right) y(x)^2 dx \tag{A.10}$$

A.2 MASS PROPERTIES OF COMMON SHAPES

A.2.1 Rectangle

Axial inertia of a rectangle (Figure A-3) is given by [30]:

$$I_x = \frac{m_{rectangular} \cdot b_y{}^2}{12} \tag{A.11}$$

where b_y is the height (y distance) of the rectangle (Figure A-3).The transverse inertia of a rectangular area is given by [30]:

$$I_y = \frac{m_{rectangular} \cdot b_x{}^2}{12} \tag{A.12}$$

$$I_z = \frac{m_{rectangular} \cdot b_x \cdot b_y}{12} \tag{A.13}$$

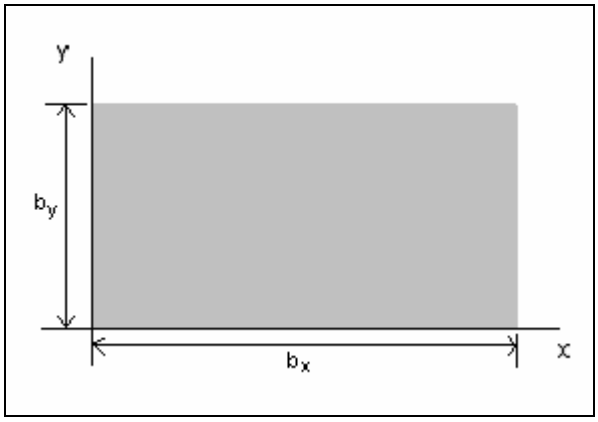

Figure A-3 Rectangular area

A.2.2 Triangle

Axial inertia of a triangle is given by [30]:

$$I_x = \frac{m_{triangular} \cdot b_y{}^2}{18} \tag{A.14}$$

Transverse inertia of a triangle is given by:

$$I_y = \frac{m_{triangular} \cdot b_x{}^2}{18} \tag{A.15}$$

$$I_z = \frac{m_{triangular} \cdot b_x \cdot b_y}{18} \tag{A.16}$$

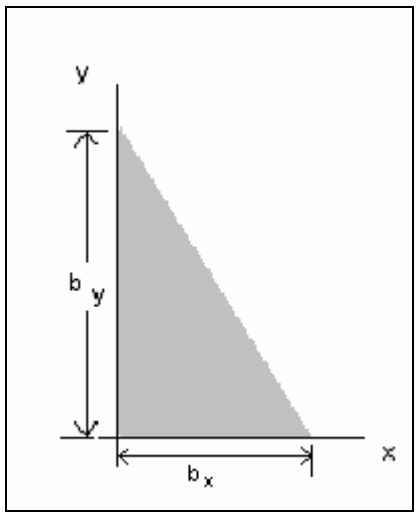

Figure A-4 Triangular area

A.3 CALCULATING THE MASS PROPERTIES OF COMPOSITE GEOMETRIES

For a body of n parts, the mass properties are the combination of the properties of each of the subparts. The mass of each part is simply added to find the total mass. However, to find centre of gravity location and calculate the inertia values of the master body some mathematics is involved. The center of gravity location can be computed as follows [31]:

$$m = \int dm \tag{A.17}$$

$$\int r dm = 0 \tag{A.18}$$

where r denotes the centre of gravity location of the master body (Figure A-5.) Then the centre of gravity location of a body consisting n parts becomes:

$$r = \frac{\sum_{i=1}^{n} r_i \cdot m_i}{\sum_{i=1}^{n} m_i} \tag{A.19}$$

The inertia values of a body made of n parts can be computed once the centre of gravity locations are found. Consider the general fin geometry of Figure 2.4. The fin is made up of three triangles and a rectangle. Then the axial inertias of the fin can be calculated as [17]:

$$I_{x_{total}} = \sum \left(I_x + m \cdot (d_y)^2 \right) \tag{A.20}$$

where d_y is the y distance between the centre of the fin and the centre of gravity of the subpart (Figure A-6).

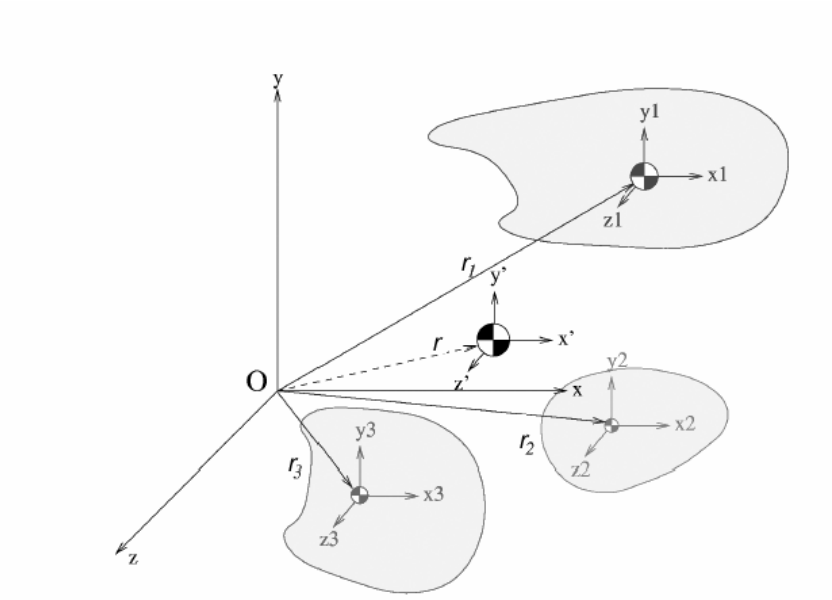

Figure A-5 The centre of gravity location for a body of n parts

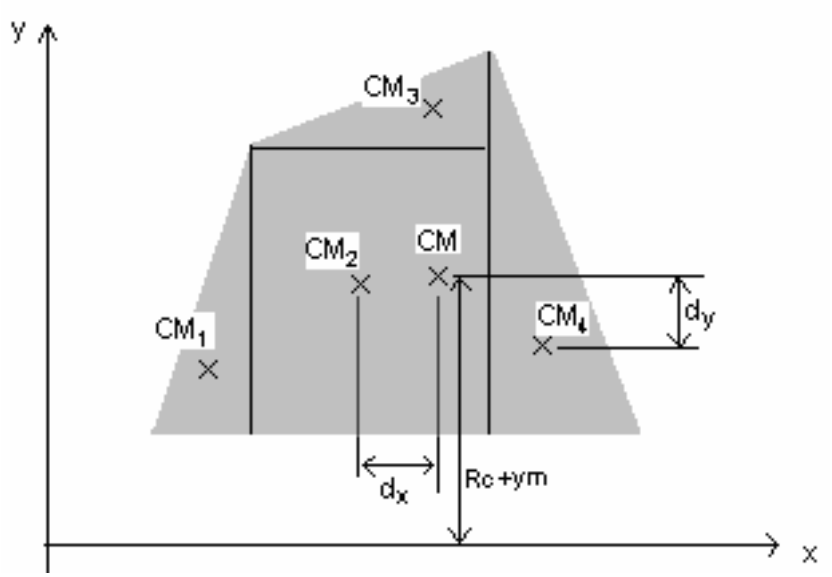

Figure A-6 Subparts for a general fin

The transverse inertia calculation for the fins is handled similarly [17]:

$$I_{y_{total}} = \sum \left(I_y + m \cdot (d_x)^2 \right) \tag{A.21}$$

$$I_{z_{total}} = \sum \left(I_z + m \cdot (d_x)^2 \right) \tag{A.22}$$

where d_x is the x distance between the centre of the fin and the centre of gravity of the subpart (Figure A-6).

However, these transverse inertias are with respect to the local reference frames of each fin and must be transferred to the models frame of reference (Figure A-7). This is done by transforming the local frame of reference of each fin (x_i, y_i, z_i) to the model's frame of reference (X, Y, Z) by first a rotation of θ_i angle (Figure A-8) about x_i axis and then application of parallel axis theorem [32]. The transformation matrix is defined as:

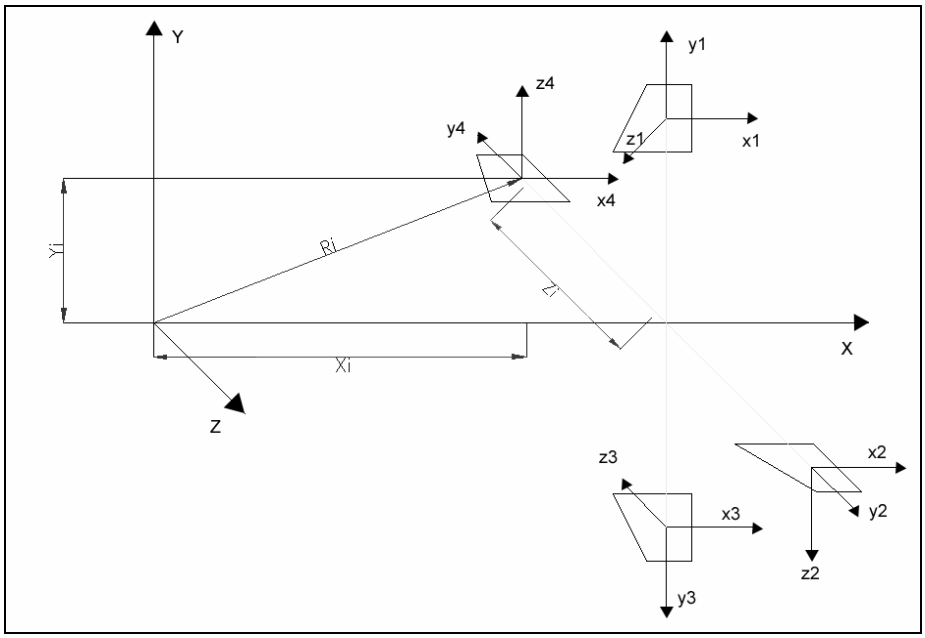

Figure A-7 Local and global reference frames for a 4 finned model

$$R_i = \begin{bmatrix} 1 & 0 & 0 \\ 0 & \cos(\theta_i) & \sin(\theta_i) \\ 0 & -\sin(\theta_i) & \cos(\theta_i) \end{bmatrix} \tag{A.23}$$

The inertia tensor for a fin in local reference frame can be defined as:

$$(I_i)_{x_i y_i z_i} = \begin{bmatrix} I_x & 0 & 0 \\ 0 & I_y & 0 \\ 0 & 0 & I_z \end{bmatrix} \tag{A.24}$$

Then the inertia tensor for the rotated local frame is obtained:

$$(I_i)_{(x_i y_i z_i)'} = R_i \cdot (I_i)_{x_i y_i z_i} \cdot R_i^T \tag{A.25}$$

The next step is to apply the parallel axis theorem:

$$(I_i)_{XYZ} = (I_i)_{(x_i y_i z_i)'} + \begin{bmatrix} Y_i^2 + Z_i^2 & -X_i \cdot Y_i & -X_i \cdot Z_i \\ -X_i \cdot Y_i & X_i^2 + Z_i^2 & -Y_i \cdot Z_i \\ -X_i \cdot Z_i & -Y_i \cdot Z_i & X_i^2 + Y_i^2 \end{bmatrix} \cdot m_i \tag{A.26}$$

where m_i is the mass of the i^{th} fin.

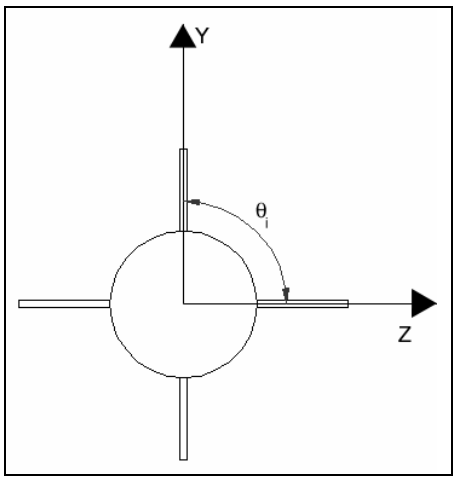

Figure A-8 Fin orientation

The total inertia of the fins can be found by simply adding the inertia tensors of the fins:

$$I_{fin} = \sum_{i=!}^{n_{fin}} (I_i)_{XYZ} \tag{A.27}$$

where n_{fin} is the total number of fins. The axial and transverse inertia contribution of the fins to the model is simply:

$$I_{fin_x} = I_{fin}[1,1] \tag{A.28}$$

$$I_{fin_y} = I_{fin}[2,2] \tag{A.29}$$

APPENDIX B

DETAILS OF THE SOLUTION FOR TEST CASE 1

The optimum solution is denoted with bold and italic rows in the following tables. Mass is in grams and the location of centre of gravity is measured in centimeters from nose.

B.1 RESULTS AT MACH 1.5 WITH WEIGHTING FACTOR SET 1

Table B-1 Results for Test case – 1 at Mach 1.5 with weighting factor set 1

Case #	Nose	Body	Tail	ErrCg(%)	ErrI(%)	FOM	Flag
1	Steel	Steel	Steel	13.63	2.02	5.35	1
2	Steel	Steel	Aluminum	0.04	7.59	2.80	1
3	Steel	Aluminum	Steel	20.72	31.87	17.65	1
4	Steel	Aluminum	Aluminum	3.75	41.80	15.27	1
5	Steel	Aluminum	Brass	29.73	9.52	13.20	1
6	Steel	Brass	Aluminum	1.49	3.20	1.82	1
7	Steel	Brass	Brass	9.48	5.30	5.06	1
8	Steel	Brass	Steel	7.76	4.79	4.31	1
9	Steel	Steel	Brass	16.15	1.45	6.01	1
10	Aluminum	Aluminum	Aluminum	12.85	3.69	5.56	1
11	Aluminum	Aluminum	Steel	35.35	5.36	13.65	1
12	Aluminum	Steel	Aluminum	7.69	5.25	4.54	1
13	Aluminum	Steel	Steel	24.22	17.13	13.89	1
14	Aluminum	Steel	Brass	25.92	13.42	13.24	1
15	Aluminum	Brass	Steel	33.78	3.67	12.84	1
16	Aluminum	Brass	Brass	23.79	12.63	12.25	1
17	Aluminum	Brass	Aluminum	6.03	9.16	5.30	1
18	Aluminum	Aluminum	Brass	33.55	2.53	12.14	1
19	Brass	Brass	Brass	12.55	3.05	5.34	1
20	Brass	Brass	Aluminum	0.11	3.07	1.31	1
21	Brass	Aluminum	Brass	29.49	10.22	13.36	1
22	Brass	Aluminum	Aluminum	16.02	26.25	14.24	1
23	Brass	Aluminum	Steel	27.47	15.99	14.61	1
24	***Brass***	***Steel***	***Aluminum***	***0.03***	***2.53***	***1.08***	***1***
25	Brass	Steel	Steel	6.08	8.56	5.01	1
26	Brass	Steel	Brass	10.97	14.92	8.77	1
27	Brass	Brass	Steel	10.27	3.08	4.59	1

Table B-2 Results for Test case – 1 at Mach 1.5 with weighting factor set 1 (cont'd)

Case #	x1	x2	x3	Mass	Cg	Ix/Iy
1	33.19	0.96	39.21	405.4	19.39	0.0071
2	0.87	0.14	37.42	764.4	17.06	0.0067
3	30.55	0.99	38.07	351.0	20.60	0.0050
4	27.33	0.98	34.33	256.3	17.71	0.0042
5	33.67	0.93	39.21	362.3	22.14	0.0066
6	20.40	0.20	39.21	790.8	16.81	0.0071
7	32.40	0.98	39.21	404.5	18.69	0.0069
8	32.48	0.98	39.21	391.7	18.39	0.0069
9	33.27	0.96	39.21	418.4	19.82	0.0072
10	32.24	0.98	39.21	140.2	19.26	0.0070
11	30.77	0.99	39.21	252.4	23.10	0.0077
12	10.32	0.20	39.21	682.7	18.38	0.0077
13	31.73	0.99	39.21	318.5	21.20	0.0085
14	31.16	0.96	39.08	378.2	21.49	0.0083
15	1.48	0.99	10.62	1072.3	22.83	0.0070
16	31.20	0.99	39.07	354.1	21.13	0.0082
17	12.48	0.25	39.21	713.8	18.10	0.0080
18	27.39	0.96	39.16	323.0	22.79	0.0075
19	33.11	0.97	39.21	427.3	19.21	0.0071
20	17.14	0.32	20.50	761.2	17.09	0.0071
21	33.82	0.92	39.21	379.7	22.10	0.0065
22	6.62	0.52	9.33	457.4	19.80	0.0054
23	33.34	0.93	38.87	359.5	21.76	0.0061
24	***37.22***	***0.39***	***39.21***	***680.1***	***17.07***	***0.0075***
25	32.40	0.98	39.21	392.5	18.11	0.0067
26	31.80	0.98	38.77	419.5	18.94	0.0062
27	32.89	0.96	39.21	429.1	18.82	0.0071

B.2 RESULTS AT MACH 1.5 WITH WEIGHTING FACTOR SET 2

Table B-3 Results for Test case – 1 at Mach 1.5 with weighting factor set 2

Case #	Nose	Body	Tail	ErrCg(%)	ErrI(%)	FOM	Flag
1	Steel	Steel	Steel	6.21	7.87	5.71	1
2	Steel	Steel	Aluminum	0.03	7.58	3.20	1
3	Steel	Aluminum	Steel	27.86	15.49	17.41	1
4	Steel	Aluminum	Aluminum	3.75	41.80	18.27	1
5	Steel	Aluminum	Brass	28.28	17.29	18.30	1
6	Steel	Brass	Aluminum	1.58	1.50	1.37	1
7	Steel	Brass	Brass	14.73	0.45	6.16	1
8	Steel	Brass	Steel	6.57	1.20	3.29	1
9	Steel	Steel	Brass	13.06	11.91	10.07	1
10	Aluminum	Aluminum	Aluminum	12.85	3.69	6.64	1
11	Aluminum	Aluminum	Steel	35.35	5.36	16.33	1
12	Aluminum	Steel	Aluminum	2.60	2.27	2.00	1
13	Aluminum	Steel	Steel	23.74	16.41	16.13	1
14	Aluminum	Steel	Brass	25.27	16.29	16.69	1
15	Aluminum	Brass	Steel	33.78	3.67	15.19	1
16	Aluminum	Brass	Brass	23.95	17.32	16.58	1
17	Aluminum	Brass	Aluminum	10.88	12.60	9.51	1
18	Aluminum	Aluminum	Brass	36.24	6.09	16.99	1
19	Brass	Brass	Brass	11.64	15.95	11.12	1
20	Brass	Brass	Aluminum	0.08	3.05	1.41	1
21	Brass	Aluminum	Brass	28.65	11.15	16.00	1
22	Brass	Aluminum	Aluminum	2.96	43.20	18.52	1
23	Brass	Aluminum	Steel	25.08	26.49	20.70	1
24	***Brass***	***Steel***	***Aluminum***	***0.03***	***0.40***	***0.31***	***1***
25	Brass	Steel	Steel	11.10	4.78	6.43	1
26	Brass	Steel	Brass	13.84	19.43	13.39	1
27	Brass	Brass	Steel	6.95	5.82	5.19	1

Table B-4 Results for Test case – 1 at Mach 1.5 with weighting factor set 2 (cont'd)

Case #	x1	x2	x3	Mass	Cg	Ix/Iy
1	31.94	0.98	39.21	391.5	18.13	0.0067
2	15.35	0.13	26.94	760.2	17.06	0.0067
3	33.28	0.94	38.93	344.1	21.82	0.0062
4	27.31	0.98	34.31	256.3	17.71	0.0042
5	32.91	0.95	38.82	350.7	21.89	0.0060
6	24.24	0.52	33.08	683.3	16.80	0.0072
7	33.14	0.96	39.21	423.7	19.58	0.0073
8	17.88	0.82	39.21	891.3	18.19	0.0074
9	32.00	0.98	38.82	406.1	19.30	0.0064
10	32.24	0.98	39.21	140.2	19.26	0.0070
11	30.75	0.99	39.21	252.4	23.10	0.0077
12	27.91	0.99	36.75	270.1	17.51	0.0071
13	31.66	0.99	39.21	320.4	21.12	0.0085
14	31.60	0.99	39.21	334.6	21.38	0.0085
15	1.47	0.99	10.61	1072.3	22.83	0.0070
16	31.60	0.99	39.21	344.0	21.15	0.0086
17	23.62	0.53	28.28	597.0	18.92	0.0082
18	30.41	0.99	39.21	268.0	23.25	0.0077
19	31.37	0.99	38.47	435.9	19.05	0.0061
20	17.28	0.32	20.50	762.5	17.08	0.0071
21	33.75	0.92	39.18	374.2	21.96	0.0065
22	26.70	0.98	33.70	270.8	17.57	0.0041
23	32.14	0.97	38.24	348.3	21.35	0.0054
24	***36.46***	***0.34***	***38.23***	***701.3***	***17.07***	***0.0073***
25	33.11	0.97	39.21	404.0	18.96	0.0069
26	31.18	0.99	38.26	433.5	19.43	0.0059
27	32.64	0.98	39.21	401.0	18.25	0.0069

B.3 RESULTS AT MACH 2.5 WITH WEIGHTING FACTOR SET 1

Table B-5 Results for Test case – 1 at Mach 2.5 with weighting factor set 1

Case #	Nose	Body	Tail	ErrCg(%)	ErrI(%)	FOM	Flag
1	Steel	Steel	Steel	13.63	2.02	5.35	1
2	Steel	Steel	Aluminum	0.04	7.59	2.80	1
3	Steel	Aluminum	Steel	29.30	11.54	13.73	1
4	Steel	Aluminum	Aluminum	2.54	33.65	12.19	1
5	Steel	Aluminum	Brass	38.80	15.90	18.49	1
6	Steel	Brass	Aluminum	1.27	4.39	2.14	1
7	Steel	Brass	Brass	29.77	11.27	0.00	0
8	Steel	Brass	Steel	10.36	2.59	4.46	1
9	Steel	Steel	Brass	30.92	12.43	0.00	0
10	Aluminum	Aluminum	Aluminum	12.51	3.93	5.53	1
11	Aluminum	Aluminum	Steel	31.01	6.73	12.72	1
12	Aluminum	Steel	Aluminum	7.71	5.41	4.60	1
13	Aluminum	Steel	Steel	24.22	17.13	13.89	1
14	Aluminum	Steel	Brass	37.78	1.24	13.31	1
15	Aluminum	Brass	Steel	20.46	4.60	8.48	1
16	Aluminum	Brass	Brass	28.07	27331.10	0.00	0
17	Aluminum	Brass	Aluminum	14.45	10.59	8.49	1
18	Aluminum	Aluminum	Brass	54.03	2.40	19.07	1
19	Brass	Brass	Brass	31.48	27331.10	0.00	0
20	Brass	Brass	Aluminum	3.35	0.10	1.41	1
21	Brass	Aluminum	Brass	42.95	17.47	20.41	1
22	Brass	Aluminum	Aluminum	3.70	33.52	12.51	1
23	Brass	Aluminum	Steel	28.11	11.01	13.16	1
24	***Brass***	***Steel***	***Aluminum***	***0.03***	***2.53***	***1.08***	***1***
25	Brass	Steel	Steel	0.13	15.09	5.23	1
26	Brass	Steel	Brass	33.76	19.55	18.08	1
27	Brass	Brass	Steel	11.64	1.78	4.62	1

Table B-6 Results for Test case – 1 at Mach 2.5 with weighting factor set 1 (cont'd)

Case #	x1	x2	x3	Mass	Cg	Ix/Iy
1	33.19	0.96	39.21	405.4	19.39	0.0071
2	0.87	0.14	37.42	764.4	17.06	0.0067
3	33.59	0.92	39.04	354.2	22.07	0.0064
4	15.71	0.86	32.74	386.3	17.50	0.0048
5	31.06	0.53	38.54	761.4	23.69	0.0061
6	14.24	0.33	28.03	771.5	16.85	0.0070
7	30.18	0.38	30.65	1123.9	22.15	0.0065
8	32.70	0.97	39.21	414.9	18.84	0.0071
9	29.71	0.37	30.19	1103.5	22.35	0.0064
10	32.16	0.99	39.21	140.8	19.20	0.0070
11	19.49	0.89	39.21	427.9	22.36	0.0078
12	4.51	0.27	39.21	683.4	18.38	0.0077
13	31.73	0.99	39.21	318.5	21.20	0.0085
14	25.55	0.57	33.11	916.3	23.52	0.0074
15	30.10	0.98	38.75	384.0	20.56	0.0076
16	38.73	########	39.21	#########	21.86	2.0000
17	24.67	0.78	31.32	447.2	19.53	0.0081
18	2.58	0.94	22.69	793.0	26.29	0.0075
19	33.31	########	39.21	#########	22.44	2.0000
20	4.35	0.55	38.92	797.2	16.50	0.0073
21	29.18	0.48	33.64	811.2	24.40	0.0060
22	27.77	0.84	34.77	324.6	17.70	0.0048
23	33.96	0.91	39.21	368.1	21.86	0.0065
24	***37.22***	***0.39***	***39.21***	***680.1***	***17.07***	***0.0075***
25	29.15	0.99	38.83	468.4	17.05	0.0062
26	20.34	0.75	27.91	926.0	22.83	0.0059
27	33.27	0.96	39.21	421.4	19.05	0.0072

B.4 RESULTS AT MACH 2.5 WITH WEIGHTING FACTOR SET 2

Table B-7 Results for Test case – 1 at Mach 2.5 with weighting factor set 2

Case #	Nose	Body	Tail	ErrCg(%)	ErrI(%)	FOM	Flag
1	Steel	Steel	Steel	8.84	6.26	6.12	1
2	Steel	Steel	Aluminum	0.04	7.59	3.21	1
3	Steel	Aluminum	Steel	27.86	15.49	17.41	1
4	Steel	Aluminum	Aluminum	10.04	34.17	17.77	1
5	Steel	Aluminum	Brass	47.37	3.36	20.42	1
6	Steel	Brass	Aluminum	1.58	1.50	1.37	1
7	Steel	Brass	Brass	43.38	12.44	22.48	1
8	Steel	Brass	Steel	6.57	1.20	3.29	1
9	Steel	Steel	Brass	43.73	3.12	18.92	1
10	Aluminum	Aluminum	Aluminum	12.85	3.69	6.64	1
11	Aluminum	Aluminum	Steel	35.35	5.36	16.33	1
12	Aluminum	Steel	Aluminum	2.64	0.11	1.21	1
13	Aluminum	Steel	Steel	23.74	16.41	16.13	1
14	Aluminum	Steel	Brass	50.33	18.13	27.56	1
15	Aluminum	Brass	Steel	22.45	17.65	16.10	1
16	Aluminum	Brass	Brass	44.22	8.93	21.43	1
17	Aluminum	Brass	Aluminum	10.88	12.60	9.51	1
18	Aluminum	Aluminum	Brass	54.59	0.48	22.18	1
19	Brass	Brass	Brass	19.49	27331.10	0.00	0
20	Brass	Brass	Aluminum	2.98	5.47	3.52	1
21	Brass	Aluminum	Brass	43.28	15.17	23.55	1
22	Brass	Aluminum	Aluminum	3.71	37.92	16.73	1
23	Brass	Aluminum	Steel	25.83	25.77	20.71	1
24	***Brass***	***Steel***	***Aluminum***	***0.03***	***0.40***	***0.31***	***1***
25	Brass	Steel	Steel	8.65	6.82	6.27	1
26	Brass	Steel	Brass	26.54	20.44	0.00	0
27	Brass	Brass	Steel	9.18	4.06	5.38	1

Table B-8 Results for Test case – 1 at Mach 2.5 with weighting factor set 2 (cont'd)

Case #	x1	x2	x3	Mass	Cg	Ix/Iy
1	32.56	0.98	39.21	383.2	18.58	0.0068
2	0.89	0.14	36.92	764.4	17.06	0.0067
3	33.28	0.94	38.93	344.1	21.82	0.0062
4	3.45	0.91	24.48	460.0	18.78	0.0048
5	32.58	0.71	36.17	611.4	25.15	0.0070
6	24.24	0.52	33.08	683.3	16.80	0.0072
7	21.81	0.87	27.25	796.2	24.47	0.0064
8	17.88	0.82	39.21	891.3	18.19	0.0074
9	17.89	0.81	22.18	910.5	24.53	0.0071
10	32.16	0.98	39.18	140.2	19.26	0.0070
11	30.75	0.99	39.21	252.4	23.10	0.0077
12	15.57	0.86	31.63	533.9	17.52	0.0073
13	31.66	0.99	39.21	320.4	21.12	0.0085
14	17.91	0.81	22.20	862.5	25.66	0.0086
15	31.62	0.99	39.21	329.6	20.90	0.0086
16	25.35	0.71	29.02	848.9	24.61	0.0079
17	23.62	0.53	28.28	597.0	18.92	0.0082
18	3.10	0.99	23.91	764.0	26.38	0.0073
19	37.37	########	39.21	##########	20.39	2.0000
20	16.65	0.54	29.32	724.9	16.56	0.0069
21	32.62	0.40	34.79	832.8	24.45	0.0062
22	18.07	0.87	31.10	377.3	17.70	0.0045
23	32.19	0.96	38.27	350.3	21.48	0.0054
24	***36.46***	***0.34***	***38.23***	***701.3***	***17.07***	***0.0073***
25	32.80	0.98	39.21	394.4	18.54	0.0068
26	21.85	0.10	39.21	1208.9	21.60	0.0058
27	32.95	0.97	39.21	407.5	18.63	0.0070

APPENDIX C

DETAILS OF THE SOLUTION FOR TEST CASE 2

The optimum solution is denoted with bold and italic rows in the following tables. Mass is in grams and the location of centre of gravity is measured in centimeters from nose.

C.1 RESULTS AT MACH 0.6 WITH WEIGHTING FACTOR SET 1

Table C-1 Results for Test case – 2 at Mach 0.6 with weighting factor set 1

Case #	Nose	Body	Tail	ErrCg(%)	ErrI(%)	FOM	Flag
1	Steel	Steel	Steel	22.27	2.83	8.78	1
2	Steel	Steel	Aluminum	6.55	4.92	4.21	1
3	Steel	Aluminum	Steel	13.12	41.46	18.51	1
4	Steel	Aluminum	Aluminum	5.78	24.25	10.20	1
5	Steel	Aluminum	Brass	15.10	42.24	19.44	1
6	***Steel***	***Brass***	***Aluminum***	***6.30***	***1.55***	***2.92***	***1***
7	Steel	Brass	Brass	22.79	2.71	8.94	1
8	Steel	Brass	Steel	21.69	1.03	8.00	1
9	Steel	Steel	Brass	23.03	5.54	9.94	1
10	Aluminum	Aluminum	Aluminum	25.15	14.06	13.22	1
11	Aluminum	Aluminum	Steel	42.40	18.89	20.68	1
12	Aluminum	Steel	Aluminum	18.18	2.78	7.21	1
13	Aluminum	Steel	Steel	32.92	3.16	12.34	1
14	Aluminum	Steel	Brass	34.32	0.74	12.01	1
15	Aluminum	Brass	Steel	34.87	0.55	12.30	1
16	Aluminum	Brass	Brass	36.22	1.17	12.97	1
17	Aluminum	Brass	Aluminum	16.49	4.47	7.22	1
18	Aluminum	Aluminum	Brass	43.38	19.44	21.18	1
19	Brass	Brass	Brass	22.06	2.52	8.63	1
20	Brass	Brass	Aluminum	5.77	2.73	3.24	1
21	Brass	Aluminum	Brass	12.78	42.47	18.75	1
22	Brass	Aluminum	Aluminum	0.67	32.90	11.51	1
23	Brass	Aluminum	Steel	10.99	41.58	17.85	1
24	Brass	Steel	Aluminum	8.19	4.58	4.75	1
25	Brass	Steel	Steel	20.84	4.45	8.85	1
26	Brass	Steel	Brass	22.33	7.34	10.33	1
27	Brass	Brass	Steel	14.25	13.05	9.60	1

Table C-2 Results for Test case – 2 at Mach 0.6 with weighting factor set 1 (cont'd)

Case #	x1	x2	x3	Mass	Cg	Ix/Iy
1	23.58	0.92	27.25	1228.5	15.65	0.0404
2	10.46	1.08	20.96	1163.3	13.64	0.0395
3	17.55	0.93	27.25	959.2	14.48	0.0243
4	20.63	1.13	25.44	578.4	13.54	0.0315
5	17.90	0.93	27.25	972.9	14.73	0.0240
6	***16.45***	***1.29***	***24.14***	***911.0***	***13.61***	***0.0409***
7	23.23	0.93	27.25	1305.6	15.72	0.0405
8	23.24	0.93	27.25	1284.1	15.58	0.0412
9	23.35	0.93	27.25	1254.3	15.75	0.0393
10	21.94	0.93	27.19	457.6	16.02	0.0357
11	27.19	0.64	29.68	731.0	18.23	0.0337
12	10.36	1.45	22.80	689.4	15.13	0.0427
13	13.89	1.18	25.12	943.4	17.01	0.0403
14	14.93	1.12	25.61	978.1	17.19	0.0413
15	0.75	0.58	23.01	1476.6	17.26	0.0418
16	0.09	0.53	3.10	1515.5	17.44	0.0411
17	8.14	1.60	21.52	702.5	14.91	0.0397
18	25.22	0.72	29.02	728.7	18.35	0.0335
19	23.62	0.92	27.25	1324.5	15.62	0.0405
20	10.48	1.08	20.78	1239.1	13.54	0.0405
21	17.70	0.93	27.25	1013.9	14.44	0.0239
22	17.65	0.11	30.40	963.4	12.89	0.0279
23	17.51	0.93	27.25	996.7	14.21	0.0243
24	0.08	0.08	30.40	1497.6	13.85	0.0397
25	23.56	0.93	27.25	1255.0	15.47	0.0397
26	23.87	0.87	27.25	1332.5	15.66	0.0385
27	17.12	0.86	27.74	1501.4	14.62	0.0362

C.2 RESULTS AT MACH 0.6 WITH WEIGHTING FACTOR SET 2

Table C-3 Results for Test case – 2 at Mach 0.6 with weighting factor set 2

Case #	Nose	Body	Tail	ErrCg(%)	ErrI(%)	FOM	Flag
1	Steel	Steel	Steel	16.84	14.07	12.63	1
2	Steel	Steel	Aluminum	6.69	4.00	4.49	1
3	Steel	Aluminum	Steel	12.43	41.50	21.77	1
4	Steel	Aluminum	Aluminum	5.89	24.41	12.24	1
5	Steel	Aluminum	Brass	14.07	42.37	22.77	1
6	Steel	Brass	Aluminum	6.03	4.91	4.60	1
7	Steel	Brass	Brass	22.79	2.71	10.46	1
8	Steel	Brass	Steel	21.69	1.03	9.35	1
9	Steel	Steel	Brass	16.98	18.41	14.48	1
10	Aluminum	Aluminum	Aluminum	25.32	14.96	16.20	1
11	Aluminum	Aluminum	Steel	42.39	18.70	24.58	1
12	Aluminum	Steel	Aluminum	16.69	6.85	9.55	1
13	Aluminum	Steel	Steel	33.21	0.04	13.49	1
14	Aluminum	Steel	Brass	34.14	2.85	14.99	1
15	Aluminum	Brass	Steel	35.08	0.43	14.50	1
16	Aluminum	Brass	Brass	33.68	2.96	14.86	1
17	Aluminum	Brass	Aluminum	16.36	3.03	7.90	1
18	Aluminum	Aluminum	Brass	43.27	19.96	25.43	1
19	Brass	Brass	Brass	21.20	4.95	10.73	1
20	***Brass***	***Brass***	***Aluminum***	***7.07***	***0.29***	***3.18***	***1***
21	Brass	Aluminum	Brass	11.99	42.50	22.00	1
22	Brass	Aluminum	Aluminum	0.66	32.90	13.62	1
23	Brass	Aluminum	Steel	10.37	41.57	20.98	1
24	Brass	Steel	Aluminum	5.69	3.21	3.78	1
25	Brass	Steel	Steel	20.17	9.87	12.26	1
26	Brass	Steel	Brass	15.08	17.20	13.21	1
27	Brass	Brass	Steel	14.25	13.05	11.22	1

Table C-4 Results for Test case – 2 at Mach 0.6 with weighting factor set 2 (cont'd)

Case #	x1	x2	x3	Mass	Cg	Ix/Iy
1	19.20	0.93	27.25	1320.5	14.96	0.0357
2	13.88	1.13	22.65	1062.2	13.66	0.0399
3	16.66	0.93	27.25	978.5	14.39	0.0243
4	20.58	1.13	25.41	579.0	13.55	0.0314
5	16.66	0.93	27.25	999.9	14.60	0.0240
6	10.77	1.23	21.08	1107.9	13.57	0.0396
7	23.22	0.93	27.25	1305.6	15.72	0.0405
8	23.23	0.93	27.25	1284.1	15.58	0.0412
9	5.03	1.08	25.85	1599.8	14.97	0.0339
10	21.32	0.98	26.83	445.9	16.04	0.0354
11	26.96	0.65	29.57	725.7	18.23	0.0338
12	8.02	1.59	21.52	684.5	14.94	0.0387
13	14.71	1.13	25.48	950.5	17.05	0.0416
14	14.33	1.15	25.36	972.7	17.17	0.0404
15	16.35	0.12	23.80	1478.0	17.29	0.0418
16	14.80	1.12	25.61	1021.7	17.11	0.0428
17	8.00	1.59	21.52	714.1	14.89	0.0403
18	24.13	0.77	28.54	708.2	18.34	0.0333
19	23.03	0.93	27.25	1336.2	15.51	0.0395
20	***13.88***	***1.05***	***22.14***	***1183.3***	***13.71***	***0.0415***
21	16.66	0.93	27.25	1037.6	14.33	0.0239
22	17.62	0.11	30.40	963.3	12.88	0.0279
23	16.66	0.93	27.25	1016.1	14.13	0.0243
24	15.15	1.12	23.23	1074.5	13.53	0.0403
25	21.55	1.02	26.46	1199.6	15.38	0.0375
26	17.30	0.86	27.80	1469.2	14.73	0.0344
27	17.10	0.86	27.74	1501.2	14.62	0.0362

C.3 RESULTS AT MACH 1.2 WITH WEIGHTING FACTOR SET 1

Table C-5 Results for Test case – 2 at Mach 1.2 with weighting factor set 1

Case #	Nose	Body	Tail	ErrCg(%)	ErrI(%)	FOM	Flag
1	Steel	Steel	Steel	22.27	2.83	8.78	1
2	Steel	Steel	Aluminum	8.74	2.39	4.16	1
3	Steel	Aluminum	Steel	13.12	41.46	18.51	1
4	Steel	Aluminum	Aluminum	5.78	24.25	10.20	1
5	Steel	Aluminum	Brass	14.18	44.37	19.87	1
6	Steel	Brass	Aluminum	15.29	11.38	9.22	1
7	Steel	Brass	Brass	18.30	40.88	20.12	1
8	Steel	Brass	Steel	21.69	1.03	8.00	1
9	Steel	Steel	Brass	18.50	40.85	20.21	1
10	Aluminum	Aluminum	Aluminum	25.15	14.06	13.22	1
11	Aluminum	Aluminum	Steel	42.40	18.89	20.68	1
12	Aluminum	Steel	Aluminum	18.18	2.78	7.21	1
13	Aluminum	Steel	Steel	32.78	4.72	12.81	1
14	Aluminum	Steel	Brass	39.58	9.60	16.69	1
15	Aluminum	Brass	Steel	34.87	0.55	12.30	1
16	Aluminum	Brass	Brass	42.91	12.21	18.73	1
17	Aluminum	Brass	Aluminum	16.49	4.47	7.22	1
18	Aluminum	Aluminum	Brass	43.40	23.80	22.64	1
19	Brass	Brass	Brass	16.84	43.01	20.35	1
20	Brass	Brass	Aluminum	11.35	3.80	5.48	1
21	Brass	Aluminum	Brass	12.33	45.17	19.53	1
22	Brass	Aluminum	Aluminum	0.67	32.90	11.51	1
23	Brass	Aluminum	Steel	10.99	41.58	17.85	1
24	***Brass***	***Steel***	***Aluminum***	***5.92***	***1.87***	***2.94***	***1***
25	Brass	Steel	Steel	21.10	5.50	9.30	1
26	Brass	Steel	Brass	16.88	44.23	20.77	1
27	Brass	Brass	Steel	20.96	0.80	7.69	1

Table C-6 Results for Test case – 2 at Mach 1.2 with weighting factor set 1 (cont'd)

Case #	x1	x2	x3	Mass	Cg	Ix/Iy
1	23.58	0.92	27.25	1228.5	15.65	0.0404
2	10.36	0.65	20.53	1351.2	13.92	0.0406
3	17.55	0.93	27.25	959.2	14.48	0.0243
4	20.63	1.13	25.44	578.4	13.54	0.0315
5	5.96	1.11	25.61	1050.9	14.62	0.0231
6	17.09	1.14	21.77	974.5	14.76	0.0463
7	10.04	1.56	21.88	1174.9	15.14	0.0246
8	23.24	0.93	27.25	1284.1	15.58	0.0412
9	7.82	1.59	21.13	1265.2	15.17	0.0246
10	21.94	0.93	27.19	457.6	16.02	0.0357
11	27.19	0.64	29.68	731.0	18.23	0.0337
12	10.36	1.45	22.80	689.4	15.13	0.0427
13	13.48	1.20	24.93	941.0	17.00	0.0396
14	20.04	1.15	25.36	901.9	17.87	0.0456
15	0.75	0.58	23.01	1476.6	17.26	0.0418
16	18.35	1.08	22.72	1079.6	18.29	0.0467
17	8.14	1.60	21.52	702.5	14.91	0.0397
18	22.21	0.79	27.85	718.5	18.36	0.0317
19	9.65	1.59	21.58	1207.2	14.96	0.0237
20	13.81	0.85	19.30	1296.6	14.25	0.0432
21	5.58	1.16	25.24	1087.3	14.38	0.0228
22	17.65	0.11	30.40	963.4	12.89	0.0279
23	17.51	0.93	27.25	996.7	14.21	0.0243
24	***17.81***	***1.10***	***24.91***	***1041.6***	***13.56***	***0.0424***
25	23.87	0.87	27.25	1308.6	15.50	0.0393
26	9.82	1.59	21.64	1183.3	14.96	0.0232
27	23.61	0.92	27.25	1303.1	15.48	0.0413

C.4 RESULTS AT MACH 1.2 WITH WEIGHTING FACTOR SET 2

Table C-7 Results for Test case – 2 at Mach 1.2 with weighting factor set 2

Case #	Nose	Body	Tail	ErrCg(%)	ErrI(%)	FOM	Flag
1	Steel	Steel	Steel	16.84	14.07	12.63	1
2	Steel	Steel	Aluminum	7.25	1.71	3.80	1
3	Steel	Aluminum	Steel	12.43	41.50	21.77	1
4	Steel	Aluminum	Aluminum	0.39	29.35	12.08	1
5	Steel	Aluminum	Brass	14.18	44.37	23.63	1
6	Steel	Brass	Aluminum	9.68	0.23	4.26	1
7	Steel	Brass	Brass	17.95	39.15	23.07	1
8	Steel	Brass	Steel	21.69	1.03	9.35	1
9	Steel	Steel	Brass	18.25	43.18	24.81	1
10	Aluminum	Aluminum	Aluminum	25.32	14.96	16.20	1
11	Aluminum	Aluminum	Steel	42.39	18.70	24.58	1
12	Aluminum	Steel	Aluminum	16.69	6.85	9.55	1
13	Aluminum	Steel	Steel	35.66	2.54	15.56	1
14	Aluminum	Steel	Brass	35.57	1.62	15.12	1
15	Aluminum	Brass	Steel	35.08	0.43	14.50	1
16	Aluminum	Brass	Brass	32.96	8.59	16.88	1
17	Aluminum	Brass	Aluminum	16.36	3.03	7.90	1
18	Aluminum	Aluminum	Brass	37.38	31.11	27.54	1
19	Brass	Brass	Brass	17.30	41.47	23.78	1
20	***Brass***	***Brass***	***Aluminum***	***7.07***	***0.29***	***3.18***	***1***
21	Brass	Aluminum	Brass	12.51	44.98	23.19	1
22	Brass	Aluminum	Aluminum	0.66	32.90	13.62	1
23	Brass	Aluminum	Steel	10.37	41.57	20.98	1
24	Brass	Steel	Aluminum	1.00	11.96	5.43	1
25	Brass	Steel	Steel	21.07	4.93	10.66	1
26	Brass	Steel	Brass	15.24	40.15	22.42	1
27	Brass	Brass	Steel	14.22	13.06	11.21	1

Table C-8 Results for Test case – 2 at Mach 1.2 with weighting factor set 2 (cont'd)

Case #	x1	x2	x3	Mass	Cg	Ix/Iy
1	19.20	0.93	27.25	1320.5	14.96	0.0357
2	14.71	1.06	23.12	1100.0	13.73	0.0409
3	16.66	0.93	27.25	978.5	14.39	0.0243
4	19.53	0.45	30.40	893.4	12.85	0.0294
5	5.96	1.11	25.61	1050.9	14.62	0.0231
6	5.88	0.45	19.23	1493.0	14.04	0.0417
7	10.46	1.52	22.19	1178.2	15.10	0.0253
8	23.23	0.93	27.25	1284.1	15.58	0.0412
9	9.19	1.59	21.58	1178.3	15.14	0.0236
10	21.31	0.98	26.83	445.9	16.04	0.0354
11	26.96	0.65	29.57	725.7	18.23	0.0338
12	8.02	1.59	21.52	684.5	14.94	0.0387
13	28.71	0.11	29.47	1411.1	17.36	0.0405
14	13.23	0.85	24.92	1208.5	17.35	0.0409
15	16.35	0.12	23.80	1478.0	17.29	0.0418
16	16.09	0.72	27.98	1293.3	17.02	0.0452
17	8.00	1.59	21.52	714.1	14.89	0.0403
18	10.61	0.98	26.77	722.9	17.58	0.0287
19	7.17	1.65	20.60	1340.0	15.01	0.0243
20	***13.88***	***1.05***	***22.14***	***1183.3***	***13.71***	***0.0415***
21	16.35	1.07	26.03	971.2	14.40	0.0229
22	17.62	0.11	30.40	963.3	12.88	0.0279
23	16.66	0.93	27.25	1016.1	14.13	0.0243
24	3.78	1.71	19.87	1221.3	12.93	0.0366
25	23.74	0.90	27.25	1282.1	15.50	0.0395
26	7.87	1.59	21.64	1304.1	14.75	0.0249
27	17.09	0.86	27.74	1502.4	14.62	0.0362